Lightweight purlins stiffened with polyurethane foam

HAMK
UNIVERSITY OF APPLIED SCIENCES

Bachelor's thesis

Degree Programme in Construction Engineering

BECONU07B3 22.11.2011

Sujan Shakya

HAMK
UNIVERSITY OF APPLIED SCIENCES

BACHELOR'S THESIS

Degree programme in Construction Engineering
Visamäentie 35 B
13100 HÄMEENLINNA

Title	Lightweight steel purlins stiffened with polyurethane foam
Author	Sujan Shakya
Supervised by	Lassi Martikainen
Approved on	_____._____.20_____
Approved by	

HAMK
UNIVERSITY OF APPLIED SCIENCES

ABSTRACT

VISAMÄKI
Degree programme in Construction Engineering

Author Sujan Shakya **Year** 2011

Subject of Bachelor's thesis Lightweight steel purlins stiffened with polyurethane foam

ABSTRACT

The objective of this thesis was to implement new ways to stiffen the cold-formed steel (CFS) profiles in steel purlin systems. The use of polyurethane foam as stiffeners in purlin system is an innovative approach and is worth testing. This thesis was commissioned by Sheet Metal Center (SMC) and tests were conducted in SMC test hall from March 2011 till August 2011.

The aim of this thesis was to find an innovative method of stiffening cold-formed steel purlins against various buckling modes. Polyurethane boards (PU-boards) can be used as longitudinal stiffeners in the cold-formed C-profiles/purlins which will reinforce the profiles against buckling. The combination of PU-board of high stiffness-low strength and lightweight purlin of high strength-low stiffness were used to conduct the test to obtain beams with high strength and high stiffness.

The metal sheets used for the C-profile manufacture were S280+Z275 of thickness 0.5mm and S350+Z275 of thickness 1.0mm. In total, 20 tests were carried out which included two different cross-sections from each sheet-steel types. A four point bending setup was used to conduct the bending stiffness test. The average tangent bending stiffness of unstiffened profiles for S280+Z275 and S350+Z275 were 324,64 kNm^2 and 829,23 kNm^2 respectively. When profile webs of each sheet-steel material type were stiffened by polyurethane foam, values of tangent bending stiffness increased by 3% to 4% respectively. Similarly for web and flange stiffened profiles, the values leaped up to 11% and 9% respectively. Using PU-board as flange stiffeners were able to yield approximately an additional 10% of the bending stiffness compared to unstiffened beam. This means that the flanges are very critical members regarding the bending stiffness of the C-profile and stiffening flanges against buckling modes can be a very effective way to increase the bending stiffness of CFS-profiles.

Keywords cold-formed steel, C-purlin, polyurethane foam, bending stiffness, stiffeners.

Pages 51 p. + appendices 27 p.

CONTENTS

1 INTRODUCTION

This thesis project was commissioned by Sheet Metal Center (SMC). SMC is a research and development unit under the administration of HAMK University of Applied Sciences that works both as an educational and training institute as well as an enterprise. It was established in 1998 to provide various weathering tests and structural analysis on various structures as their service to the customers. Later, SMC started working as a hybrid of a business point and an educational institute. SMC also provides work placement and thesis topics in various fields of construction engineering to many graduating students of HAMK. (HAMK 2011.)

The aim of this thesis is to analyze the performance of PU-boards used in stiffening C-profiles to increase the bending stiffness of the stiffened profiles. The specimens created will be tested in the test hall of SMC and the test results are compared in order to obtain a productive conclusion.

The use of cold-formed steel products is gaining popularity in construction industry and it is very critical for any industry to succeed economically and environmentally. To meet such demands, factors that affect industrial economy and the surrounding environment like technical issues, design criteria of load-bearing sheets and products, technical findings and inventions must be kept going on so as to update any changes that is on the goodwill of the industry. Innovations of grooves and bents in cold-formed profiles have helped the profiles to become more efficient as the grooves and bends work as they increase load bearing capacities of the profiles and sheets. Similarly, use of polyurethane boards as stiffeners is an innovative approach and is worth testing. This is a new approach towards the methods of stiffening CFS profiles by other materials rather than only grooves and bends that are/could be made in the profile cross-section.

This thesis will be focusing on a different method of stiffening cold-formed steel purlins against various buckling modes. Polyurethane boards can be used as longitudinal stiffeners in the cold-formed C-profiles/purlins which will reinforce the profiles against buckling. The PU-boards have contrasting characteristics compared to C-profile as C-profile high strength and low stiffness whereas PU-board is relatively stiffer but has low material strength. The combination of these contrasting materials both of which are used widely in construction industry should yield favorable results of C-profiles with high strength as well as high stiffness.

Calculations regarding the determination of bending resistance of the unstiffened C-profile were completed according to Eurocode 3. Eurocode 3 provides us an approach to design a cold-formed C-profile cross-section on the basis of “effective width method” where the large extent compressed parts of the member element are regarded ineffective and are omitted from design consideration and effective parts are considered to undergo uniform bending stresses.

2 COLD-FORMED STEEL PURLINS

2.1 Introduction

The use of cold-formed steel (CFS) as structural members was introduced in the mid nineteenth century in the United States and Great Britain. However, many limitations were set when using CFS as structural members in building constructions until the introduction of the very first specification for the design of cold-formed steel structural members. This specification was published for the very first time by American Iron and Steel Institute (AISI 1946). (Young, n.d. 119-120.)

After the official publication of the code, the use of CFS structural members has increased dramatically over the years. From domestic houses to large city complexes, the use of CFS structural members of different forms, different shapes and sizes have played significant role in building industry in many different ways. Despite of having high deflection to loading ratio due to it being a slenderness member, cold-formed steel profiles have stood up for their good strength- to-weight ratio. The manufacturing process of fabricating CFS profiles, namely brake-pressing and roll forming of steel sheets makes it possible to produce CFS profiles of various cross-sectional shapes which encourage creative designs in building construction. (The Steel Framing Alliance n.d, 2.) Also, cold-forming method increases the yield strength of the material due to strain hardening.

"New products in thin steel sheets, combined with improved plating and insulating materials, make steel an interesting option with an increasing number of applications in modern construction." (European Lightweight Steel-Frame Construction 2005, 2).

Moreover, its flexibility in various shapes and cross-sections has made cold-formed profiles friendlier in many applications in construction industry. In addition, nestable cross-section designs enable compact packaging and shipping. Some of the advantages of CFS purlins over other building materials are as follows:

- Cost effective
- Shorter and predictable construction schedule
- Highest strength-to-weight ratio of any building material
- 100% recyclable
- Noncombustible- does not burn or contribute as fire load during the spread of fire
- Inorganic- will not rot, warp, split, crack or creep
- Dimensionally stable- does not expand or contract with moisture content
- Consistent material quality- produced in strict accordance with standard requirements
- High strength results in safer structures, less maintenance and slower aging of the structure etc.
- Suitable for automated mass-production

Due to the above mentioned advantages, CFS framing system has been developed under the influence of "open" construction system like in timber construction and it has started replacing other building materials already. This system has a lot to offer as the system relies on methods and techniques based on smart principles and flexible assemblies and not on a particular project or any given situations. Hence, this system is called "third-generation system". (European Light-Weight Steel Construction, 6) Cold-formed steel framing system refers to a structural framing system comprising cold-formed steel members like beams, columns, joists, studs etc. Places where the climate is very humid or places prone to termite or woodworm infestations, lightweight steel structures prove to be very effective in those regions. Wooden studs, wooden beams and columns, wooden truss in timber buildings are substituted by CFS studs, profiles, CFS purlins and CFS trussing system in CFS framing system. In this way, cost of maintenance for CFS framed building decreases making this "third generation" the very first choice of structural designers. (European Light-Weight Steel Construction, 6)

Load-bearing panels and composite panels do not only carry the normal load that is acting vertically downwards on them but also act as diaphragms to resist forces in their own planes given that they are interconnected to each other and to the connecting members correctly.

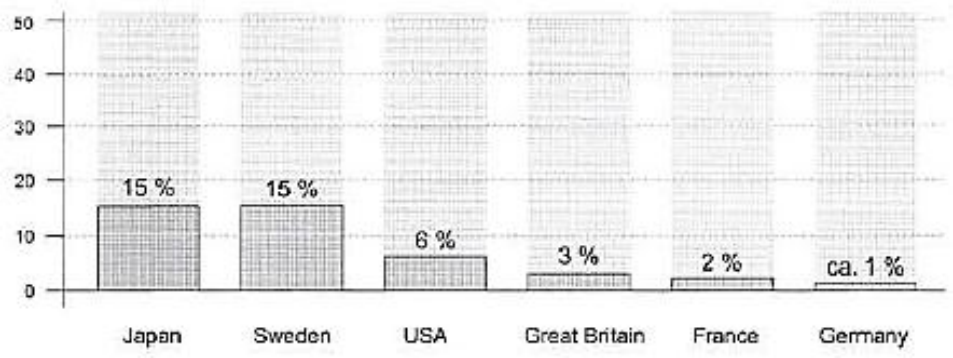

Figure 1 Percentage of self-supporting steel framing used in multi-story residential buildings (European Lightweight Steel-Framed Construction 2005, 2)

Figure 1 represents the data corresponding to the use of self-supporting steel framing systems in multi-story residential buildings in different countries around the world. Similarly, Figure 2 and Figure 3 show the wide applications of cold-formed sheet products in construction industry that has already started replacing other building products in some parts of the globe.

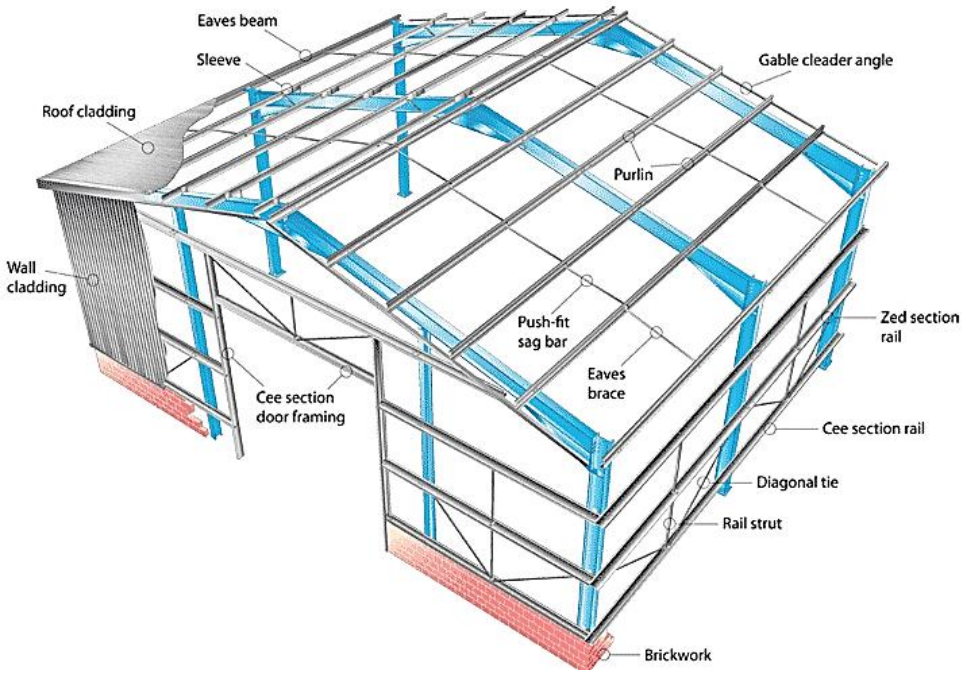

Figure 2 Use of cold-formed steel profiles in a building (Steadman & Son n.d.)

Figure 3 Connections between hot rolled beam and cold-formed Z-purlins. (Metsec, n.d.)

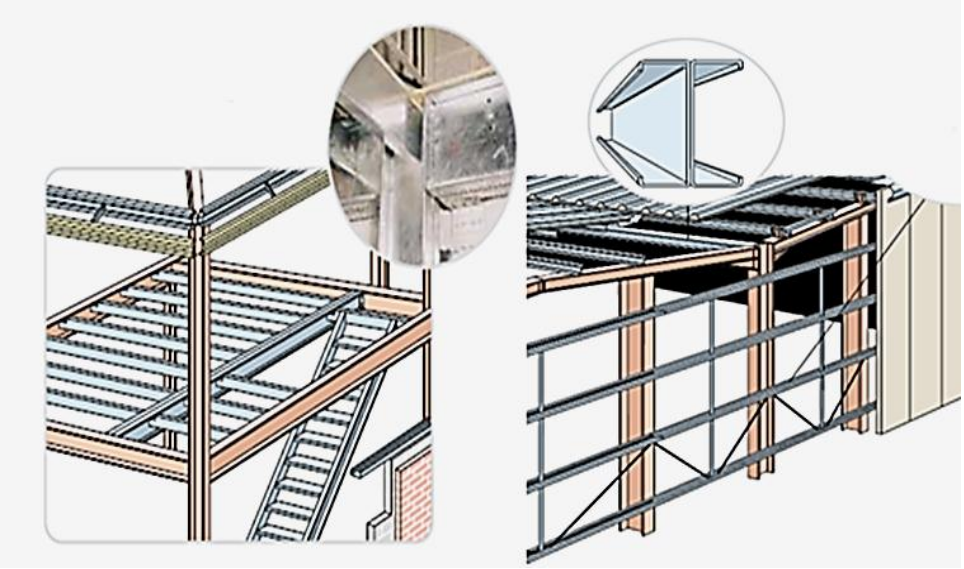

Figure 4 Use of CFS purlin system in floor construction and roof construction respectively (Kingspan multibeam 2007, 5)

In Figure 4, we can see different applications of C-profiles in a steel framed building. C-profiles used in the roof as a primary or secondary beam will experience forces from self-weight of the roof structure, snow load and wind load on the roofing sheet. C-profiles will generate a large amount of deflection as the span of the profile increases because it has a very low stiffness ratio. For serviceability limit design, a structural member must acquire as less deflection as possible. Similarly, in case of floor construction, in order to decrease deflection at the mid span of the floor, it requires more profiles to carry imposed loads with less deflection. As the number of purlins increases or an extra member is introduced in the system, the cost of the whole construction increases. So, a new design or a system is required that can withstand design values of imposed loads with low deflections and this project is an attempt to implement that system.

There are many cross-section shapes and sizes in CFS purlins that have been developed in recent years. However, some of the very typical cross-sections commonly used in building industry are C shaped purlins, Z or Sigma purlins and Hat profiles etc. These profiles are often used as load bearing members in roofs, floors, walls etc. as well as structural members like columns, beams, joists etc. Typical forms of CFS cross-sections are shown in Figure 5.

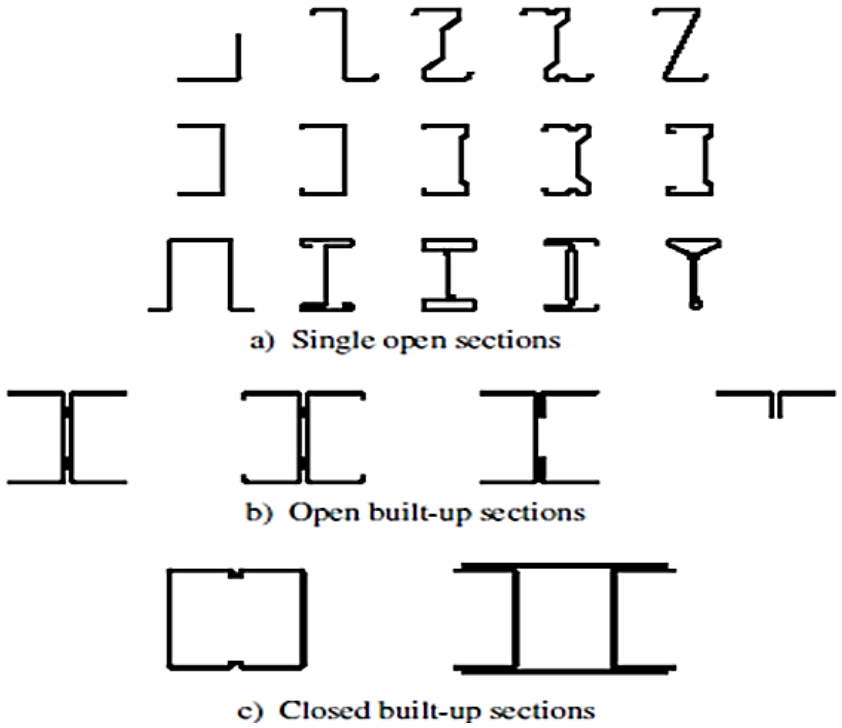

Figure 5 Typical forms of section for cold-formed members (EN 1993-1-3:2006, 8)

Similarly, Figure 6 illustrates different types of cross-sections for cold-formed members and sheets. Profile members shown in Figure 6 includes very typical cross-sections e.g. C, hat and all profile sheets. However, complicated cross-sections shown in Figure 6 are manufactured as desired by the customer or required by design plan. Due to the alterations and/or repetitions of grooves and bends in a profile cross-section, grooves and bends provide much greater strength compared to the typical profile cross-sections.

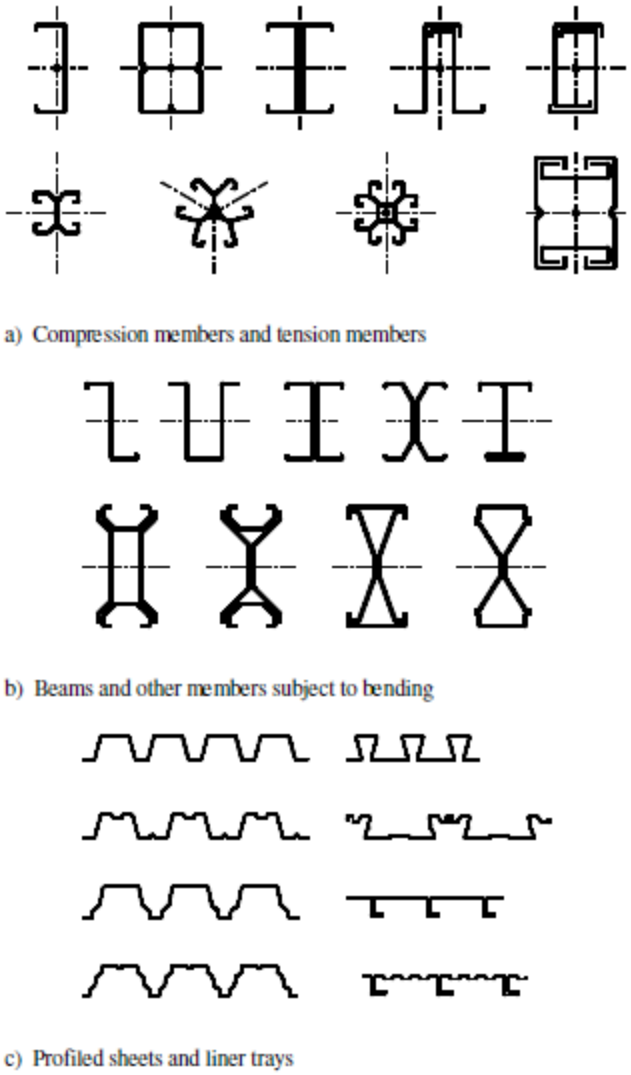

Figure 6 Cold-formed members and profile sheets (EN 1993-1-3:2006, 9)

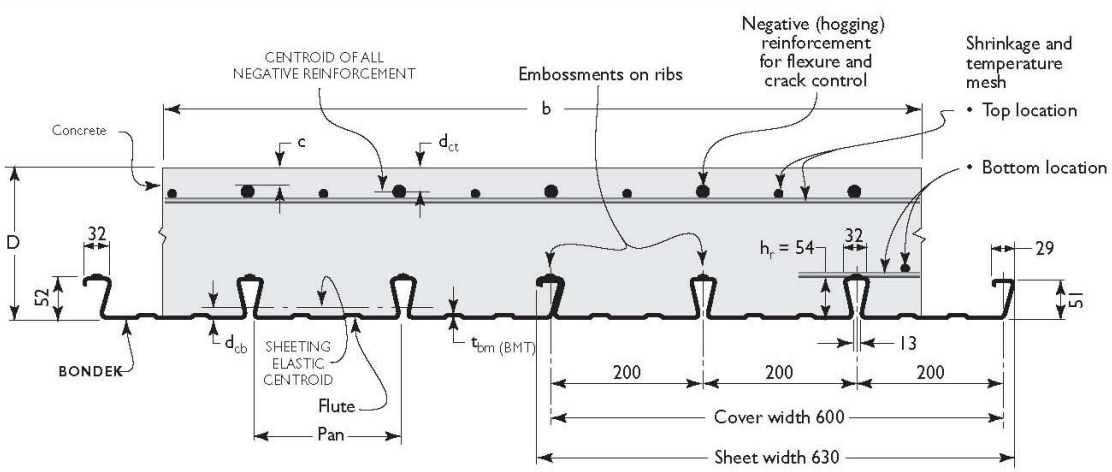

Figure 7 BONDEK composite slab (Structural decking n.d.)

Figure 6 also shows some popular sheeting designs used in steel construction as roofing sheet, sheets for floor constructions and for some composite slab designs. Composite slabs are in-situ concrete slabs reinforced by

sheeting of different cross-sections. An example of composite slab is shown in Figure 7.

Cold-formed profiles and sheets, due to their slender character, will experience different buckling modes considering the loadings and support conditions. Some of the buckling phenomena that may occur in CFS elements are local buckling, distortional buckling, overall buckling, lateral distortional buckling, flexural torsional buckling etc. Among them, global buckling is a very common buckling in every loading case and is inevitable to prevent. When a cold-formed C-profile experiences flexural or axial load, it experiences local and distortional buckling along with overall buckling of the beam considering a laterally restrained support condition.

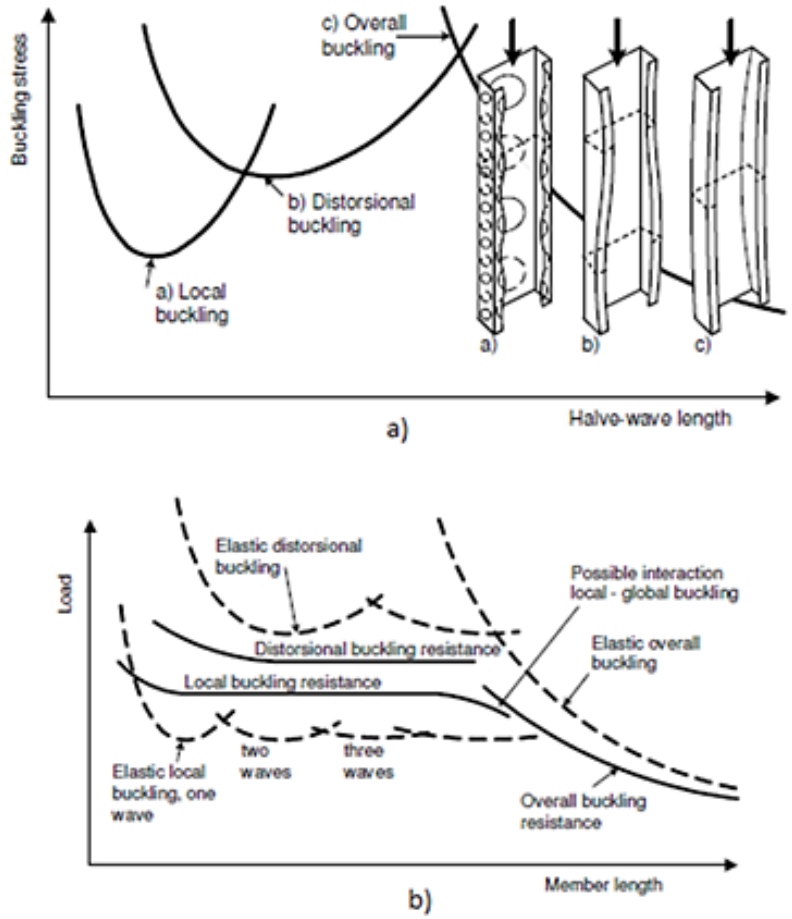

Figure 8 a) Examples of elastic critical stress for various buckling modes as function of half-wavelength and examples of buckling modes. b) Examples of elastic buckling resistance as function of member length (EN 1993-1-3:2006, 25)

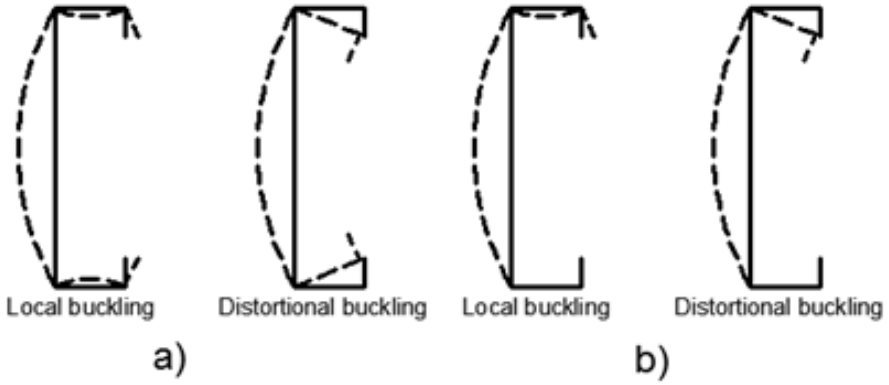

Figure 9 Buckling of cross-section containing edge stiffener under a) pure compression b) bending load (Gardner & Nathercot 2005, 140)

Figure 8 demonstrates the trend of buckling phenomena and relations on how buckling of profile elements vary with member length. Also, Figure 9 illustrates the buckling phenomena occurring in C-profile cross-section under compressive load and bending load respectively.

Similarly, Figure 8 gives us an idea of various buckling loads and buckling resistances on a cold-formed profile depending on member length. In the Figure, elastic local buckling load is lower than the local buckling resistance meaning that the profile members undergo yielding because of which the members remain deformed even after the withdrawal of load. In distortional buckling and overall buckling however, the member resistance is lower than their corresponding buckling loads. This results in returning of buckled members to its original state.

Figure 9 shows that the first buckling mode of a C-profile under compressive load (which is the same in case of flexural loading of C-profiles) is local buckling. Local buckling stress of the C-profile is lowest compared to other two buckling modes. At a point after the C-profile has gone under local buckling, stresses arising on profile members reach the level of distortional buckling stress and the profile starts buckling in distortion. As the distortional stress is at its maximum, the failure mode changes into overall buckling of the profile and the beam will fail eventually.

There have been many studies on instabilities of cold-formed lightweight profiles like local, distortional, flexural-torsional buckling using many different methods such as finite strip method (FSM), direct strength method (DSM), effective width method (EWM) etc. Several studies close to this topic have been conducted related to various buckling modes under different failure modes (Shear, bending or combined). “Shear Buckling of Thin-Walled Channel Sections” by Pham and Hancock in 2007a provided solutions to the shear buckling of complete channel sections loaded in pure shear parallel with the web by using a spline finite strip analysis (Lau and Hancock, 1986). For combined bending and shear, an extension to the DSM has been studied by Pham and Hancock in “Direct Strength Design of Cold-Formed Purlins” in 2007b. Tests on cold-formed profiles under pure bending were also run using the four point bending arrangement. This arrangement provided a large central region of uniform bending moment

and no shear force in order to make bending stresses as the only predominant stress in the mid span of the test specimen. This method is very effective as the region contains only bending stress and no shear stress, making the test results on bending actions very precise. So the same test arrangement will be used in this thesis.

2.2 Stiffeners

In Figure 5 and Figure 7, we can see different types of cross-sectional shapes of profiles, sheets being flat surfaced containing simple cross-sections as well as sheets containing various shapes with grooves and bends in their cross-sections. Grooves and bends made in CFS profiles and load bearing sheets act like stiffeners making the members much stiffer, resisting buckling failures thereby increasing the overall resistance of the members. Typically, stiffeners are the steel angle or plate or combination of plates attached to a slender beam in order to prevent its buckling nature by increasing its stiffness. Stiffeners can be longitudinal or transverse depending on their position on the beam. Different forms of stiffeners are shown in Figure 10 and 11 respectively. Also, depending on stiffening flange or web of the profile, stiffeners can still be categorized into the following catagories:

- Longitudinal flange stiffeners which may either be edge stiffeners or intermediate stiffeners which mean that there will be an additional bent or bents on the edge of the flange.

- Longitudinal web stiffeners which may be intermediate web stiffeners meaning that the grooves on the web continue along the span of the beam making the beam stiffer on the web part.

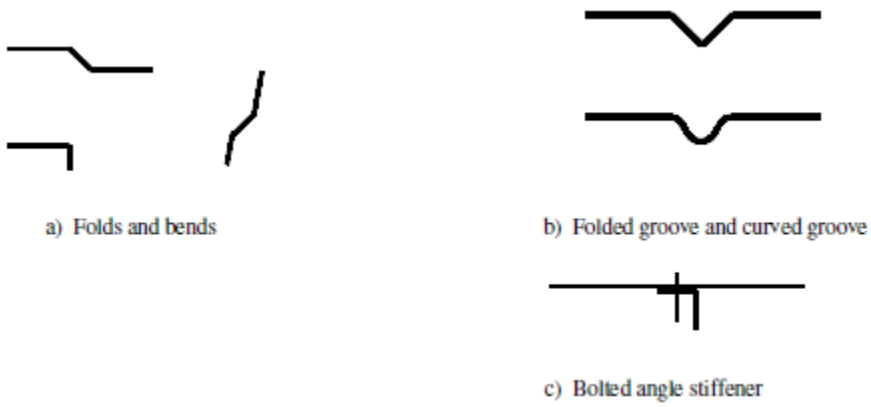

Figure 10 Typical forms of stiffeners for cold-formed members and sheeting (EN 1993-1-3:2006, 10)

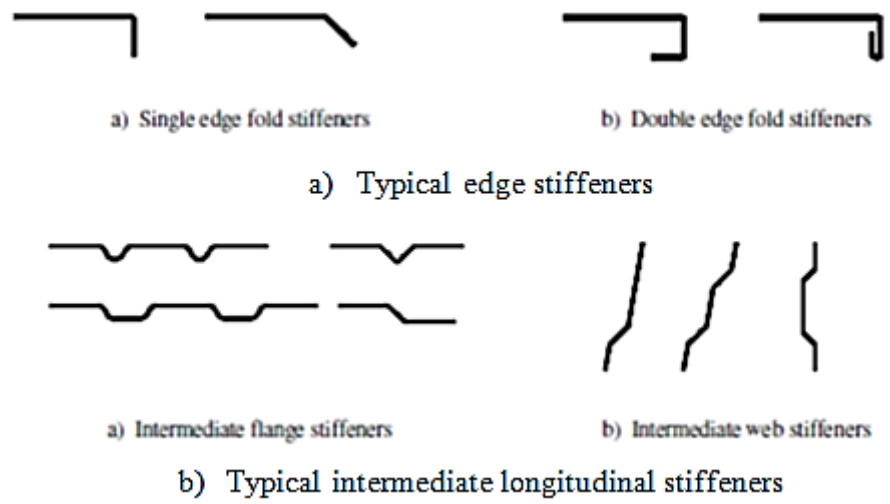

Figure 11 Typical a) edge stiffeners; b) intermediate longitudinal stiffeners (EN 1993-1-3:2006, 10)

On a simply supported beam or a column, mid span of the beam is usually the critical place when it comes to buckling loads and bending stresses. Members of the CFS profile like web and flanges hold similar case. If the nodes between webs and flanges of a cold-formed steel profile are considered as fixed supports, the middle part of each compressed member experiences critical buckling stress under various buckling conditions. Under the loading, compressed members start to experience various failure phenomena like buckling, twisting, torsion etc. So stiffeners in CFS profiles and sheets are placed in places that are prone to buckling. Stiffeners are mostly present in the middle of profile member especially in a flange apart from the case of edge stiffeners whereas the position of stiffeners in web largely depend on the loading cases (axial or flexural) and depending which side of web the buckling phenomenon takes place.
Stiffeners illustrated in Figure 10 and Figure 11 respectively, work in two typical ways.

1) Grooves and bents used as intermediate stiffeners in webs and flanges increase the material presence in the stiffened region. This, in most of the cases, increases the overall moment of inertia of the cross-section thereby increasing the overall resistance of the profile or sheet.

2) Grooves and bents used as intermediate stiffener in webs and flanges increase the stiffness of the profile/sheet as these stiffeners are assumed to contain linear or rotational springs acting at the centroid of the effective stiffener section. These imaginary linear or rotational springs provide their stiffness to the member which results in increase of stiffness of the profile. Spring stiffness can be of many different kinds depending on nature of loading, boundary conditions, profile cross-section etc. Figure 12 illustrates the modeling of elements of a cross-section with or without stiffeners.

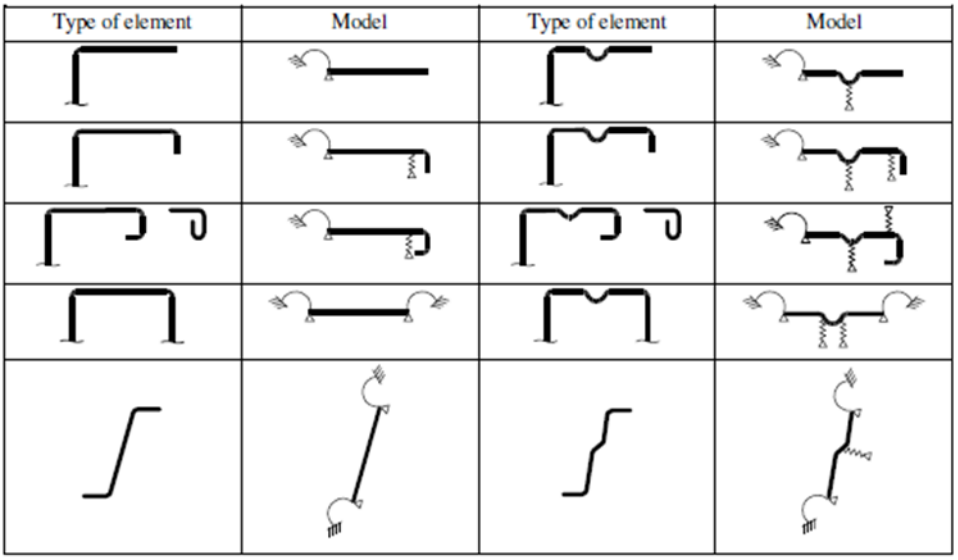

Figure 12 Structural modeling of elements of a cross-section (EN 1993-1-3:2006, 22)

Instabilities like deformation and eccentricities in any slender profile element affect the stiffness and resistance of the profile due to various load actions generated by eccentric loads and deformation. Due to the combination of actions of such generated forces, the failure of the purlin will occur in relatively lower force/load. Various buckling loads generating in slender purlin will make things more vulnerable when exposed to a smaller load. Stiffening purlins by PU-stiffeners will prevent/reduce the loads caused by deformation and buckling making the stiffened purlin to achieve higher load-resistance than unstiffened ones.

2.3 Stiffening by using polyurethane boards

Although stiffening cold-formed C-profiles with PU-boards is a new and innovative approach in the field of cold-formed steel industry, the basic idea is very similar to lightweight sandwich panels.

A sandwich panel consists of two stiff face-sheets on a thick core material. Sandwich panels have very high bending stiffness compared to its weight and hence it is often used in aeronautical, marine and vehicle industry where the weights of the structures are kept as light as possible. “However, sandwich panels are not good at carrying in-plane compressive load and it has a unique stability failure mode of its own—wrinkling” (Fagerberg 2003). This flexural wrinkling is a unique failure associated with flat and lightly profiled sandwich panels when subjected to bending or compressive loads. The wrinkling failure of the sandwich panel occurs well below the yield stress of the compressed face-sheet making it a predominant failure mode of sandwich panels. (Mahendran and McAndrew 2003, 2.)

Wrinkling is a phenomenon that shows local instability of the flat and thin profiled sheet faces of a sandwich panel associated with short waves of buckling. The compressive face of a sandwich panel in bending generates buckling waves at a stress level below the yield point of the face material.

As the amplitude of the wave increases gradually, a wrinkle is formed at the location of greatest bending moment and/or imperfections in the panel. “Wrinkling phenomenon is controlled by the vertical supports provided by the core to the face-sheet and the shear stiffness of the core material. This support provided by the core governs the wrinkling wavelength and the buckling load.” (Staal, Horrigan, Mallison & Jayaraman n.d.)

As the slender face-sheet of the sandwich panel tends to buckle in relative low flexural load or low compressive load, core material which is glued chemically, will prevent the buckling phenomena of the face-sheet by providing its own stiffness to the slender sheet. The wave created by the load will either bend in towards the core material or bend away from the core material. If the curve tends to bend away from the core material, adhesive force provided by high performance glue will prevent it buckling away from the core material. Likewise, if the wave is bending towards the core material, continuous support of the core material will reinforce the face-sheet by providing its stiffness to the sheet hence preventing it buckling inwards. As the loading stresses get higher, core material starts to crush and glue gives up and eventually the panel will fail in local buckling or wrinkling of the face-sheet. This phenomenon is illustrated in Figure 13.

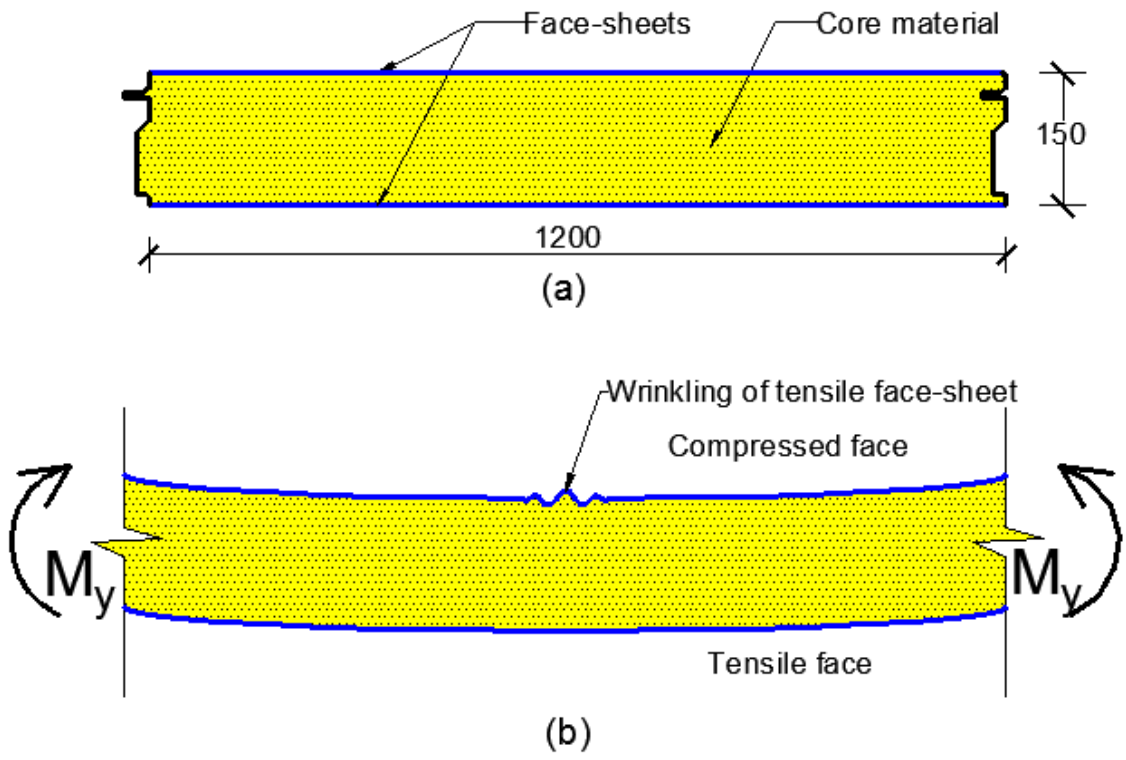

Figure 13 (a) Sandwich panel cross-section; (b) wrinkling of compressed face in sandwich panel side view

Likewise, our cold-formed C-profiles stiffened by PU-boards hold a similar case when considering the mechanism of PU-board in C-profile. When the unstiffened C-profile is loaded in flexural load, ripples of small wavelength start appearing in compressed zones of the profile due to the generated elastic local buckling stresses. As the loading in the profile increases,

stresses in and around the compressed zone increase dramatically as the profile will fail under high buckling stress. On the other hand, PU-stiffened C-profiles are able to withstand higher buckling stresses in the compressive zone of the profile. This is because PU-stiffeners/foam of the compressed zone under compressive stress will start working effectively against the buckling stresses as they provide their continuous stiffness to the corresponding compressed member. The PU-stiffeners for flanges and webs under compression start to work as continuous supports for the compressive members which will control the role of buckling in the member elements. A structural model of PU-stiffened C-profiles explaining the working mechanism of PU-foam is shown in Figure 14.

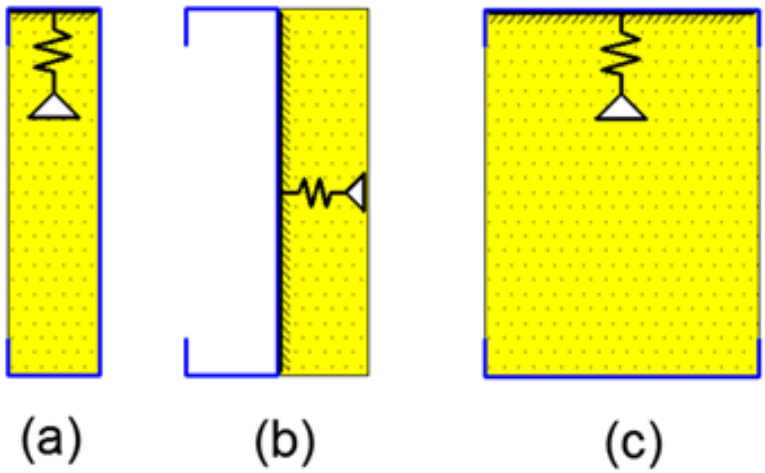

Figure 14 Structural model of PU-stiffened C-profiles illustrating bending stiffness provided by continuous support of PU-foam to the plane parts of the profile which are (a) compressive flange (b) whole web member (c) wide flange. Blue lines representing C-profiles and dotted yellow shade PU-boards.

However, wrinkling phenomenon of compressed elements in case of C-profile is not as severe in a sandwich panel. In case of sandwich panel, the width-to-thickness ratio of the compressed face is very high and has more tendency to buckle in smaller load. Unlike sandwich panel, compressed elements of C-profile have relatively smaller width meaning relatively stiffer profile-member. Moreover, wrinkling is a predominant failure mode in sandwich panel loaded in flexure whereas in case of C-profile, there are several other failure modes that can take place than local buckling of compressed member elements depending upon various loading conditions.

Local buckling of compression elements is not the only major failure mode that occurs in the profile during the loading. Web crippling of cold-formed steel member is also a very common failure mode in cold-formed steel profiles especially in case of CFS profiles with longer web member. Usually, cold-formed steel flexural members have high web element/large web slenderness ratios so webs of those profiles are likely to cripple due to high local load intensity. Figure 15 gives us an idea of web crippling in cold-formed steel flexural members. (Cold-Formed Steel Design for the Students 2008, 6.)

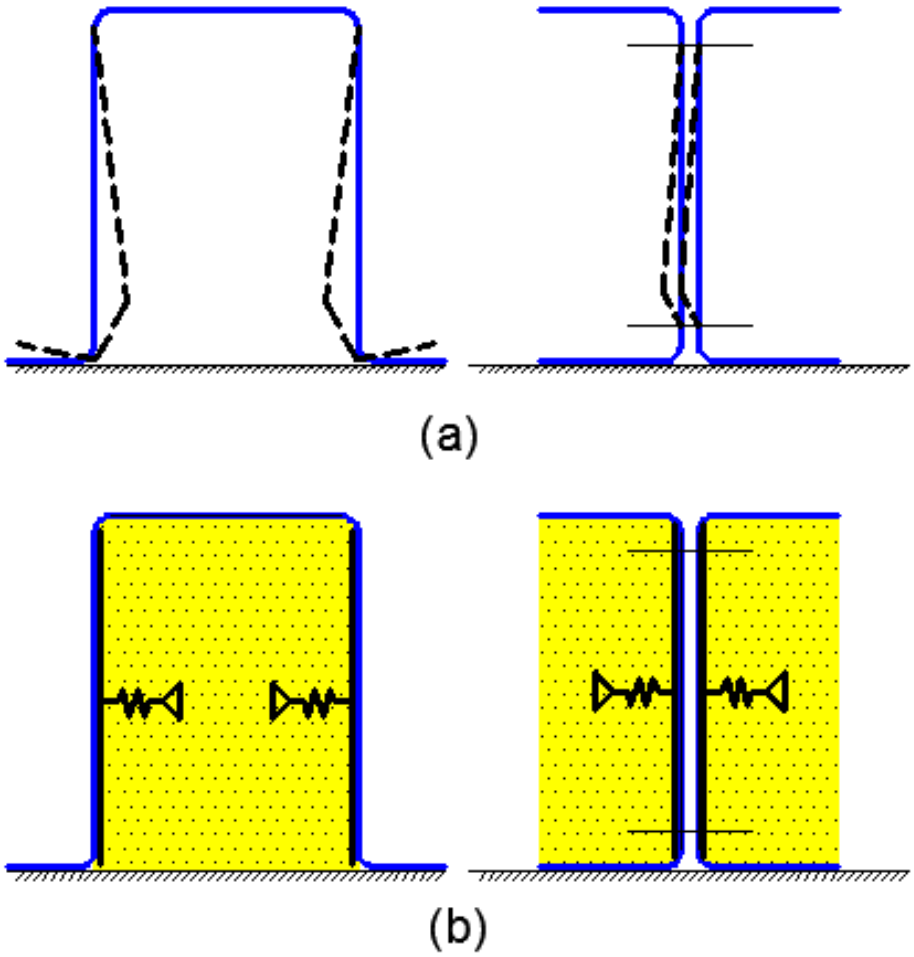

Figure 15 (a) Web crippling failure modes for single hat section and I-section profile respectively(b) web crippling failure prevented by the use of PU-foam as stiffeners

"Web crippling failure mode is rather a complicated phenomenon and it is affected by the following factors.

- non-uniform stress distribution under the applied load and adjacent portions of the web
- elastic and inelastic stability of the web element
- local yielding in the immediate region of load application
- bending produced by eccentric load or reaction when it is applied on the bearing flange at a distance beyond the curved transition of the web
- initial out-of-plane imperfection of plate elements
- various edge restraints provided by beam flanges and interaction between flange and web elements etc." (Cold-Formed Steel Design for the Students 2008, 6.)

Even though web crippling is one of the critical failure phenomena in higher CFS flexural member profile; such phenomenon can be prevented/reduced by introducing PU-foam in the profiles. As shown in figure 15, PU-foam fastened with the profile will provide a continuous stiff support

to the buckling web elements of the profile by giving its own compressive stiffness to the web element. In figure 15(b), a single hat profile has been stiffened by putting PU-foam in the concave part of the hat profile. As PU-foam fills the inside gap of the profile, webs of the hat profile are prevented from buckling as PU-foam provides its compressive stiffness to the web member of the hat profile. Similarly, in case of two fastened C-profiles, the web gets a continuous support from PU-foam against buckling. PU-foam stiffening each side of the C-profile prevents web crippling of the C-profile web member.

3 EXPERIMENTAL PROGRAM

3.1 Introduction

The purpose of conducting this experimental test is to implement a new alternative to stiffen the cold-formed steel profiles which, in this project, will be polyurethane boards as stiffeners. As mentioned earlier, all the theoretical analysis of determining the maximum load-bearing capacity of the test specimens rely on the requirements and standards set by Eurocode 3: design of steel structures which promotes effective width method analysis in a CFS purlin system. Also, this research, if successful, would strengthen the role of stiffeners of a different material property than the purlin itself. So, the bending stiffness tests were run on stiffened and unstiffened profiles which contained several combinations of PU-boards and C-profile. In order to accomplish the bending stiffness test on C-profiles, the test specimens were first designed and then manufactured.

Design of the test specimens include different alternatives of using different shapes of PU-boards, attach them via chemical bonding and use them as stiffeners to the C-profiles. In Figure 16, it is shown that there are altogether four different alternatives of using PU-boards for C-profile stiffening.
Manufacture of the test specimens consisted of a careful production of designed test specimens in the laboratory under a senior supervision.

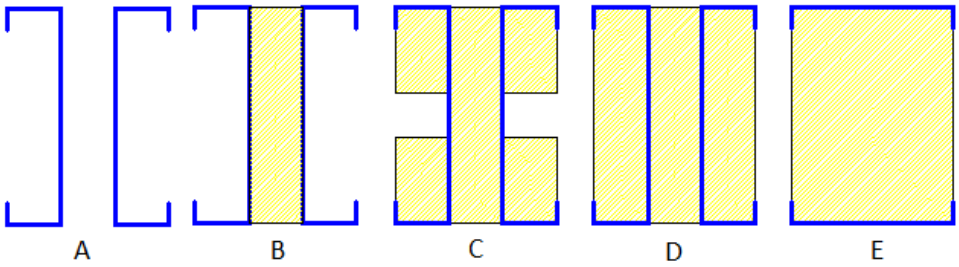

Figure 16 Various combination sketches of test series to analyze bending stiffness of the beam. Shaded parts describe PU-boards.

In Figure 16, the first four combinations A, B, C and D respectively have identical C-profile sectional properties. However, combination E consists of a different CFS profile, a slender profile consisting of a long flange and a short lip can be seen.

Combination A of the Figure 16 will be made by fastening two C-profiles mechanically. Combination B shows two C-purlins glued together on a PU-board. In combination B, profile webs are stiffened. Combination C consists of C-profiles glued together on PU-board of the same profile height as well as PU-board glued on concave part of each profile. In combination C, profile webs are stiffened and flanges are partially stiffened. Combination D shows C-profiles stiffened by PU-boards of the same profile height in between the profile and inside each profile. In combination D, profile webs are stiffened on both sides whereas flanges are stiffened,

too. Combination E consists of PU-board as wide as flange of the profile glued in between two C-purlins without lips.

Combinations illustrated in Figure 16 will be our proposed test series. By analyzing the cross-sections in Figure 16, it is easy to predict that the failure mode and buckling phenomena will be similar in combinations A, B, C and D respectively. However, Combination E will have a different action against the loading and it will provide us a different failure mode as the profile cross-section doesn't consist of a steel web but PU-boards to transfer flexural load along the beam.

3.2 Sheet-steel test materials

All the sheet-steel materials and other materials that help prepare test specimens are very commonly used in building industry and are recommended by designers and builders in Finland. The sheet-steel materials selected for the tests in this project are shown in detail in Table 1.

Table 1 illustrates the type of steel grade used in the manufacture of the cold-formed steel profiles and the standard that it is taken from. It also describes the type of coating in each sheet-steel material and the thickness of each sheet of the steel sheet. Also, the basic yield strength f_{yb} and ultimate tensile strength f_u are mentioned in Table 1. Most importantly, Table 1 describes the material type of the steel where S280 and S350 stand for structural steel of yield strengths 280 N/mm^2 and 350 N/mm^2 and Z275 means that the steel has been coated by 275g of hot dip zinc per sq. meter of the sheet. Moreover, the steel type we used, S280+Z275, has an additional epoxy coating as an ultimate surface coating. (EN 1993-1-3, 14, 2006)

Table 1 Material properties of the CFS-sheets

Type of steel	Standard	Type of Materials	Type of external layer	Thickness (mm)	f_{yb} (N/mm²)	f_u (N/mm²)
Continuous hot dip zinc coated carbon steel sheet of structural quality	EN 10326	S280+Z275	Epoxy coated	0.5mm	280	360
		S350+Z275	Zinc coated	1.0mm	350	420

From the sheet-steel materials mentioned above, the designed C-profiles were manufactured in the SMC premises. The sheets were initially cut into lengths of the perimeter of each profile. The cut sheets were bent several times by using a press brake in order to achieve the desired cross-sections without losing their material strength. The cross-sections chosen to conduct this test are illustrated in Figure 17.

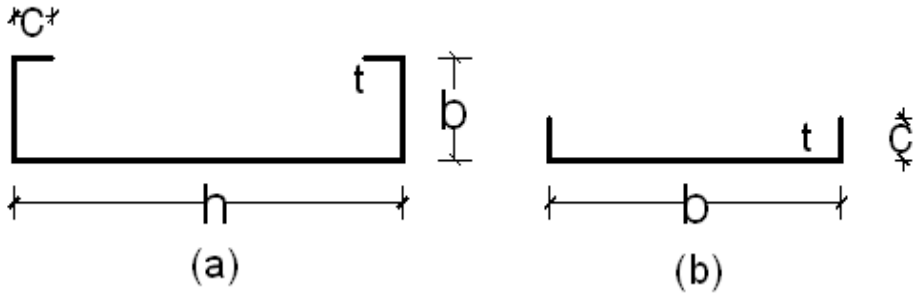

Figure 17 Cold-formed cross-sections (a) Lipped C-profile, (b) wide flange profile

In Figure 17, two typical CFS profile cross-sections used in the test are illustrated. In the Figure, h stands for the height of the profile, b for breadth, c for lip width and t for thickness, where thickness and breadth of the cross-section in this case have two variables.
Cross-sectional properties and length details of the profiles used in the tests are shown in Table 2.

Table 2 Cross-sectional properties and length details

Name of the profile	Type of material	Thickness t (mm)	Height h (mm)	Breadth b (mm)	Lip width c (mm)	Length L (mm)	Cross-section perimeter P (mm)
Lipped C-profile	S280+Z275	0.5	200	50	20	2000	340
	S350+Z275	1.0	200	50	20	2500	340
Wide flange profile	S280+Z275	0.5	-	150	20	2000	190
	S350+Z275	1.0	-	150	20	2500	190

In Table 2, the cross-section geometry of all profile cross-sections has been described. Also, the profile length of each cross-section type has been mentioned in the table. Furthermore, cross-section perimeter has been calculated which is the exact amount of sheet length to be cut to create a single CFS profile.

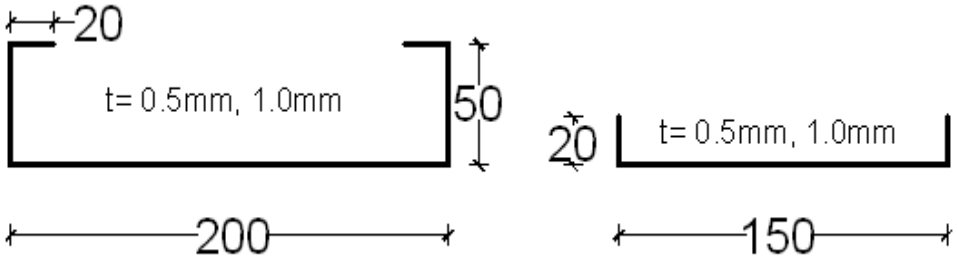

Figure 18 CFS profile with dimensions of C-profile and wide flange profile

Apart from the steel sheets that are used in the production of test specimens, several other materials were also used i.e. polyurethane boards and chemical adhesive named “Macroplast UK 8150”. Moreover, other supplementary materials were used to conduct the tests i.e. LVL boards cut into different sizes and SD3 and SD6 fasteners.

LVL strips and smaller PU-strips were used only during the test procedure. In combination A, LVL strips were fixed at each end of the profile in order to support the test beam against lateral buckling. Also, LVL strips were placed in first 2 combinations and PU-strips in combination C right under the loading points to distribute the load into the tensile region of the test beam. LVL strips and PU-strips did not contribute in the test results in any way as those materials were placed for the test to run according to plan. If these test beams are to be mass-produced, the LVL strips and PU-strips can be omitted from the manufacture process.

Figure 16 showed us the initial sketches of the combinations that were designed to be manufactured. However, during the manufacturing process, it was learnt that the manufacture of combination D in Figure 16 was impossible considering the fact that stiffeners should be able to reinforce the elements of the profile against various buckling modes which was difficult to achieve in that case. Also, the distribution of PU-board around the neutral axis of the beam doesn’t contribute in beam stiffening. So, a new set of combinations were declared which is illustrated in Figure 19.

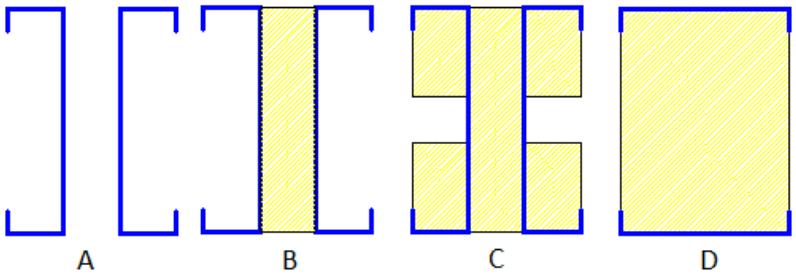

Figure 19 New set of combination for test specimen manufacture

As for PU-boards, they had to be cut in many panels of different sizes according to the combinations shown in Figure 19. A typical PU-board cross-section size used during the test specimen manufacture was 50mmx200mm. On the other hand, combination C required 50mmx80mm extra pieces as flange stiffeners. Correct sizes and their total number of boards are mentioned in Table 3. The same table was used during the cutting process of PU-boards.

The PU-boards used during the test specimen manufacture were cut from a bigger PU-panel of dimensions 1200mm x 2600mm x 50mm. The density of the PU-foam is approximately 40 kg/m^3. The thermal conductivity of the PU-foam is 0.027 W/mK. Information on the method of creating test series names is described in Table 4.

Table 3 Polyurethane board dimensions and requirements

Series name	Combination type	No. of tests	No. of 50x200 PU-board	No. of 50x80 PU-board	Total PU-sizes (Pcs)		Length of PU-board (mm)
					50x200	50x80	
S280_0,5_A_Series1	A	3	0	0	0	0	2000
S280_0,5_B_Series2	B	3	1	0	3	0	2000
S280_0,5_C_Series3	C	3	1	4	3	12	2000
S280_0,5_D_Series4	D	3	3	0	9	0	2000
S350_1,0_A_Series5	A	2	0	0	0	0	2500
S350_1,0_B_Series6	B	2	1	0	2	0	2500
S350_1,0_C_Series7	C	2	1	4	2	8	2500
S350_1,0_D_Series8	D	2	3	0	6	0	2500
TOTAL					25	20	

It was determined that 3 tests per series should be conducted. So there were 8 different series that was dependent on sheet-steel material thicknesses and 3 test specimens in each series making the total number of test specimens 24. However, due to limited time and resources, only 2 tests were conducted in the latter half of the test series.

Each test series were named in the following manner.
[Specimen material]_[material thickness]_[Combination type]_[number of series]

So the names of all series are mentioned in Table 4. Similarly, the average weight of the test beam of each series is also shown in the table. Individual weights of each test beam are described in Table 6.

Table 4 Nomenclature of test series

Material Type (...+Z275)	Material thickness (mm)	Average weight of each beam (kg/m)	Number of test series	Stiffener details	Test series name
S280	0,5	2.83	Series 1	Not stiffened	S280_0,5_A_Series1
S280	0,5	3.48	Series 2	Webs fully stiffened	S280_0,5_B_Series2
S280	0,5	4.05	Series 3	Webs and flanges stiffened	S280_0,5_C_Series3
S280	0,5	2.98	Series 4	Flanges fully stiffened	S280_0,5_D_Series4
S350	1,0	6.42	Series 5	Not stiffened	S350_1,0_A_Series5
S350	1,0	7.08	Series 6	Webs fully stiffened	S350_1,0_B_Series6
S350	1,0	7.20	Series 7	Webs and flanges stiffened	S350_1,0_C_Series7
S350	1,0	4.32	Series 8	Flanges fully stiffened	S350_1,0_D_Series8

3.3 Test specimen design and test specimen manufacture

The cold-formed C-profiles used to conduct bending stiffness test on the PU-stiffened beams were designed completely based on Eurocode “Design of steel structures, 2006”. During the manufacture of the C-profiles, factors like minimum requirements for rounded corners, geometric proportions (width-to-thickness ratio), structural modeling, flange curling ratios etc. were considered according to EN1993-1-3: 2006. The radius of rounded corners in the profile 2mm was less than five times the thickness of the profile so it has not been included in Table 2 along with other dimensions of the profile. The maximum width-to-thickness ratio for the elements of the cross section is mentioned in Figure 20. (EN 1993-1-3, 2006, 21)

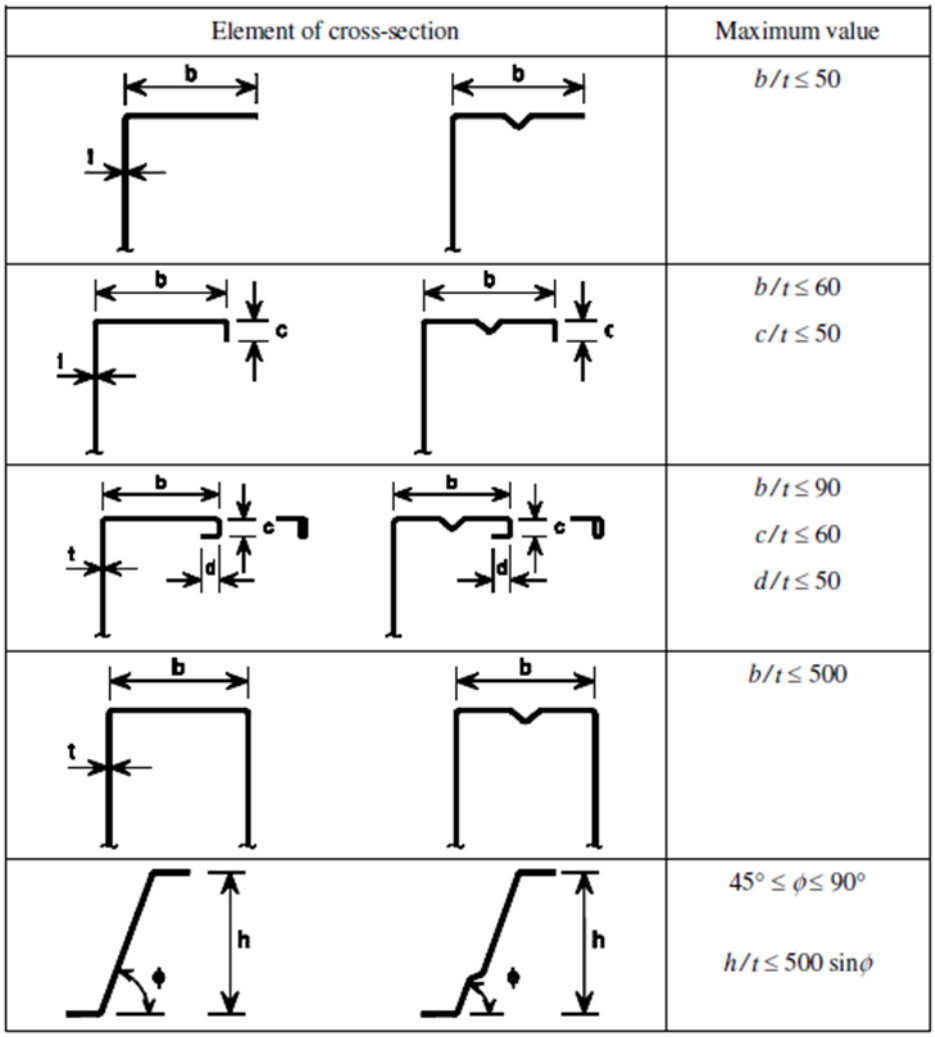

Figure 20 Maximum width-to-thickness ratios (EN 1993-1-3: 2006, 21)

For test specimen manufacture, we will be focusing on the preparation of test specimens of different test series. The main procedure to manufacture the test specimens of each series is based on glueing PU-board to each sides of C-profile with high performance glue. The only use of LVL strips in test series 1 and 5 respectively was to hold two C-profiles at a distance of 50 mm so as to avoid unwanted lateral movements and slip failure of the beam. Introduction of vertical LVL strips on the support ends and under the loading points was to reinforce the beam against uniaxial lateral buckling which is explained in test specimen S280_0,5_Series1_1 in chapter 4.

Manufacture of all the test specimens of this study were conducted in the premises of SMC. The manufacture process was completed in various phases namely,

- Cutting of sheet metal of designed material strength
- Press braking of cut sheet metal into desired cross-sections
- Cutting of PU-boards in sizes mentioned in Table 3 and thorough cleaning
- Careful cleaning of profile surfaces where glue is to be applied on

- Careful and quick glueing of PU-board to C-profile surface as glueing period of the glue after mixing the two components (glueing agent and hardening agent) is roughly 2 minutes.
- Caution and precision while attaching two components of the test specimen (PU-panel and C-profile) without any error and fixing them together with available weights and jack-screws
- After the drying of glue, a careful visual inspection of the distribution of glue in the specimen and possibly repairing of the specimen if found any flaw

Some of the pictures concerning the manufacture of the test specimens are illustrated in Figures 21 and 22 respectively. The information about the glue used during the test specimen manufacture process can be found in Appendix 3.

Figure 21 Manufacturing of a test specimen

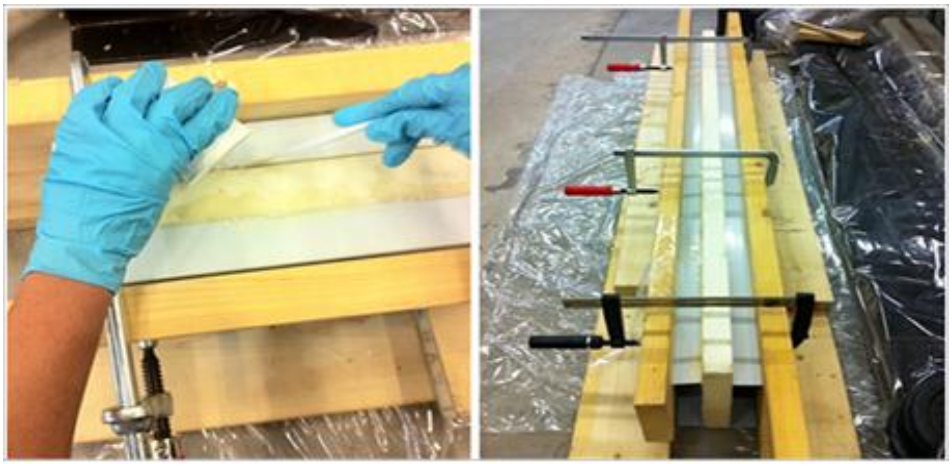

Figure 22 Glueing PU-panel to the profile and use of jack screws to get higher bonding strength between PU-panel and C-profile

3.4 Test arrangement

3.4.1 Test rig design

This experimental program consists of total 20 tests divided into 8 different test series where series consisting sheet-steel material S280 had 3 tests in each series whereas S350 series had 2 tests in each of its series. All the tests were conducted in SMC premises under the close supervision of senior advisors.

The test loading frame that was used in the tests was made in SMC whereas the loading cylinder for the test was manufactured by a German company Instron Structural Testing Systems (IST). IST is a global supplier whose testing devices are used in e.g. automotive industry, universities and R&D centers.

The test loading frame consists of two separate systems, with hydraulic cylinders of maximum loading capacities of 150 kN and 250 kN respectively. These hydraulic cylinders can be used separately as well as at the same time by positioning the cylinders depending on the aim of the test to be done. The control system of the cylinders allows programming for test-specific timed loadings, for controlling the speed of the loading, and for controlling the loading so that the tested member reaches the desired displacement and displacement rate at the specific point. Different parametric values obtained from the tests are saved automatically onto a computer in a user friendly format. (HAMK, 2011)

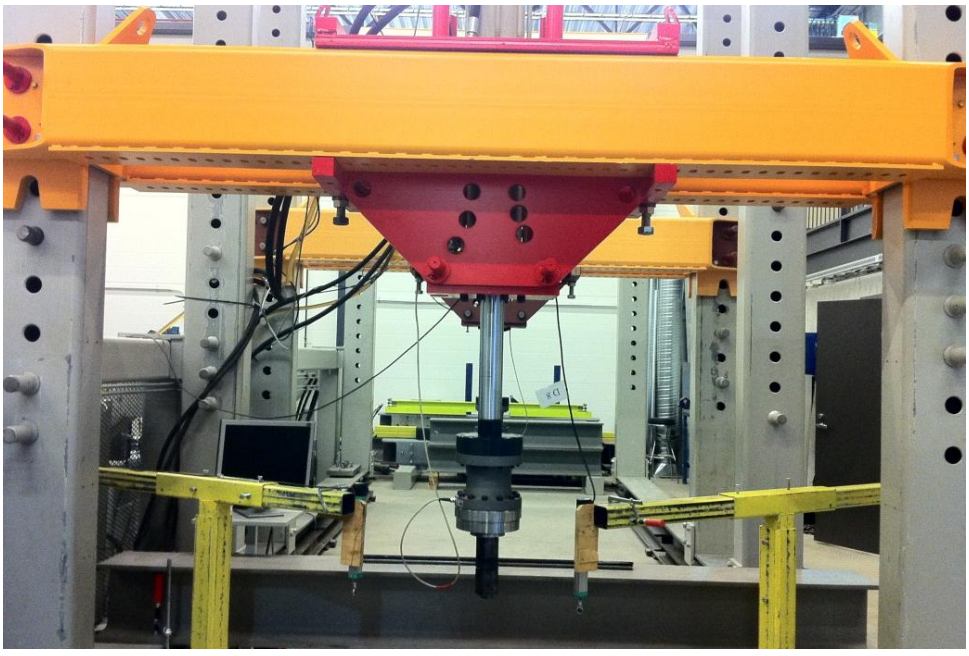

Figure 23 Instron hydraulic cylinder in the test loading frame

The test loading frame for this research, however, consists of a single hydraulic cylinder with the maximum loading capacity of 250 kN.

3.4.2 Test loading

Test rig design was based on a four point bending setup. This setup consists of a member set between two supports, two point loads acting on the member between the supports separated by some distance. As the member is loaded under these basic support conditions, a uniform bending moment diagram can be seen between the loading points as shown in Figure 24. Like in Figure 24, this test setup provides a central region of uniform bending moment and zero shear force. This means that the only possible failure mode of the beam is bending failure if all small defects are rectified and no lateral movement of the beam is allowed. If the beam experiences only bending failure, it gives us a pure data on the bending moment resistance of the beam which can be manipulated into bending stiffness and other relative resistances of the beam. By this, we can find the bending stiffness of each test specimen and analyze stiffness ratios of different test series including each test specimen.

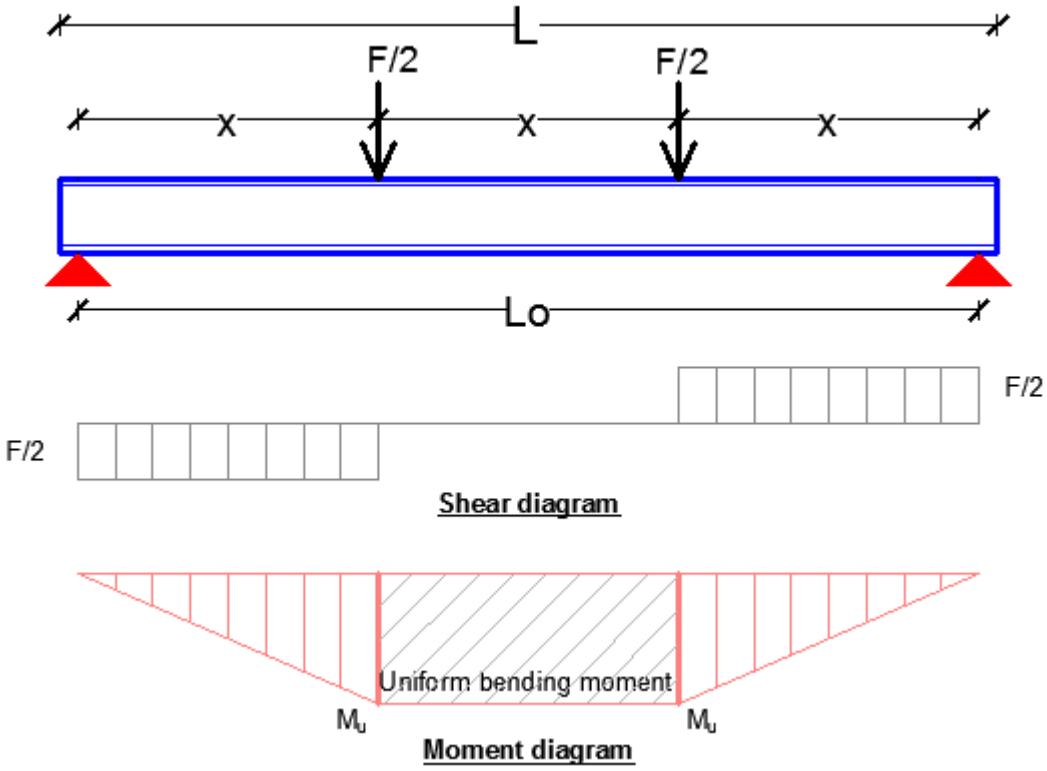

Figure 24 Four point bending setup

3.4.3 Test setup

The diagram illustrating a basic test setup for all the tests is shown in Figure 25. Figure 26 and Figure 27 describe test setups for sheet-steel material S280 and S350 respectively. The only difference between two test setups is the length of the test specimen. Test specimens of material strength S280 is 2000 mm long whereas S350 is 2500 mm long.

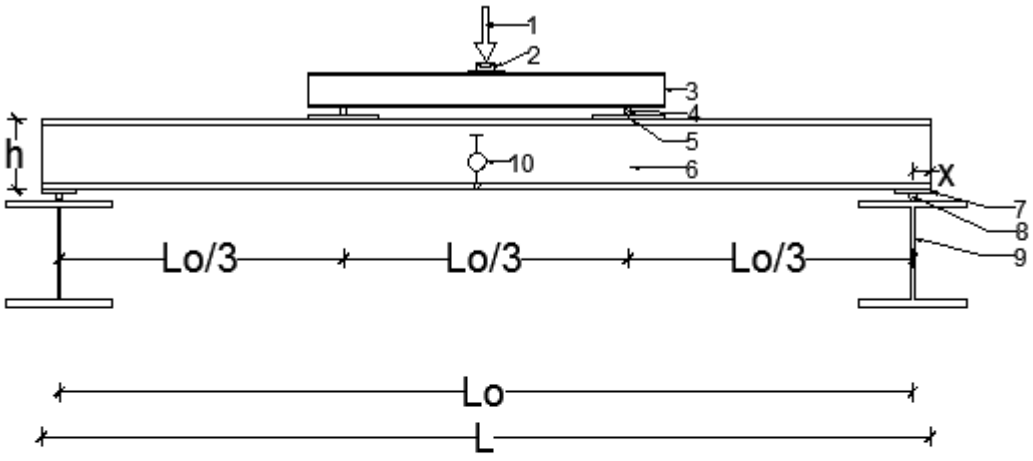

1. LOADING RAM
2. CIRCULAR PLATE WITH SPHERICAL PLAIN BEARING
3. IPE BEAM OF HEIGHT 100 mm
4. CYLINDRICAL STEEL ROD OF DIAMETER 20 mm
5. BEARING STEEL PLATE OF THICKNESS 10 mm
6. TEST SPECIMEN OF HEIGHT 200 mm
7. BEARING STEEL PLATE OF THICKNESS 10 mm
8. CYLINDRICAL STEEL ROD OF DIAMETER 20 mm
9. HOT ROLLED I BEAM AS A SOLID SUBSTRATE TO CONDUCT THE TEST
10. DEFLECTION SENSORS ON EACH SIDE OF THE TESTING BEAM

Figure 25 Basic test setup with numbering of all involved parts and devices during the test

In Figure 25, a test specimen/beam of height "h" and length "L" is loaded under two point loads. Adjacent distances between load-to-load and load-to-support is quarter the length of beam span L_0. Total length of the beam is L.

All the test specimens were tested in a similar testing environment and testing conditions. Hot rolled I beams were placed according to the beam span to create a solid substrate to conduct the tests. Positioning made a very crucial point during the test as the test specimen under the loading point must be geometrically accurate in both directions. Above the two I-beams came steel plate of thickness 10mm and a steel rod of diameter 20 mm on each side with the steel plate resting on a steel rod at symmetry. The test specimen rested over the steel plate at each end in such a manner that the actual loading span of the test specimen or the support-to-support distance is 100 mm less than the actual length of the specimen. The reduced 100 mm of the specimen, 50 mm on each side, was because the steel bar lied in the middle of the steel plate. Two pairs of steel bars of diameter 20 mm and a steel plate of thickness 10 mm lie on the specimen separated by a quarter of the length of the test beam span L_0. This time the steel plate is placed below the steel rod to prevent bearing failure of the upper flanges of the profiles of the test specimen. A small IPE beam was introduced over the steel plate and steel rod to transfer the load from the cylindrical loading ram into two point loads acting equidistant from each support points on the test specimen. A circular device of thickness 20 mm was put under the loading ram. This circular plate has an elliptical groove

where another plate with a spherical shape plate that moves freely within the groove. The purpose of this plate is to distribute the load from the loading ram onto the beam uniformly.

Also, two metal strips of dimensions 50mm x 150 mm were attached onto each test specimen in order to place the deflection sensors on each side of the testing beam to calculate the overall deflection of the beam.

On top of the test setup, there is a hydraulic cylinder that provides the maximum loading force of 250 kN connected to a cylindrical loading ram that has a spherical head. Parts that were used in the test arrangement are mentioned in the list below with respect to their numbering order.

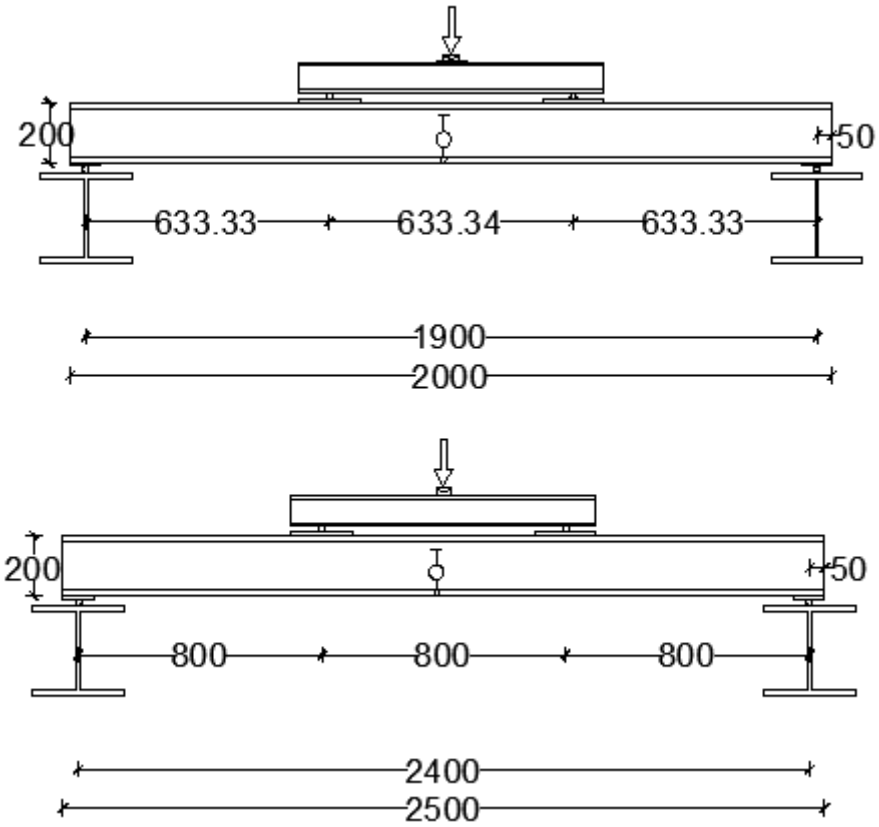

Figure 26 Test setup for (a) S280 series; (b) S350 series

Test setup for all of the test series (see table 4) is shown in Figure 26. Figure 27 below, shows us how the schematic drawings of the test setup for the series of two different cold-formed steel material types has been implemented in the test.

Figure 27 Test setup for all test series in SMC test hall

4 TEST RESULTS, EVALUATION AND COMPARISON OF TEST DATA

4.1 Failure modes

The main failure modes for most of the test specimens were combined flange and web buckling. Compressive flanges of the profiles buckled locally whereas the webs also failed locally. Some other failure modes that occurred in the test specimens were local flange buckling, lateral buckling of test beams and shear failure of PU-boards.

4.1.1 Combined flange and web buckling

Combined flange and web buckling was the common failure mode that occurred in most of the test specimens. In this failure mode, flanges of the compressive zone of the test specimen went under local buckling as ripples of short wave-length appeared in the upper flange surface. As the loading increased, webs also started to buckle locally. As the loading increases, C-profiles of the test specimen go through distortional buckling and overall buckling respectively. As compressive stresses on the upper flanges of the profiles increase, flanges start deforming as flanges start curling due to immense compressive stresses that arise in the uniform bending region/ between two loading points. During flange curling, webs of the profiles in that region also deformed. This occurred in the case of C-profiles unstiffened with PU-boards.

In case of PU-stiffened C-profiles, the situation was fairly different. In the presence of PU-boards as longitudinal stiffeners in the beam, members of the profile under compressive stress, underwent local buckling slowly or resisted higher load to deform locally than in case of unstiffened profiles. Test specimens consisting web stiffeners and flange stiffeners were capable to take more load as the stiffeners embedded in the profiles reduced/prevented early buckling of the plane parts of the profile.

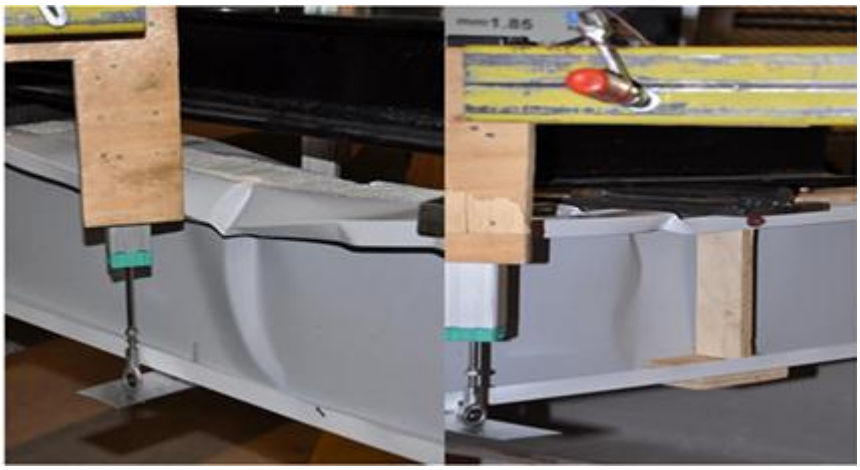

Figure 28 Combined flange and web buckling

4.1.2 Lateral buckling

Lateral buckling occurred in the unstiffened and in slender test specimens. Test specimen from each test series 1 and 5 underwent this failure as unstiffened members were unable to stabilize themselves laterally as the beam swayed towards the weaker axis. Although reinforcing the test specimens after observing the first test specimen of test series 1 undergoing lateral buckling failure, one of the test beams of test series 5 still failed in this phenomenon. However, the load resistance of test series 5-specimen was high because of its high sheet-steel material strength.

Figure 29 Lateral buckling of the test beam

In test series 1, test specimen 1, due to the profile members being very slender, C-profiles deformed laterally against a very small load. Hence, it was decided that LVL (Plywood) strips will be used, at both sides/profiles at each support points and at each loading points. This implementation proved to be worthy as other two test specimens gave a remarkably high load resistance. Similarly, the same method was used in combination B to laterally reinforce the C-profiles against lateral buckling. LVL strips were introduced in test series 1, 2, 5 and 6. Test series 3 and test series 7 had an extra PU-boards supporting flanges on each side of C-profiles connected by small PU-strips on the support points and under the loading points to simulate the contribution of LVL strips in test series 1, 2, 5 and 6.

4.1.3 Local flange buckling

Local flange buckling was observed in test series 4 test specimens. Test specimens consisting slender wide flange profiles stiffened with PU-boards of the same flange width failed under this buckling mode as compressive stress in the upper wide flange purlin was very high. As the loading was increased, region of flanges near the loading points deformed permanently creating a curl of material in the compressed flange.

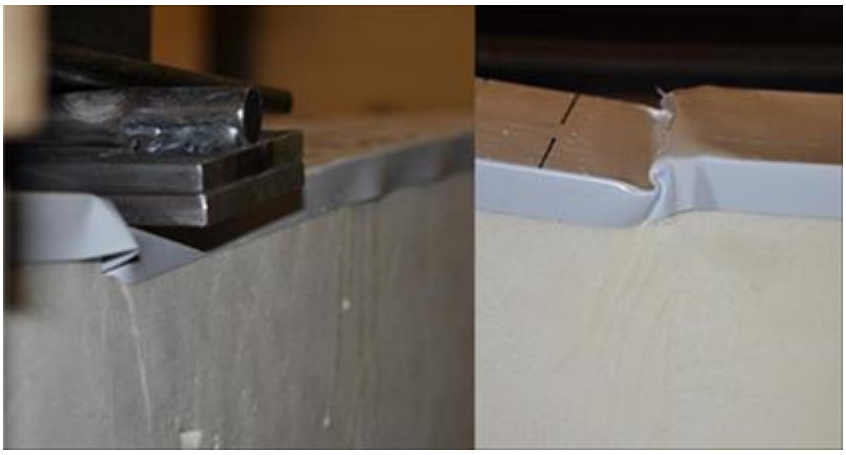

Figure 30 Local flange buckling of wide flange profile

4.1.4 Shear failure of polyurethane boards

Shear failure of PU-board was observed in test series 8 as PU-stiffeners failed in pure shear stresses. The reason that this phenomenon didn't occur in test series 4 was because of the material strength of the C-profile used in that series. In test series 4, profiles of material strength 280N/mm^2 were used whereas in test series 8, 350N/mm^2 material profiles were used. In test series 4, the compressive stress that appeared in the compressive zone of the upper wide flange profile was more than the bending stresses generated in the PU-board. Hence, the wide flange profile cross-section reached its yield point faster than PU-board reaching its critical bending stress. On the other hand, in test series 8, the strength of the C-profile was 350N/mm^2 which means that the profile could withstand more compressive stress due to bending. But the bending stiffness of PU-boards was not high enough to withstand the bending stress in the test beam. As a result, bending stiffness of PU-boards reached its limit before the profiles reached their yield point and eventually the test specimens failed due to high shear stresses in the PU-board. The angle made by the crack due to the shear failure of PU-stiffener was between 40° to 55° as it can be clearly observed in Figure 31.

Figure 31 Shear failure of the PU-board in test series 8

4.2 Analysis of the test results

Table 4 shows us the test results obtained from the tests conducted for each test series. Failure modes for each test specimen have also been described in the table. As we can see in the table, the major failure mode in the whole test was combined flange and web buckling. Average load has been calculated making it easier to compare the load resistance of each series containing the same sheet-steel material for the specimen. However, test series 4 will compared to test series 8 as both test series contain the same profile cross-section despite their varying thickness and material properties. Also, standard deviation for each test series has also been calculated to know the extent of the fluctuation of test value from its average result.

Table 5 Test results of the conducted test

Name of the series	Specimen no.	Force (kN)	Failure mode	Average (kN)	Std. Deviation (kN)
S280_0,5_A_Series1	1	0,92 [1]	Lateral buckling	5,81	0,94
	2	6,47	Flange+web buckling		
	3	5,14	Flange+web buckling		
S280_0,5_B_Series2	1	10,38	Flange+web buckling	10,31	0,70
	2	9,58	Flange+web buckling		
	3	10,97	Flange+web buckling		
S280_0,5_C_Series3	1	12,71	Flange+web buckling	11,73	1,42
	2	10,1	Flange+web buckling		
	3	12,39	Flange+web buckling		
S280_0,5_D_Series4	1	4,96	Local Buckling	5,04	0,14
	2	4,97	Local Buckling		
	3	5,2	Local Buckling		
S350_1,0_A_Series5	1	15,98	Lateral buckling	18,89	4,12
	2	21,8	Lateral+member buckling		
S350_1,0_B_Series6	1	26,1	Flange+web buckling	26,08	0,03
	2	26,06	Flange+web buckling		
S350_1,0_C_Series7	1	27,1	Flange buckling	27,94	1,19
	2	28,78	Flange buckling		
S350_1,0_D_Series8	1	4,27	Shear failure of PU	5,62	1,90
	2	6,96	Shear failure of PU		

1 This value of ultimate load for the first specimen of S280_0,5_Series1 was not taken into consideration as the test on the specimen did not provide any bending stiffness values due to predominant lateral buckling failure of the beam.

The average ultimate load provided by various combinations/beam types of two different sheet-steel material types have been compared graphically in Figure 32. Also, the average ultimate load capacities have been expressed in percentage ratio and can be observed in Figure 33.

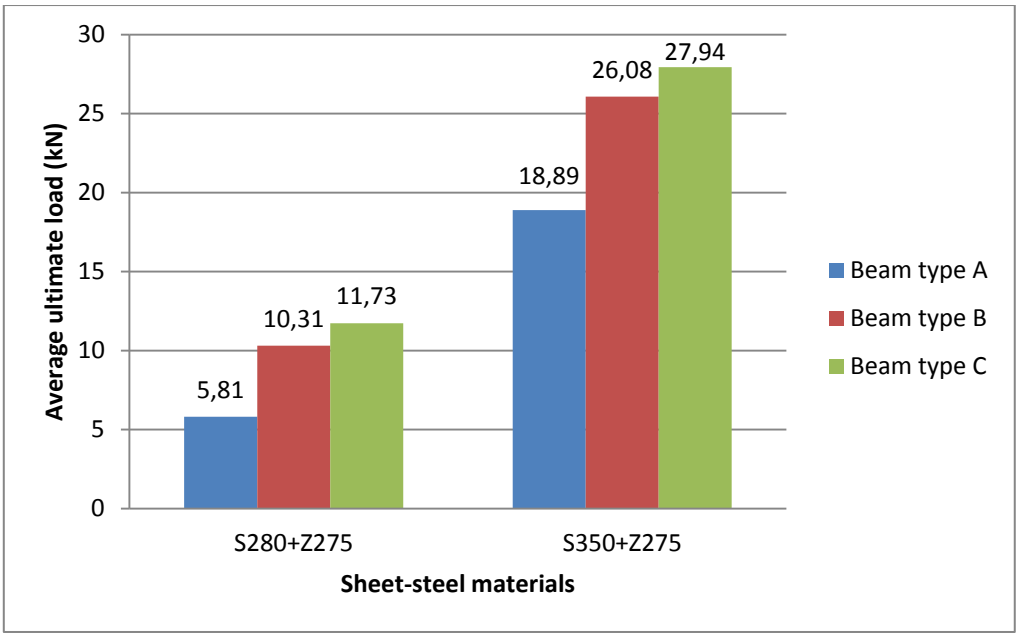

Figure 32 Average load capacities of three beam types of two different steel grades

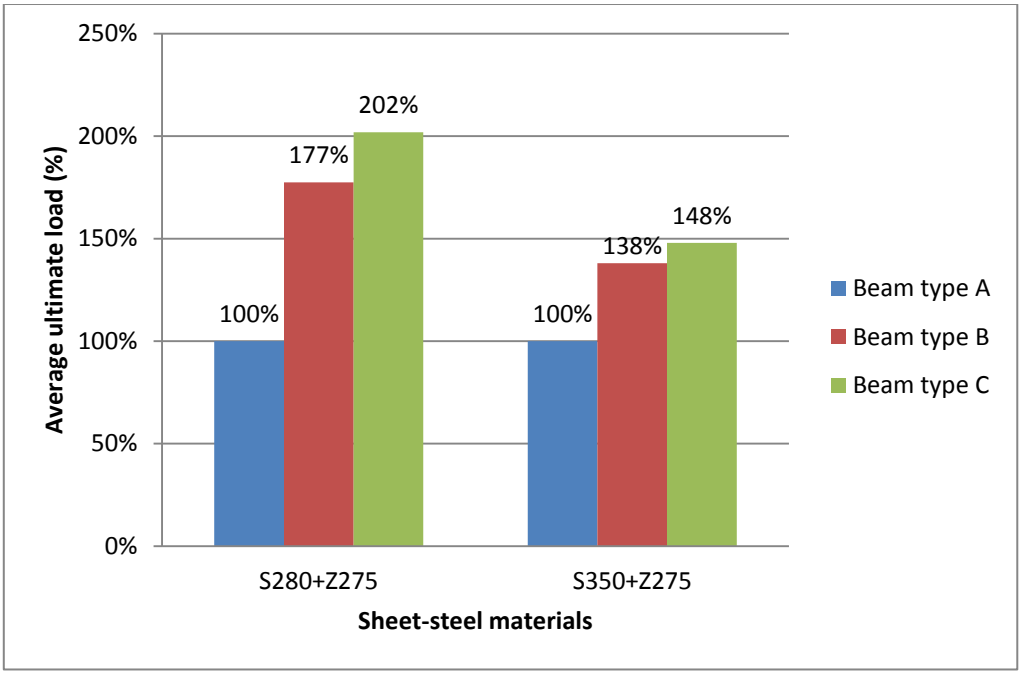

Figure 33 Percentage ratio of load resistances of beam types A, B and C with two different steel grades

The average ultimate load of test series-Series1 was 5,81 kN. Similarly, for test series 2, the average ultimate load resistance was 10,31 kN which is 77% more than that of test series1. For test series 3, the average ultimate load was 11,73 kN which is 102% more compared to test series 1. Furthermore, in test series S350, test series 5 could bear average maximum of 18,89 kN of load. On the other hand, average ultimate load capacity of test series 6 was 26,08 kN which is 38% more compared to test series 5. Test series 7 could resist 48% more load (27,94 kN) compared to the load of test series 5.

The gradual increase of both ultimate load of the beam as well as the slope of the graph of each specimen can be observed as we move from beam-type A to C in each sheet-steel material type. As we move from beam-type A to C, the amount of PU-stiffeners in a test beam also increases. It means that the PU-boards present in each PU-stiffened beam were able to function as longitudinal stiffeners. The PU-boards used in stiffening the profile reduced/prevented buckling phenomena of the beam and provided an extra stiffness to the beam. This stiffening of C-purlins provided by PU-boards is thoroughly shown below.

Failure modes rather remained the same (combined flange and web buckling) among the test conducted specimens. However, lateral and member buckling failure was observed in S350_1,0_A_Series5 specimens.

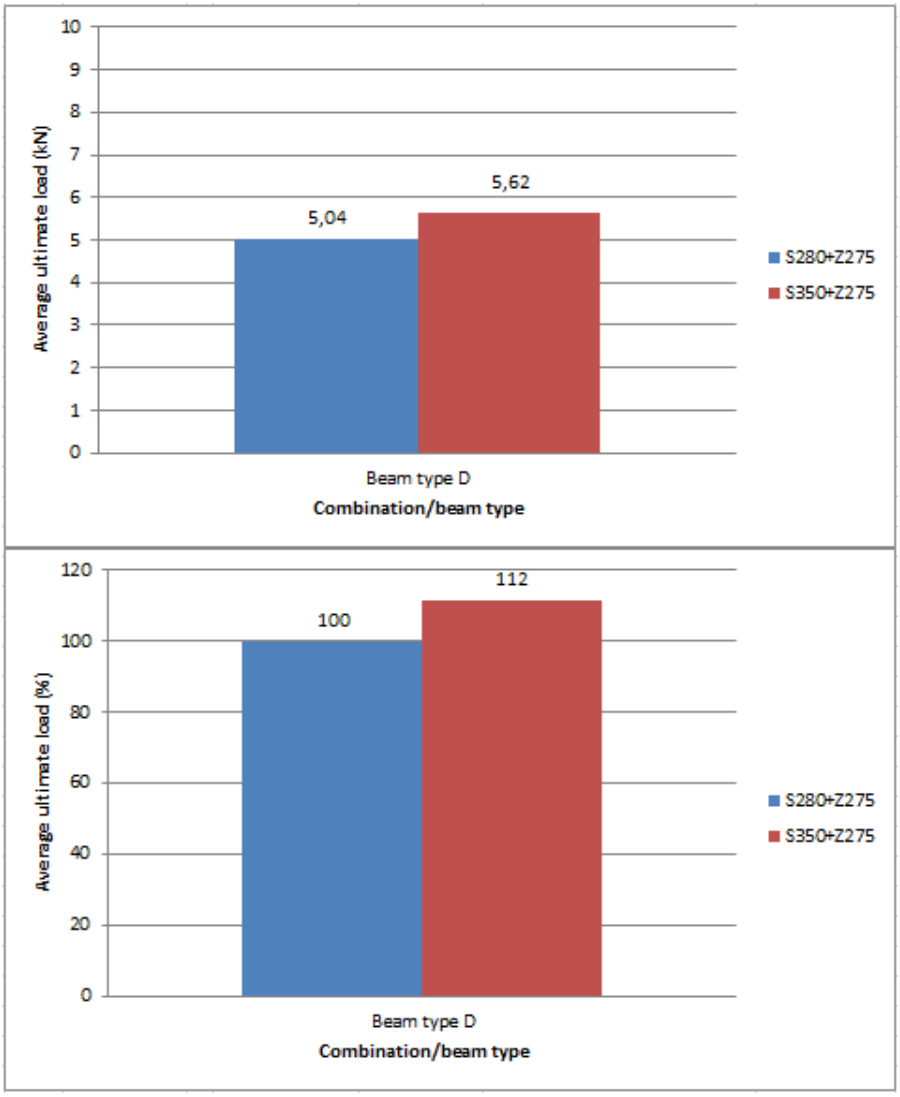

Figure 34 Avg. ultimate load of beam type D for both sheet-steel materials

Figure 34 illustrates the average load bearing capacities of beam-type D for both C-profile types. As shown in the figure, S350_1,0_D_Series8 has 12% more load bearing resistance than that of test series 4.

Figure 35 below represents graphs of test series 1, 2, and 3 consisting of the same sheet-steel material S280+Z275 and of combination A, B and C. In the figure, we can see the graphical representation of the load vs. displacement graph of each test specimen of each S280 test series.

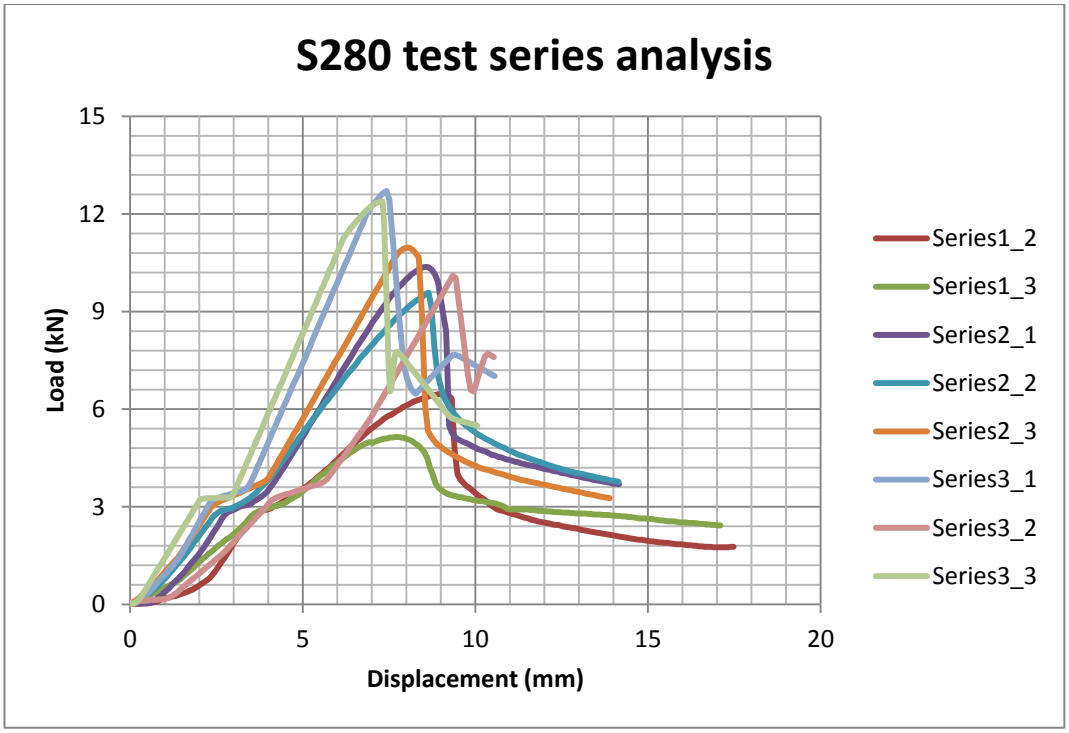

Figure 35 Test result analysis of the specimens of test series 1, 2 and 3 respectively

From the Figure, we can see that each test series has its unique slope of load against displacement curve. Although the load vs. displacement curve for each test specimen is unique, the graphs look similar when compared with the test specimens within a test series. This concludes that each test series has its own nature of the graph and failure mode or each test series have a specific slope of the curve which mathematically represents the bending stiffness of the beam of that particular test series.

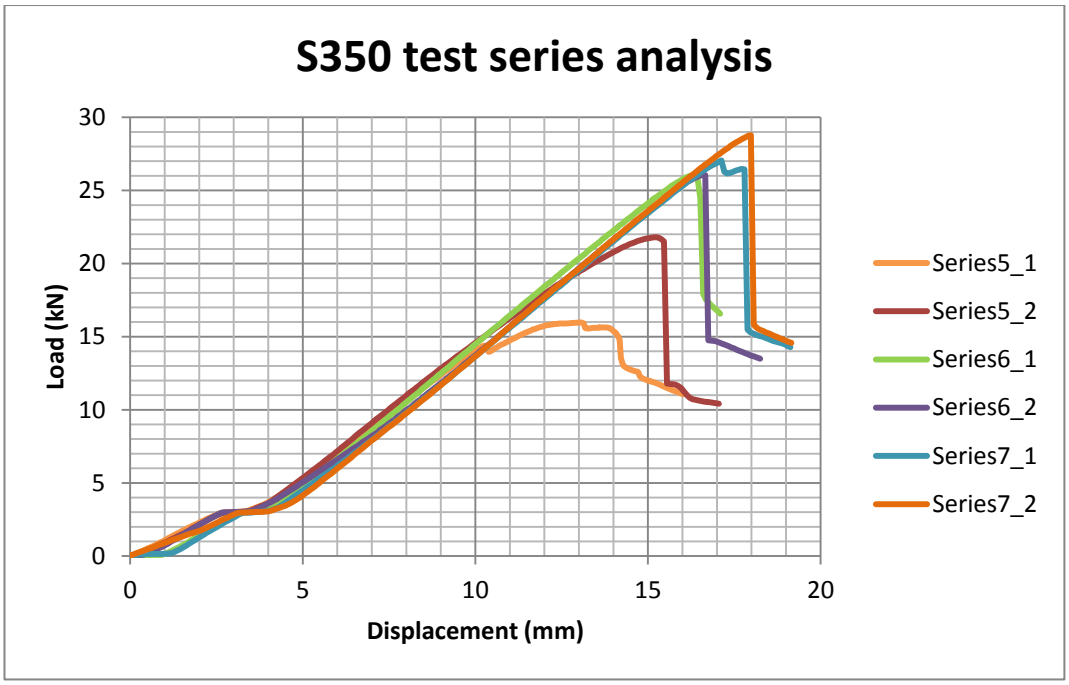

Figure 36 Test result analysis of the specimens of test series 5, 6 and 7 respectively

Similarly, Figure 36 exhibits the graphical representation of test series 5, 6 and 7 consisting of C-profiles of material S350+Z275. Although it seems that the introduction of PU-boards has increased the load-resistance of the beams exceptionally, the bending stiffness of the test specimens of the test series S350 does not seem to change in the same manner. The slope created by the graph of each test specimen looks almost identical.

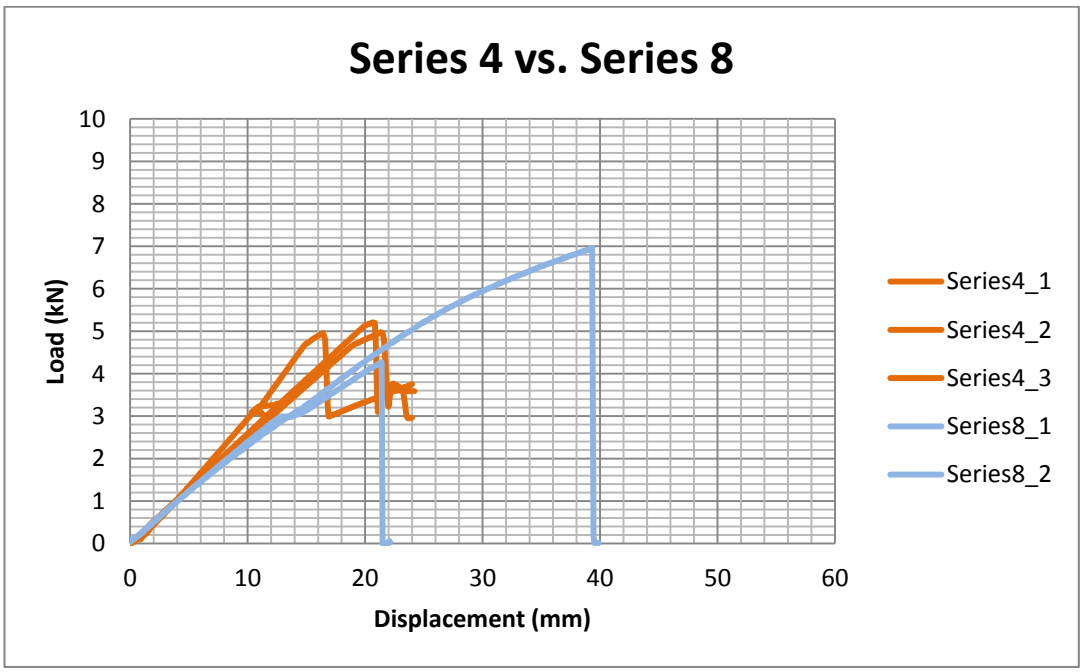

Figure 37 Test result analysis of the specimens of test series 4 and 8 respectively

However, Figure 37 comprises a different pattern than in Figures 35 and 36. From the slope angle of each test series in Figure 37, it can be observed that test series 4 specimens are relatively stiffer in comparison to

the specimens from test series 8. Also, the failure modes for the two of these test series were completely different. Test series 4 failed in local flange buckling whereas test series failed under pure shear failure of PU-boards. This happened, because, in case of test series 4, the PU-boards were able to stiffen the compressed flange of the upper wide-flange profiles against local buckling. However, in case of test series 8, the shear failure of the PU-boards of the test beam was because of the development of critical shear stresses in the PU-board. Shear stress in the PU-board was higher than any critical buckling stresses arising on the wide-flange profile as no buckling phenomena was observed during test series 8 loading. The shear resistance of the PU-board was much less compared to the buckling resistance of the compressed flange of the profile in test series 8. As the shear stresses became immense in the PU-board, it failed ultimately in shear even before the compressed profiles started showing any of the buckling modes.

As for the implementation of the test results to determine the bending stiffness of each test series, an equation is introduced to determine the deflection in case of a simply supported beam loaded by two equal concentrated loads symmetrically placed between the supports.

For a simple beam with two equally concentrated loads symmetrically placed between the two loading points and the support points, the deflection created by the force on that beam is given by,

$$\delta = \frac{F*a}{24*(E*I)}(3l^2 - 4a^2) \qquad (1)$$

where,

F	maximum force taken by the test beam before failing
a	distance between the loading point and support
l	span of the test beam

However, equation 1 applies in cases only when the bending stress caused by the applied load lies within the linear elastic region of the load vs. displacement graph. There are some linear parts of the graph that represent the bending stiffness of the beam. Hence, an imaginary tangent line can be drawn on the linear elastic region (approximately around 10% to 30% of the ultimate load of the beam) of the graph that will represent the tangent bending stiffness of the beam. Also, a straight line can be drawn between the origin and ultimate load point creating another sloped line known as "secant bending stiffness" of the beam. These two lines represent two different bending stiffnesses of the same beam. Tangent bending stiffness of slope α is greater in value compared to the secant bending stiffness that has β as inclination angle.

The statements made above can be verified in Figure 38. The figure also shows how the deflection/displacement created in the beam can be fluctuated by the load applied to the beam. However, Figure 38 only demonstrates the nature of the graph and each test specimen may have its own graphical representation of its unique nature.

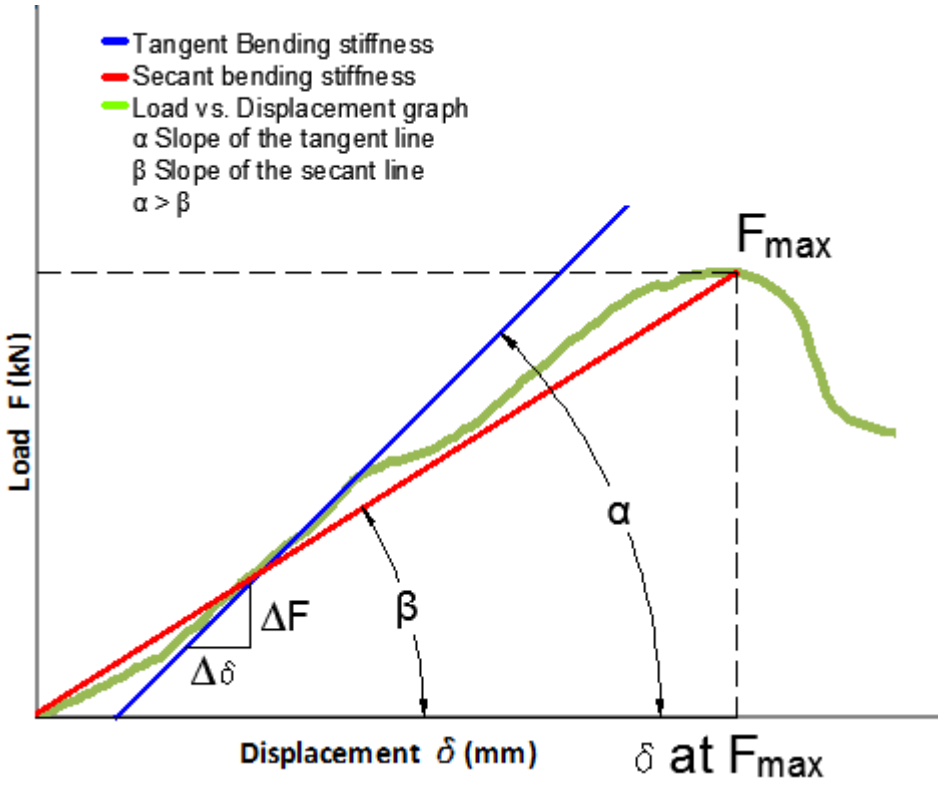

Figure 38 Load vs. displacement graph of a test beam showing tangent and secant bending stiffness of slopes α and β respectively.

In Figure 38, a normal test graph made on one of the given test specimen has been shown. A tangent line has been drawn in the graph that contains predominant linear nature of the graph. Symbols namely ΔF and $\Delta\delta$ represent small increments of load and displacement respectively on the elastic region of the graph. The slope of the inclined line drawn in the graph is α, which will be a key factor in determining the tangent bending stiffness of test specimens.

As we can see in the figure, the first linear region of the graph which represents high deflection in lesser load is due to the initial looseness and transverse flexibility of the beam. The slope of this region is not the same as the tangent bending stiffness of the beam and so is not considered during analysis. As the loading is introduced, the test beam gradually becomes stable against transverse actions and looseness. As a result, the test beam starts showing the correct stiffness of itself through the graph which is the tangent bending stiffness of that test beam.

So, equation 1 can be changed into,

$$\Delta\delta = \frac{\Delta F * a}{24 * (E * I)} * (3l^2 - 4a^2) \qquad (2)$$

In our case, the total span of the test beam was thrice the distance between loading point and support. So, the equation 2 can be changed into,

$$(E.I) = \frac{23*\Delta F*a^3}{24*\Delta\delta} \quad (3)$$

So, the bending stiffness of the test beam depends on the small change of load in the beam as the small change in loading changes the deflection of the beam under loading by a small amount. So equation 2 can further be modified into,

$$(E.I) = \frac{23*a^3}{24} * (\frac{\Delta F}{\Delta\delta}) \quad (4)$$

Since the first ratio of equation 3 being a constant, bending stiffness of any test beam in this project purely depends on the load-displacement ratio. Using equation 3, we can find both tangent bending stiffness and secant bending stiffness of each test specimen. When calculating secant bending stiffness of a test beam, the slope of the secant line is calculated. The angle made by the secant line is $\tan\beta$ whereas $\tan\alpha$ is calculated in case of the determination of tangent bending stiffness of a test beam. The individual tangent bending stiffness values of test specimens and average of each test series are compiled in Table 6.

Table 6 Tangent bending stiffness of the test specimens

Name of the series	Specimen no.	Loading distance a(mm)	Slope of the tangent line ($\tan\alpha$)	*Tan E.I. (kNm²)*	Average *Tan E.I.* (kNm²)
S280_0,5_A_Series1	1	633,33	-	-	324,64
	2	633,33	1,75	426,03	
	3	633,33	0,92	223,24	
S280_0,5_B_Series2	1	633,33	1,33	323,79	333,52
	2	633,33	1,35	328,66	
	3	633,33	1,43	348,13	
S280_0,5_C_Series3	1	633,33	1,67	406,56	359,49
	2	633,33	0,97	236,14	
	3	633,33	1,79	435,77	
S280_0,5_D_Series4	1	633,33	0,32	77,90	67,35
	2	633,33	0,25	60,86	
	3	633,33	0,26	63,30	
S350_1,0_A_Series5	1	800	1,69	829,23	829,23
	2	800	1,69	829,23	
S350_1,0_B_Series6	1	800	1,67	819,41	819,41
	2	800	1,67	819,41	
S350_1,0_C_Series7	1	800	1,67	819,41	900,37
	2	800	2,00	981,33	
S350_1,0_D_Series8	1	800	0,22	107,95	112,85
	2	800	0,24	117,76	

Also, the secant bending stiffness of the test specimens are mentioned in Table 7. Later, the two bending stiffness values are compared with one another.

Table 7 Secant bending stiffness of the test specimens

Name of the series	Specimen no.	Loading distance a(mm)	Max. load F (kN)	Displacement at max. Load δ (mm)	Slope of the secant line (tanβ)	*Sec E.I. (kNm²)*	Average *Sec E.I.* (kNm²)
S280_0,5_A_Series1	1	633,33	0,92	43,52	-	-	167,46
	2	633,33	6,47	9,07	0,71	173,66	
	3	633,33	5,14	7,76	0,66	161,25	
S280_0,5_B_Series2	1	633,33	10,38	8,57	1,21	294,87	295,78
	2	633,33	9,58	8,64	1,11	269,93	
	3	633,33	10,97	8,28	1,32	322,54	
S280_0,5_C_Series3	1	633,33	12,71	7,42	1,71	417,01	364,77
	2	633,33	10,1	9,35	1,08	262,98	
	3	633,33	12,39	7,28	1,70	414,33	
S280_0,5_D_Series4	1	633,33	4,96	16,33	0,30	73,94	63,93
	2	633,33	4,97	21,36	0,23	56,65	
	3	633,33	5,2	20,68	0,25	61,22	
S350_1,0_A_Series5	1	800	15,98	13,06	1,22	600,37	653,91
	2	800	21,8	15,12	1,44	707,44	
S350_1,0_B_Series6	1	800	26,1	16,3	1,60	785,67	778,44
	2	800	26,06	16,58	1,57	771,22	
S350_1,0_C_Series7	1	800	27,1	17,1	1,58	777,61	781,50
	2	800	28,78	17,98	1,60	785,39	
S350_1,0_D_Series8	1	800	4,27	21,41	0,20	97,86	92,34
	2	800	6,96	39,33	0,18	86,83	

Comparison of tangent bending stiffness of test series 1, 2, 3 of sheet-steel type S280+Z275 and 5, 6, 7 of sheet-steel type S350+Z275 are presented as graphical representation in Figure 39. In the figure, percentage comparison of tangent bending stiffness has also been made in order to determine the most effective combination of C-profile and PU-stiffener.

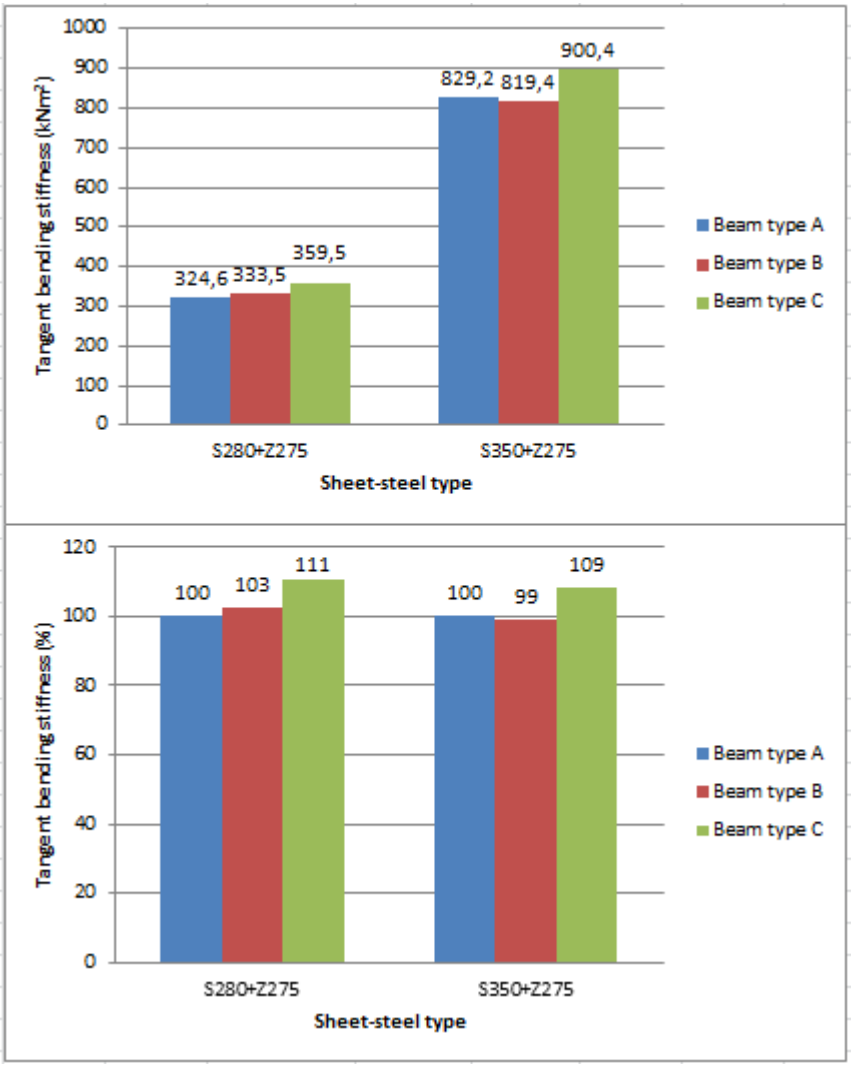

Figure 39 Comparison of tangent bending stiffness of beam types A, B and C of each sheet-steel type.

Similarly, comparison of secant bending stiffness of test series 1, 2, 3 of sheet-steel type S280+Z275 and 5, 6, 7 of sheet-steel type S350+Z275 are presented as graphical representation in Figure 40. In the figure, percentage comparison of secant bending stiffness has also been made in order to determine the most effective combination of C-profile and PU-stiffener.

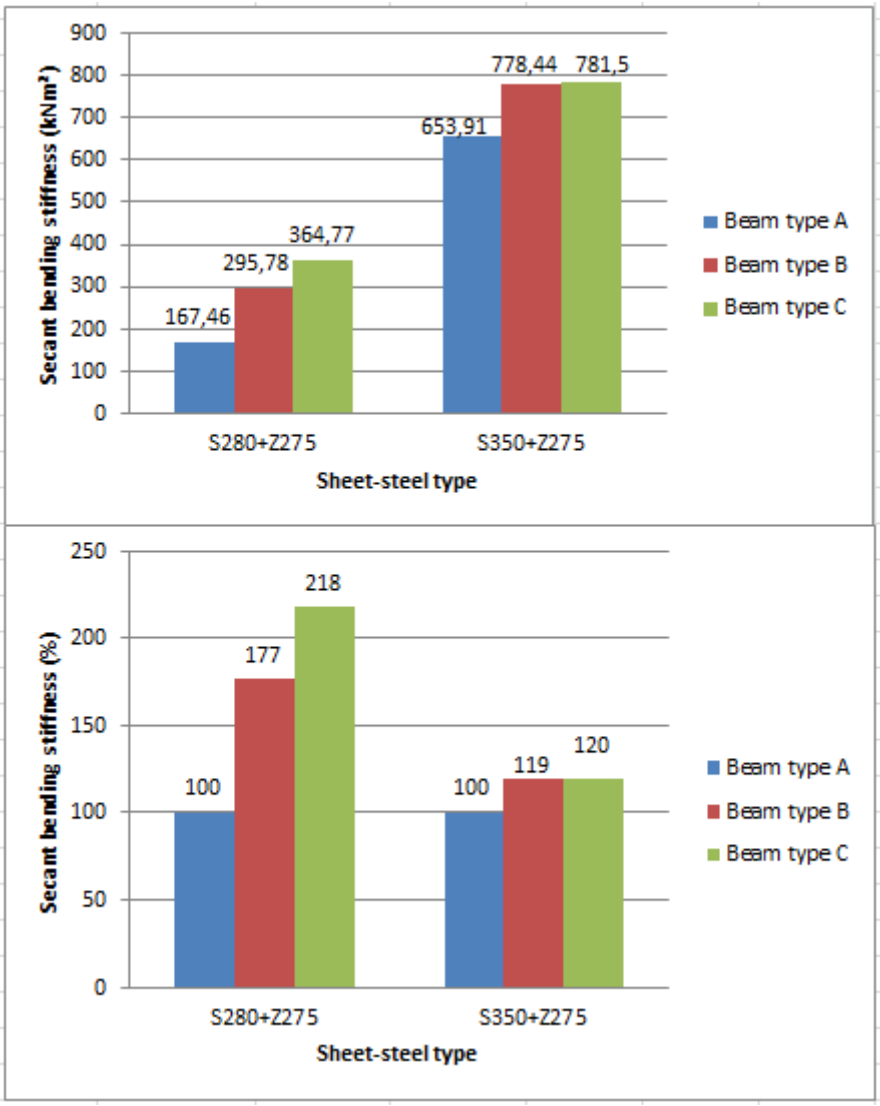

Figure 40 Comparison of secant bending stiffness of beam types A, B and C of each sheet-steel type

Also, both tangent bending stiffness and secant bending stiffness for beam-type D have been mentioned in Figure 41.

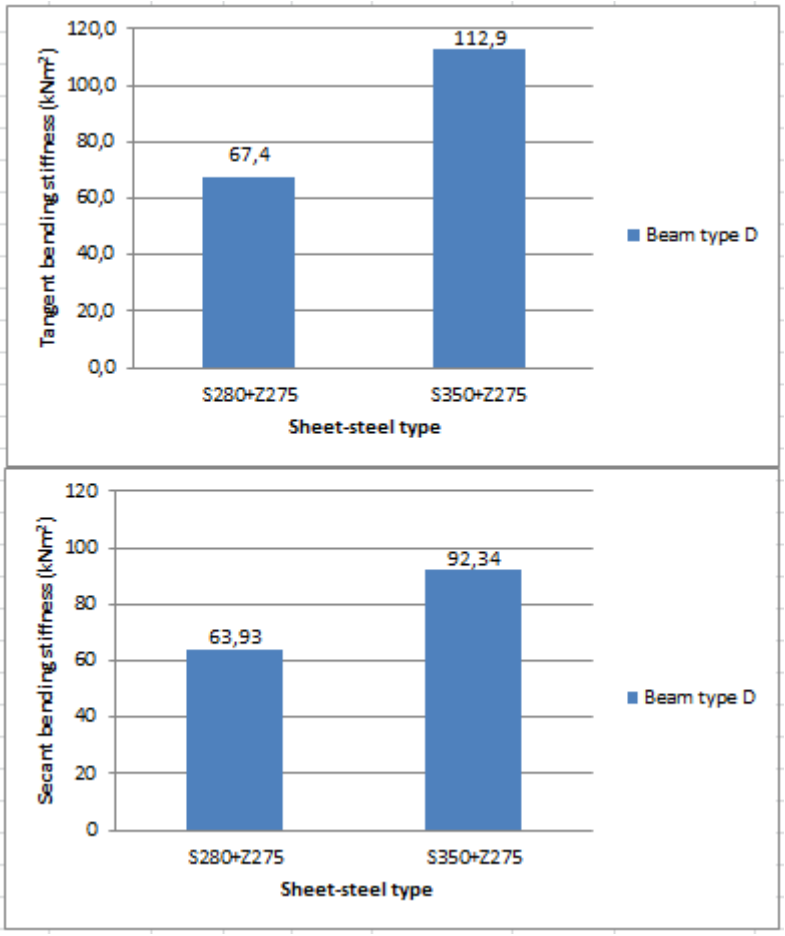

Figure 41 Tangent bending stiffness and secant bending stiffness values of beam type D for both sheet-steel types.

Figure 39 demonstrates the comparison chart regarding average tangent bending stiffness values for beam types A, B and C. In Figure 39, it can be observed that the performance of PU-stiffeners in both of the sheet-steel types is very similar to one another. As it can be seen in the figure, for sheet-steel type S280+Z275, the calculated average value of tangent bending stiffness for test series 1 is 324,6 kNm^2. Similarly, test series 2 indicates 333,5 kNm^2 which is 3% more compared to test series 1 whereas according to the data, test series 3 is 11% more stiffer compared to series 1.

Similarly, for sheet-steel type S350+Z275, average tangent bending stiffness values for test series 5 is 829 kNm^2. For test series 6, the value is 819,4 kNm^2 which is almost equal to the test series 5. In case of test series 7, the average tangent bending stiffness value is 900,4 kNm^2, 9% stiffer than series 5.

These varying results of tangent bending stiffness of each test series within a same sheet-steel material type depend on the position of PU-stiffeners in the beam. Despite specimens made of S350+Z275 sheet-steel material type are thicker (1.0mm) and longer (2.5 m) than that of S280+Z275 (0.5mm and 2.0 m), the C-profile cross-section are of the same dimension. This enables both of the specimens to exhibit similar nature of buckling phenomena and failure modes. In beam type A (for both sheet-steel types),

two C-profiles without any PU-stiffeners are mechanically connected with one another. When beam type A specimens are loaded, buckling occurs in the compressed profile members creating ripples on their respective plane surfaces. Due to the slenderness ratio of the beam being very low, the compressed profile members experience early local buckling stress as waves appear in webs and flanges of the profiles. As buckling stresses become dominant over load-resistance of the beam, the beam experiences local buckling failure. In case of beam type B specimens, C-profiles are glued on each side of the PU-board making PU-board web stiffeners for the profiles. As the beam is loaded, compressed profile members start exhibiting buckling phenomena. Compressed flanges start showing buckling behavior while profile webs do not show any sign of buckling behavior as both of the profile webs are stiffened by the 50 mm thick PU-board. As the stiffened webs of the profiles show more resistance against the buckling load, unstiffened flanges, however, tend to execute the same buckling behavior like in beam type A. The presence of PU-stiffeners in the web of the profile enhanced load resistance and bending stiffness of the profiles.

Beam type C specimens consisted of PU-stiffeners in profile-webs as well as the profile-flanges were well stiffened by glueing long and continuous PU-strips on each flange from the concave side of each profile cross-section. Beam type C specimens contain more polyurethane hence having more weight than other beam types. When the beam was loaded, it was inevitable that this beam type C specimens would be more load resistant than other beam types if unless the specimens were poorly made. Unlike in beam types A and B, this beam type did not show any buckling behavior. Compressed parts of the profile were stiffened by PU-boards already and the PU-board and strips were able to reduce/prevent any deformation in the profile cross-section caused by local buckling. As PU-stiffeners prevented any local deformations in the compressed parts of the profile, the beam experienced distortional buckling behavior after the local buckling load was less than the load resistance provided by the beam. During distortional buckling, flanges on the compressive zone tilted downwards and compressed part of the web bent towards the PU-board side- a typical behavior of a profile experiencing distortional buckling under flexural load. Figure 8a describes how a CFS profile can shift from one buckling mode to another if the stress level is not high enough for failure, we can see the same behavior in beam type C. As the amount of load applied in the beam is increased, bending moment around the mid-span of the beam increased too. This resulted in the generation of distortional buckling where the bending moment was the highest, making the beam vulnerable to the deformations caused by distortional buckling.

This brings to a fact that stiffening of compressed flanges of C-profile plays a vital role in the bending stiffness of the beam. Although, stiffening of compressed profile webs of the profile provides some stiffness to the beam but it is very low compared to the stiffness provided by web and flange stiffened profiles.

For both sheet-steel types, the performance of PU-boards as stiffener was fairly similar. Beam type C held the maximum value of tangent bending

stiffness for both sheet-steel types. According to the retrieved data, it can be expressed that the use of PU-stiffeners can increase the bending stiffness of stiffened C-profiles by approximately 10% than the ones without PU-stiffeners.

On the other hand, the secant bending stiffness of test specimens gives us a phenomenal difference in stiffness values of each test series. However, the average value secant bending stiffness of each test series must be less than that of tangent bending stiffness and it is less in every test series. The average value of secant bending stiffness for test series 5 is 167,46 kNm^2. For test series 6, the value is 295,78 kNm^2, 77% stiffer than series 5. Test series 7 holds 364,77 kNm^2 which is 118% more of test series 5. (Figure 40)

Figure 41 demonstrates both stiffness values for beam type D of both sheet-steel material types. Average tangent bending stiffness of test series 4 and 6 are 67,4 kNm^2 and 112,9 kNm^2 respectively. Similarly, average secant bending stiffness values of series 4 and 6 are 63,93 kNm^2 and 92,34 kNm^2 respectively.

However, tangent bending stiffness of the beam is more precise than secant bending stiffness as tangent bending stiffness only considers a linear inclination of the elastic region of the graph whereas secant bending stiffness is determined by considering maximum load capacity of the beam and the displacement of the beam during the maximum loading.

From Table 5 and the analysis done above, it can be concluded that,

$$F_{u_{beam\ type\ A}} \leq F_{u_{beam\ type\ B}} \leq F_{u_{beam\ type\ C}} \quad (5)$$

Similarly, taking Table 6 as reference, the tangent bending stiffness of both sheet-steel types for beam type B is similar to beam type A and beam type C greater than beam type B. This relation can be observed in equation 5.

$$(EI)_{beam\ type\ A} \approx (EI)_{beam\ type\ B} \leq (EI)_{beam\ type\ C} \quad (6)$$

Also, calculated values of bending stiffness of C-profiles with brutto and effective cross-section for both sheet-steel materials are shown in Table 8. The values shown in the table are for unstiffened C-profile beam that consists of two identical profiles.

Table 8 Calculated values of bending stiffness of unstiffened C-profiles with brutto and effective cross-sections for both sheet-steel material types

Sheet-steel material	*EI* for brutto cross-section (kNm^2)	*EI* for effective cross-section (kNm^2)
S280+Z275	413,09	216,47
S350+Z275	815,82	628,18

Brutto value of bending stiffness of a C-profile is the total bending stiffness provided by the profile when the cross-section is fully functioning and doesn't contain any ineffective parts. This case exists only when the purlin experiences pure tensile load only. When a purlin is loaded in pure compression or in bending, the compressed part of the purlin will create ineffective parts in the cross-section meaning those regions will be unable to take any compressive or bending stresses. This is due to the slender nature of the purlin. So whenever a purlin is loaded in compression or in bending, compressed zones of the slender purlin will automatically create ineffective parts and these ineffective parts cannot be considered as load-bearing profile members. Hence a new bending stiffness is required where the bending stiffness is calculated by considering the effective cross-section of the profile. Effective bending stiffness is always less than the brutto bending stiffness of a purlin. The calculations regarding the determination of the bending stiffness of S350 sheet-steel material type for brutto and effective cross-section C-profile is shown in Appendix 4. Same calculation method can be used for S280 sheet-steel material.

Comparing the tangent bending stiffness of unstiffened C-profiles of both sheet-steel materials to the calculated effective bending stiffness of unstiffened C-profiles for both sheet-steel materials will lead us to equation 6 and 7.

$$\frac{EI_{tan_{S280}}}{EI_{eff_{S280}}} = \frac{324{,}64}{216{,}47} = 1{,}5 \qquad (7)$$

$$\frac{EI_{tan_{S350}}}{EI_{eff_{S350}}} = \frac{829{,}23}{628{,}18} = 1{,}32 \qquad (8)$$

Equation 6 and equation 7 give us a ratio between the value obtained from the carried test and the value calculated considering the effective cross-section of the C-profile. The ratio obtained in equations 6 and 7 seem to be a viable ratio as the values obtained from the test results always must be greater than the design value (calculated value). Equation 7 and 8 shows us the ratio of the test results to the design value for the bending stiffnesses for both sheet-steel types namely, S280 and S350 are 1,5 and 1,32 respectively.

5 CONCLUSIONS

The objective of this thesis was to implement a new method to stiffen the cold-formed steel profiles in steel purlin systems rather than just using grooves and bends in the cross-section of the profile. This thesis also demonstrated a way to determine the bending stiffness of the PU-stiffened C-profiles. Comparative data were collected on different alternatives of PU-profile combinations. The main focus of this thesis was to find an innovative method of stiffening cold-formed steel purlins against various buckling modes. Polyurethane boards can be used as longitudinal stiffeners in the cold-formed C-profiles/purlins which will reinforce the profiles against buckling. The use of PU-board is an innovative approach and is worth testing. The PU-boards have contrasting characteristics compared to C-profile as C-profile has high strength and low stiffness whereas PU-board is relatively stiffer but has low material strength. These contrasting materials which are used widely in construction industry were used to conduct our test to obtain beams with high strength and high stiffness.

The materials that were required to conduct the tests were mainly two sheet-steel types namely S280+Z275 epoxy painted of thickness 0.5 mm and S350+Z275 zinc coated of thickness 1.0 mm. These steel sheets were bent in order to achieve two different profile cross-sections from each sheet. PU-boards were cut into desired dimensions as these boards would be stiffening the profiles. Profiles and PU-boards were glued together to form different sets of beam types (Figure 19). Names were given to each test specimen according to their sheet-steel material type, thickness of the profile and beam/combination type. A specimen number was given for each test series. Test arrangements were made in order to conduct the test and four point bending setup was made.

In this thesis, 20 tests were conducted altogether with 8 test series. Test series 1 to 4 had 3 test specimens each while test series 5 to 8 consisted of two specimens each. The results obtained were very consistent as it was as expected before the tests were conducted. Stiffened profiles were more load-resistant than unstiffened ones in both sheet-steel material types. However, the results for the maximum load resistance were more distinctive in case of S280+Z275 as the load resistance increased up to 102%. Similarly, the maximum average value of tangent bending stiffness is held by beam type C, raising the stiffness ratio to unstiffened C-profiles by approximately 10% in both sheet-steel material types. Also, the ratio between the bending stiffness values obtained from the tests and values obtained from calculation for the effective cross-section of unstiffened C-profiles for both sheet-steel materials were 1,50 and 1,32 respectively.

This leads to a fact that the PU-boards were successful to function as an alternative method of stiffening cold-formed lightweight purlins against various buckling modes. Performance of a PU-board enhanced, especially when used in compressed flanges against local buckling while PU-board as a web stiffener had less effect on the tangent bending stiffness of the beam. On the basis of this it can be concluded that flanges play a vital role in the bending stiffness of a C-profile and stiffening the flanges could

prove to be a very effective way to increase the bending stiffness of the profile.

Since the method of stiffening lightweight purlins by polyurethane is a cheap and effective way to increase the bending stiffness of the beam, there is a tendency that these stiffened C-profiles can be mass-produced. Changing profile cross-section dimensions, altering positions of PU-board as necessary, altering the thickness of PU-board between two profiles can be done in order to make it more applicable in the construction industry. However, there should be more tests regarding the performance of polyurethane if alterations are to be made.

Some of the test results did not meet the expectations as there may have been a few flaws regarding specimen preparation or some errors during test setup. Test series S280_0,5_A_Series1_1 specimen was one of them as the test specimen was not reinforced against lateral actions due to the loading. Also, in case of test specimen S280_0,5_B_Series2_2, one of the position of LVL/plywood board under the loading point was misplaced which might have altered the test results.

All the graphs and Figures of all test specimens of all test series are described in Appendix 1 and Appendix 2.

This project can be improved to obtain more accurate and detailed data if the manufacture of test specimens are done more carefully and under closed senior supervision. The use of cold-formed profiles with smaller thickness is recommended as the results clearly showed that stiffening of thin C-profiles by PU-boards gives more productive results in this project.

SOURCES

Anchorage reinforcement n.d. ’Deck of facts online. Accessed 27th September 2011.
http://www.bluescopesteelasia.com/bluescopesteel/product/structuraldecking/deckingprint.cfm?content=term&ID=65bbb582-fce9-4d7f-b61c-f5e18323564d

Ben Young. ’Local buckling and shift of effective centroid of slender sections. Accessed 26th September 2011, pdf-file.
http://www.hkisc.org/proceedings/2006421/9_Ben-Young.pdf

EN 1993-1-3. 2006. Design of steel structures. Part 1-1: General rules and rules for buildings. Accessed 2nd July 2010, pdf-file.
http://sales.sfs.fi/servlets/SFSContractServlet?action=enterContract&contractId=10105

EN 1993-1-3. 2006. Design of steel structures. Part 1-3: General rules. Supplementary rules for cold-formed members and sheeting. Accessed 2nd July 2010, pdf-file.
http://sales.sfs.fi/servlets/SFSContractServlet?action=enterContract&contractId=10105

Fagerberg, L. 2003. ’Wrinkling of sandwich panels for marine applications. Accessed 28th September 2011, pdf-file.
kth.diva-portal.org/smash/get/diva2:9408/FULLTEXT01

Garner, L. and Nathercot, D.A. 2005. ’Designers’ guide to EN 1993-1-1 Eurocode 3: Design of steel structures, general rules and rules for buildings.
London, Thomas Telford Ltd, 2005.

HAMK 2011. ’Sheet Metal Center. Accessed 26th September 2011.
http://portal.hamk.fi/portal/page/portal/HAMK/Tutkimus_ja_kehitys/Osaamiskeskittymat/Ohutlevykeskus

Hancock, G. J. and Pham, C. H. 2007a. ’Shear buckling of thin-walled channel sections. Accessed 27th September 2011, pdf-file.
http://sydney.edu.au/engineering/civil/publications/r885.pdf

Hancock, G. J. and Pham, C. H. 2007b. ’Direct strength design of cold-formed purlins. Accessed 27th September 2011, pdf-file.
http://sydney.edu.au/engineering/civil/publications/r882.pdf

Kingspan multibeam 2007. ’Rail and purlin system. Accessed 27th September 2011, pdf-file.
http://www.kingspanliterature.co.uk/kip/ire/pdf/product-literature/kingspan_multibeam.pdf

Lau, S. C. W. & Hancock, G. J. 1986.'Buckling of thin flat-walled structures by a spline finite strip method, thin-walled structures, Vol. 4, pdf-file.
http://www.sciencedirect.com.proxy.hamk.fi:2048/science/article/pii/0263823186900340

Mahendran, M. and Mcandrew, D. 2003. 'Flexural wrinkling strength of lightly profiled sandwich panels with transverse joint in the foam core. Accessed 28th September 2011, pdf-file.
http://eprints.qut.edu.au/7619/1/7619.pdf

Metsec n.d. 'Z-section butt purlin system. Accessed 27th September 2011.
http://www.metsec.com/products/cold-rolled-steel-purlins/steel-purlins-Z-sections.asp

Pierre Bourrier. 'European Lightweight Steel-framed Construction. Accessed 6th September 2011, pdf-file.
http://www.constructalia.com/en_EN/publications/european-lightweight-steel-frame-construction/4773203/279970/page.jsp

Scott D. Cortese. 'Investigation of single span Z-section purlins supporting standing seam roof system considering distortional buckling. Accessed 26th September 2011, pdf-file.
http://scholar.lib.vt.edu/theses/available/etd-07272001-205847/unrestricted/Thesis.pdf

Staal, R.A, Horrigan, D.P.W, Mallison, G.D and Jayaraman, K n.d. 'Wrinkling stresses in honeycomb sandwich panels using discrete and continuum core representations, pdf-file.
http://extra.ivf.se/eccm13_programme/abstracts/1935.pdf

Steadman and Son. 'Metal roofing and cladding systems. Accessed 26th September 2011.
http://www.steadmans.co.uk/product/purlins/index.htm

The Steel Framing Alliance. 'A builder's guide to steel frame construction. Accessed 26th September 2011, pdf-file.
http://www.steelframing.org/PDF/SFA_Framing_Guide_final%202.pdf

Wei-Wen Yu center for Cold-Formed Steel Structures 2008. 'Cold-formed steel design for the students. Accessed 28th September 2011, pdf-file.
http://www.ccfssonline.org/Student/other/SDM%20Chapter%20C%20-%200708.pdf

TEST GRAPHS AND FIGURES OF S280 TEST SERIES

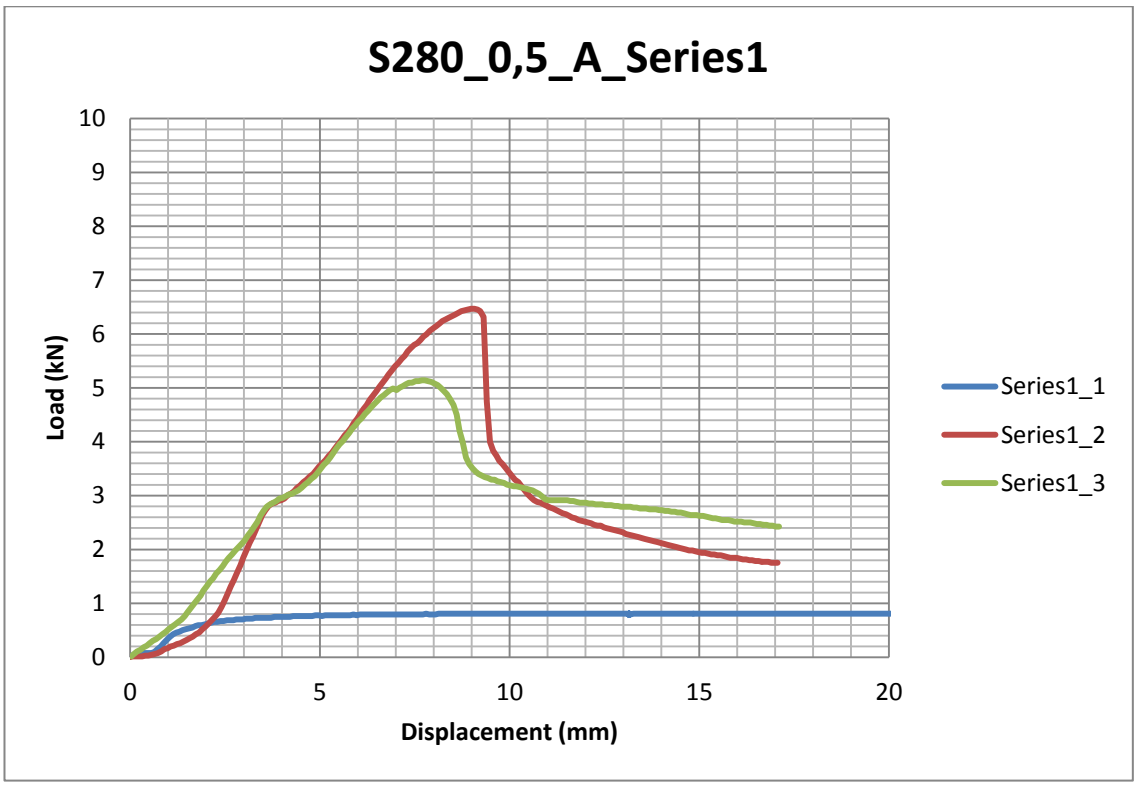

Figure 1 S280_0,5_A_Series1

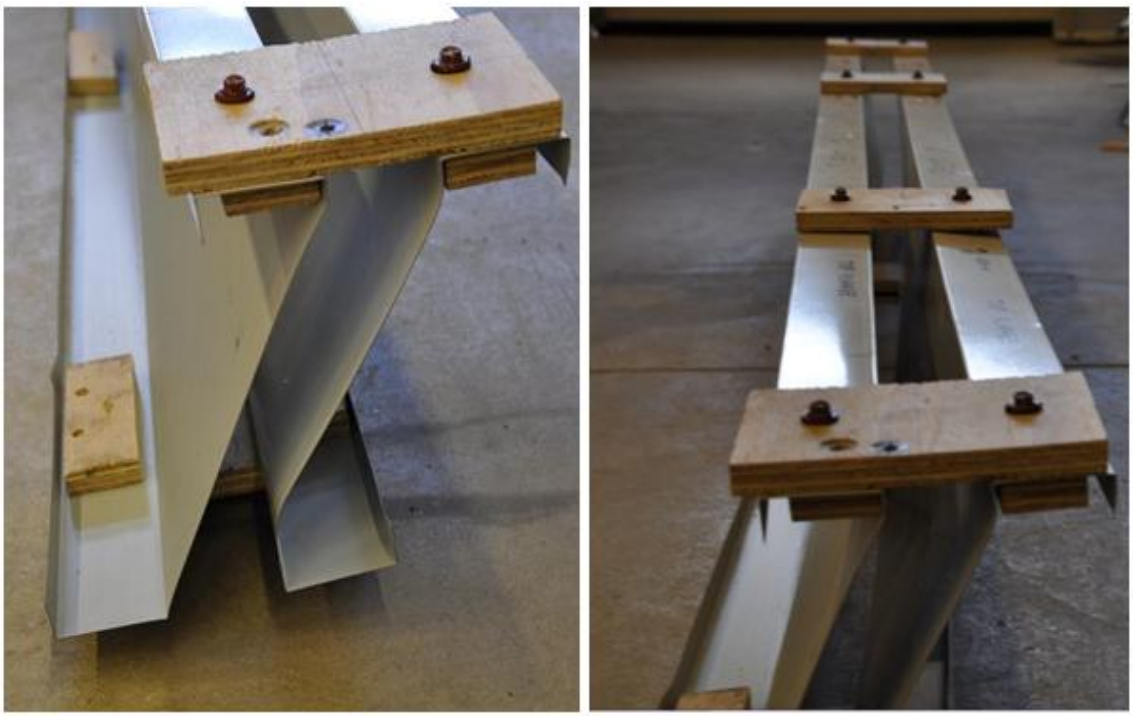

Figure 2 Lateral buckling failure (Series1_1)

Figure 3 Local member buckling failure (Series 1_2)

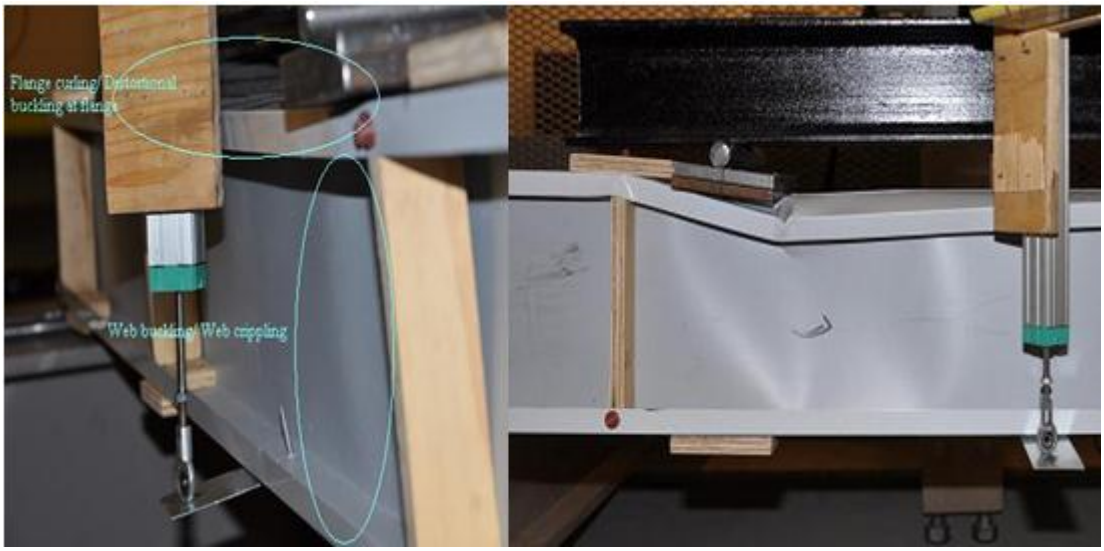

Figure 4 Local flange and web buckling failure/web crushing (Series 1_3)

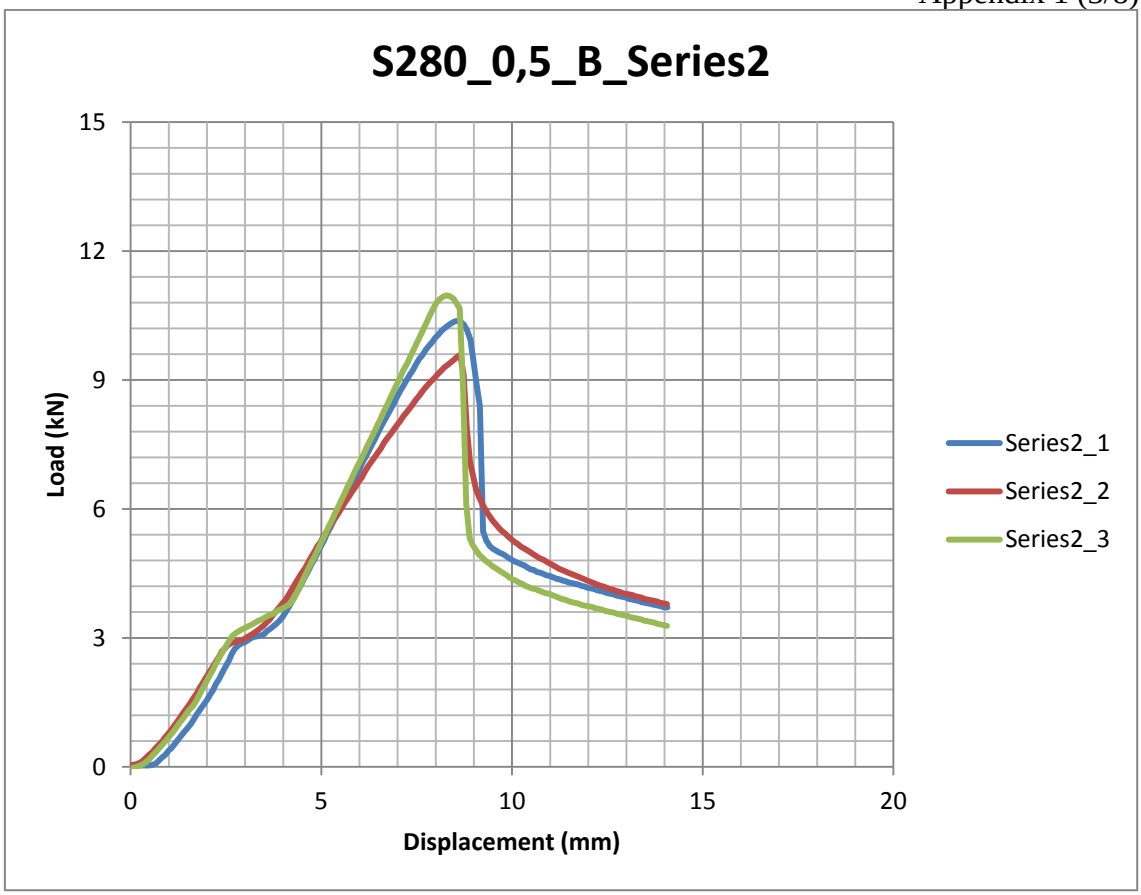

Figure 5 S280_0,5_B_Series2

Figure 6 Local flange buckling failure (Series 2_1)

Figure 7 Local flange buckling failure (Series 2_2)

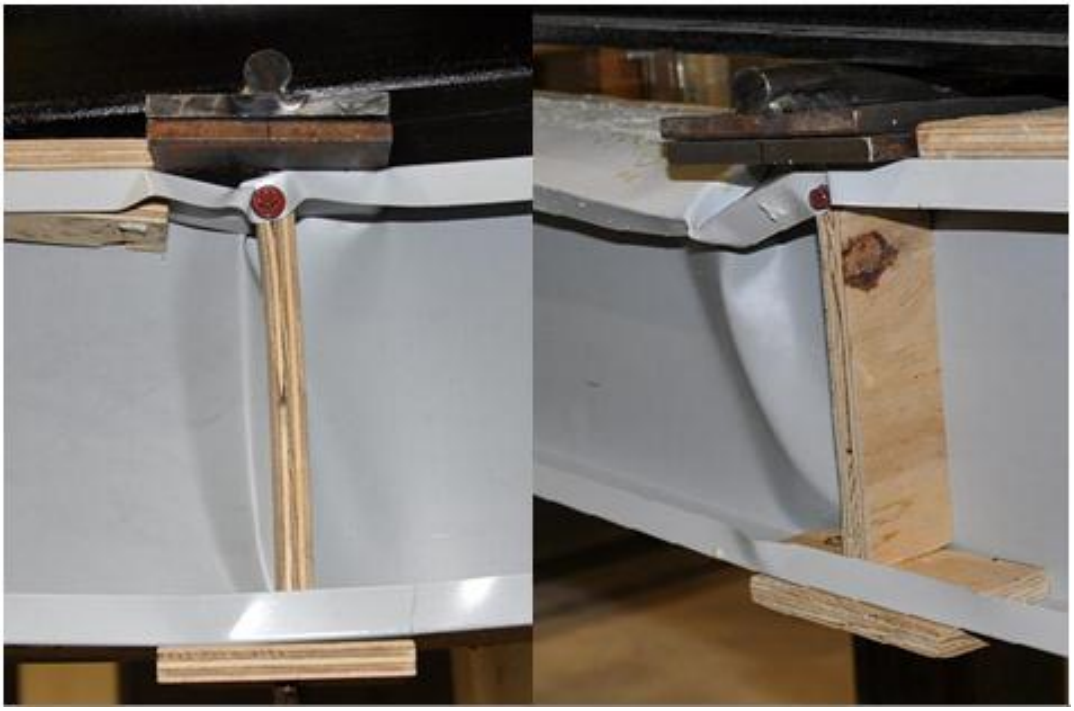

Figure 8 Local flange and web buckling failure (Series 2_3)

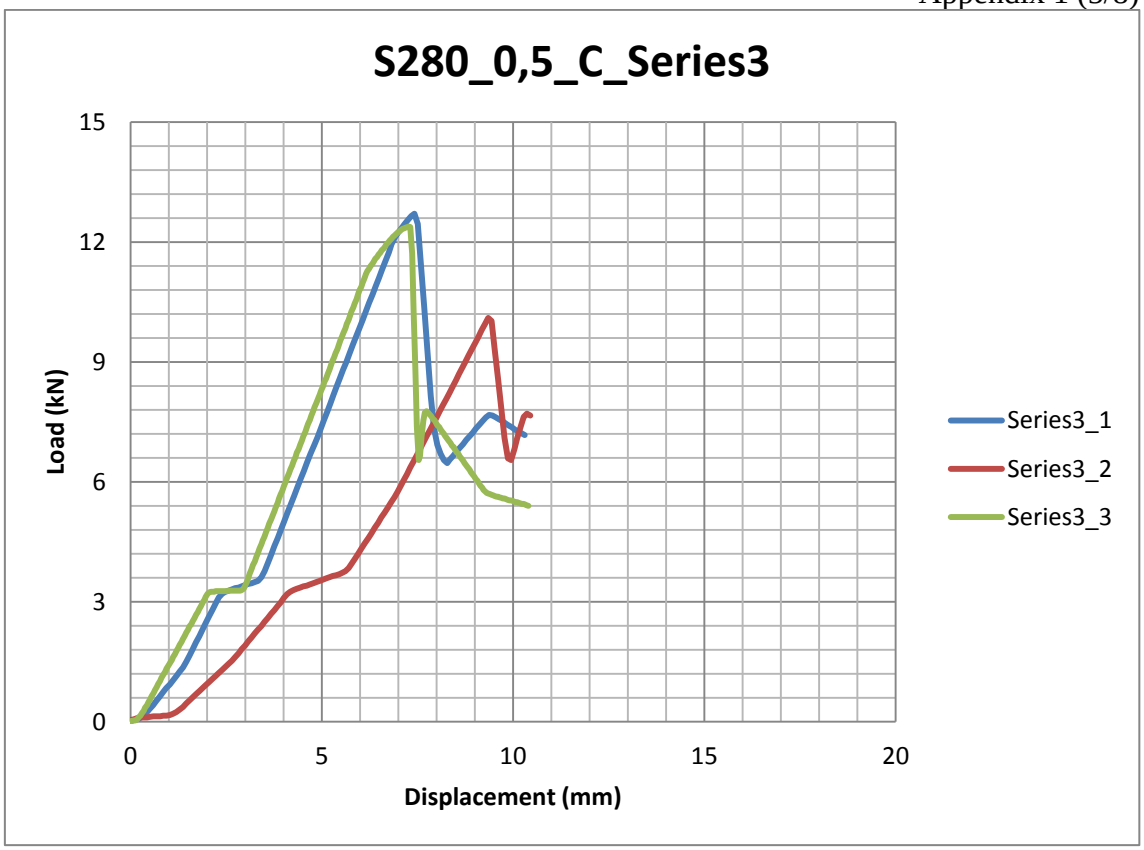

S280_0,5_C_Series3_1 maximum load 12,71 kN

Figure 9 Local flange buckling failure (Series 3_1)

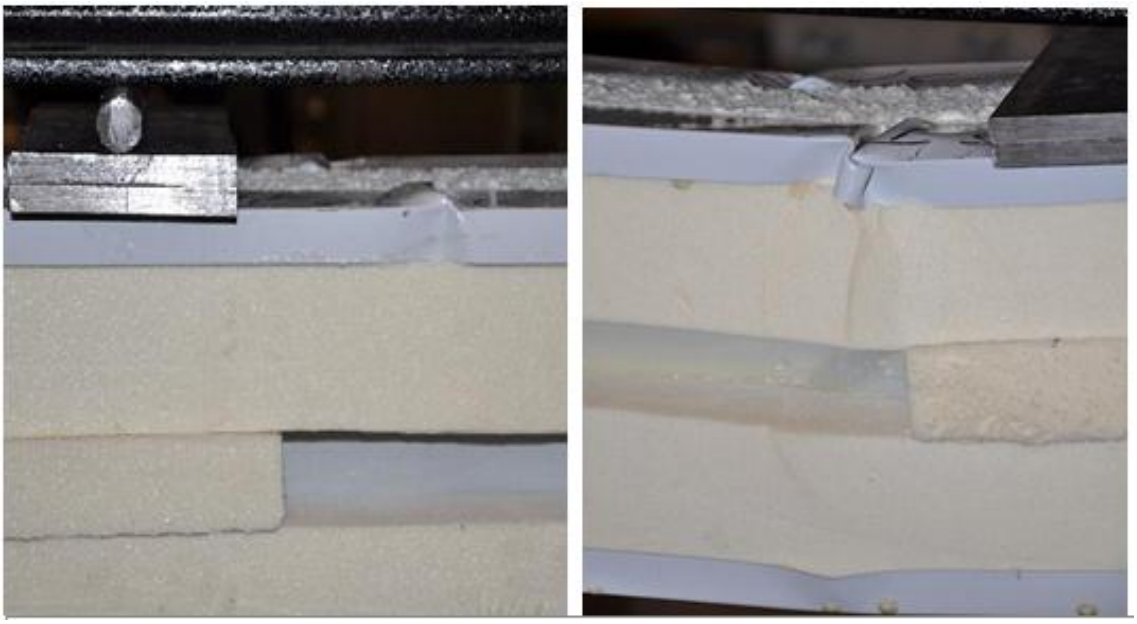

Figure 10 Local flange buckling failure between the loading points (Series 3_2)

Figure 11 Local flange buckling failure between the loading points (Series 3_3)

Figure 12 S280_0,5_C_Series4

Figure 13 Local flange buckling failure next to the loading points (Series 4_1)

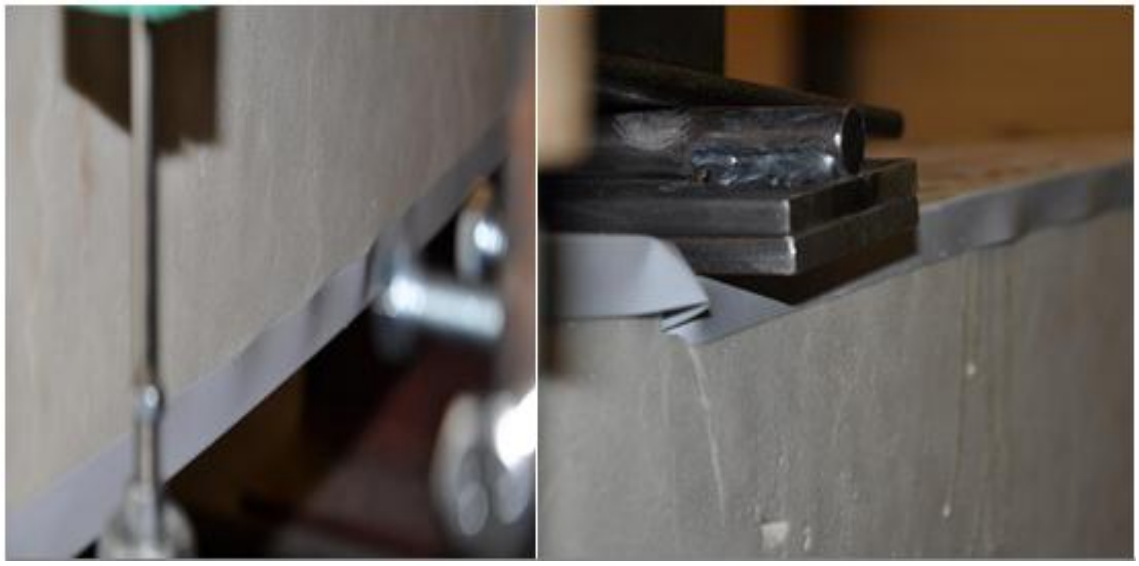

Figure 14 Local flange buckling failure next to the loading points (Series 4_2)

Figure 15 Local flange buckling failure next to the loading points (Series 4_3)

TEST GRAPHS AND FIGURES OF S350 TEST SERIES

Figure 1 S350_1,0_A_Series5

Figure 2 Lateral buckling failure (Series 5_1)

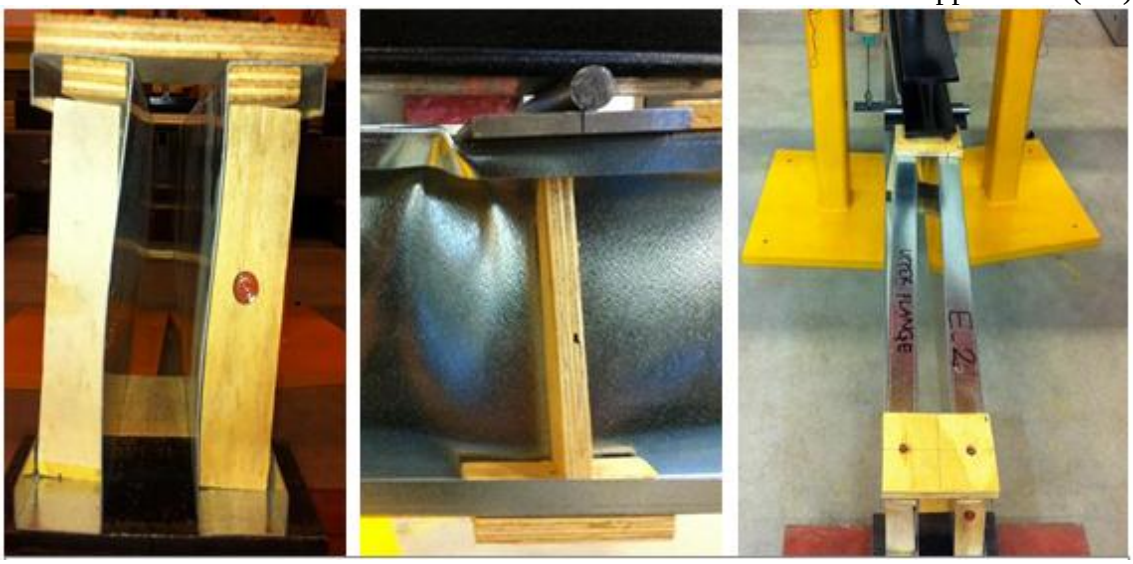

Figure 3 Lateral buckling failure (Series 5_2)

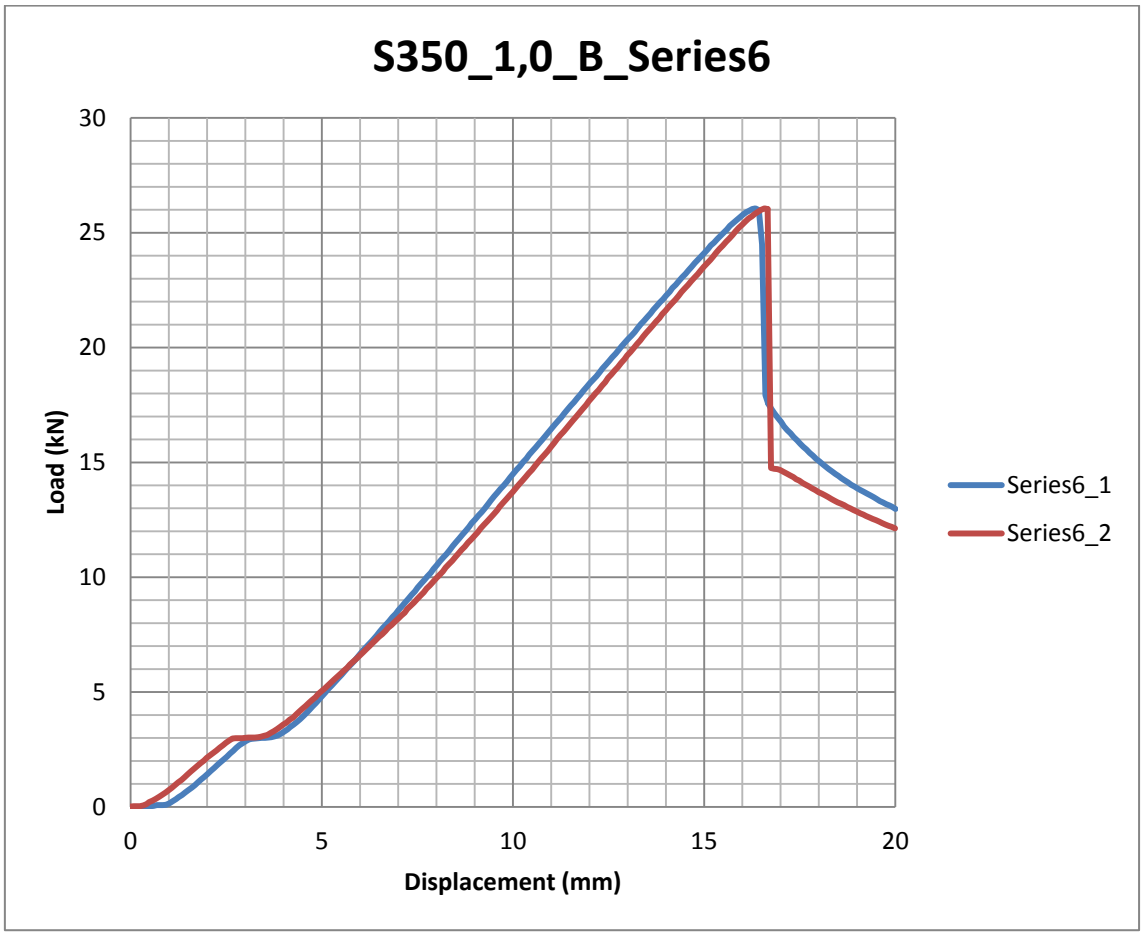

Figure 4 S350_1,0_B_Series6

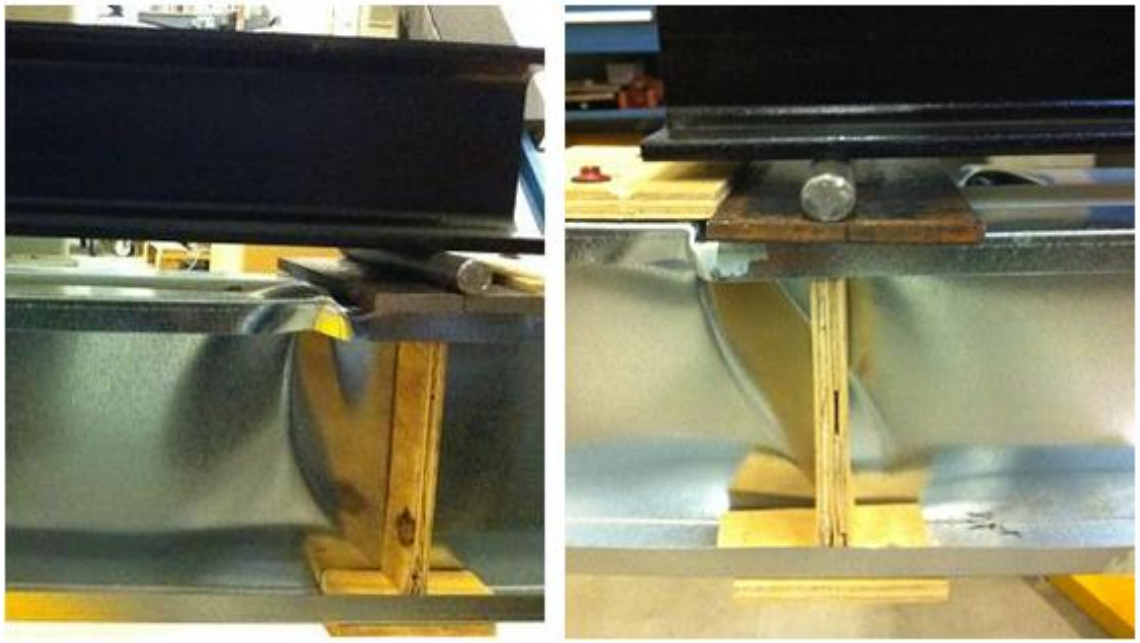

Figure 5 Local member buckling failure (Series 6_1)

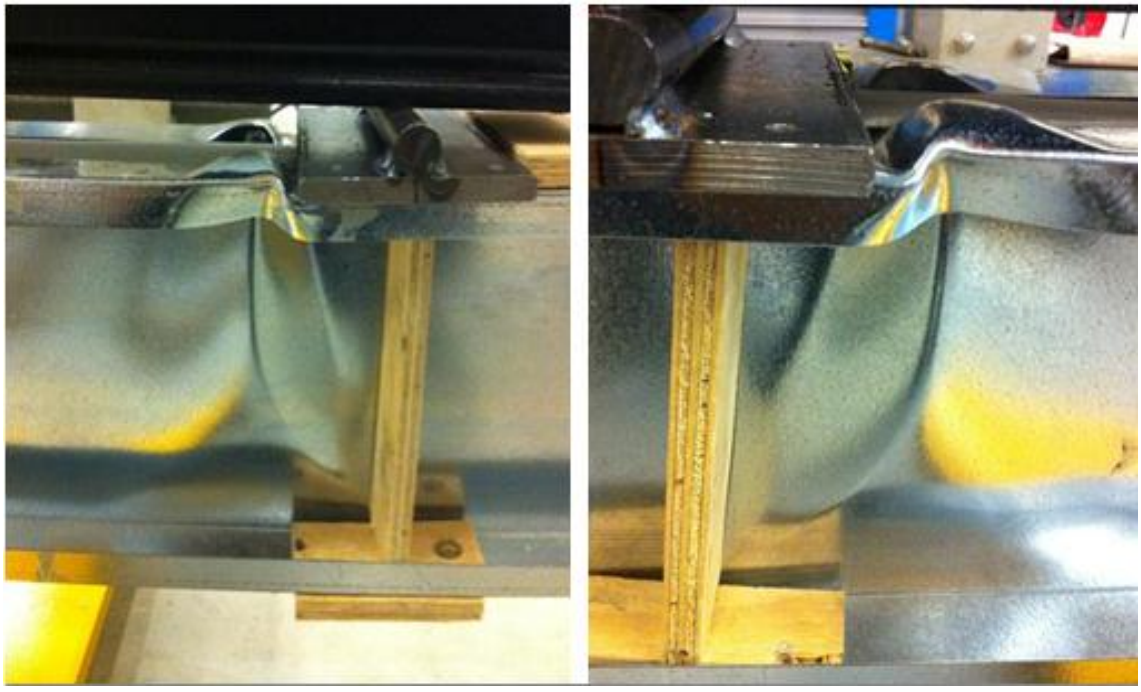

Figure 6 Local member buckling failure (Series 6_2)

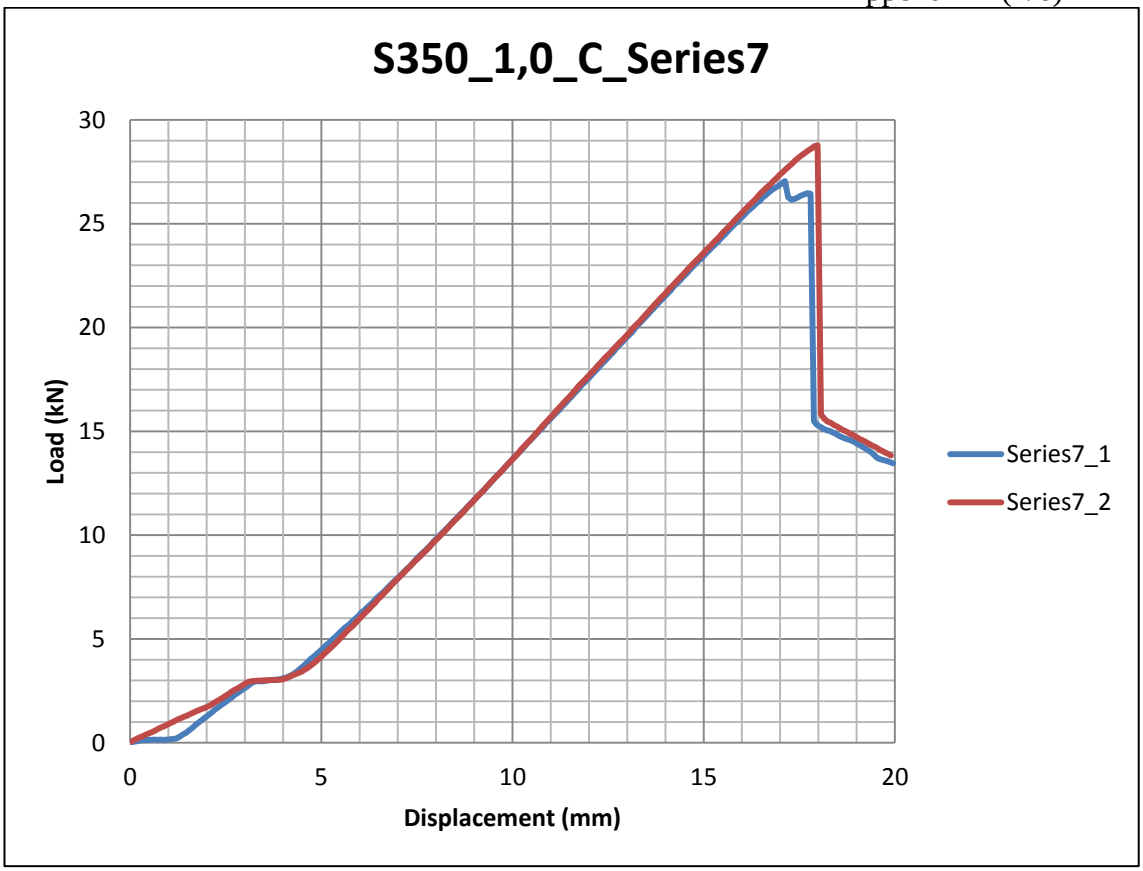

Figure 7 S350_1,0_C_Series7

Figure 8 Local flange buckling+ PU failure (Series7_1)

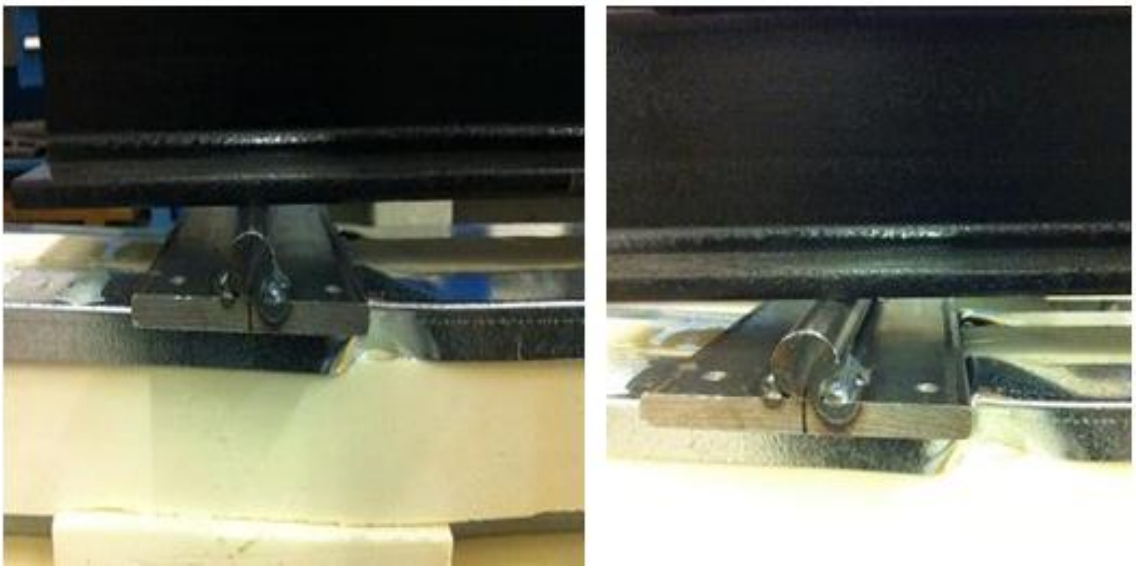

Figure 9 Local flange buckling (Series 7_2)

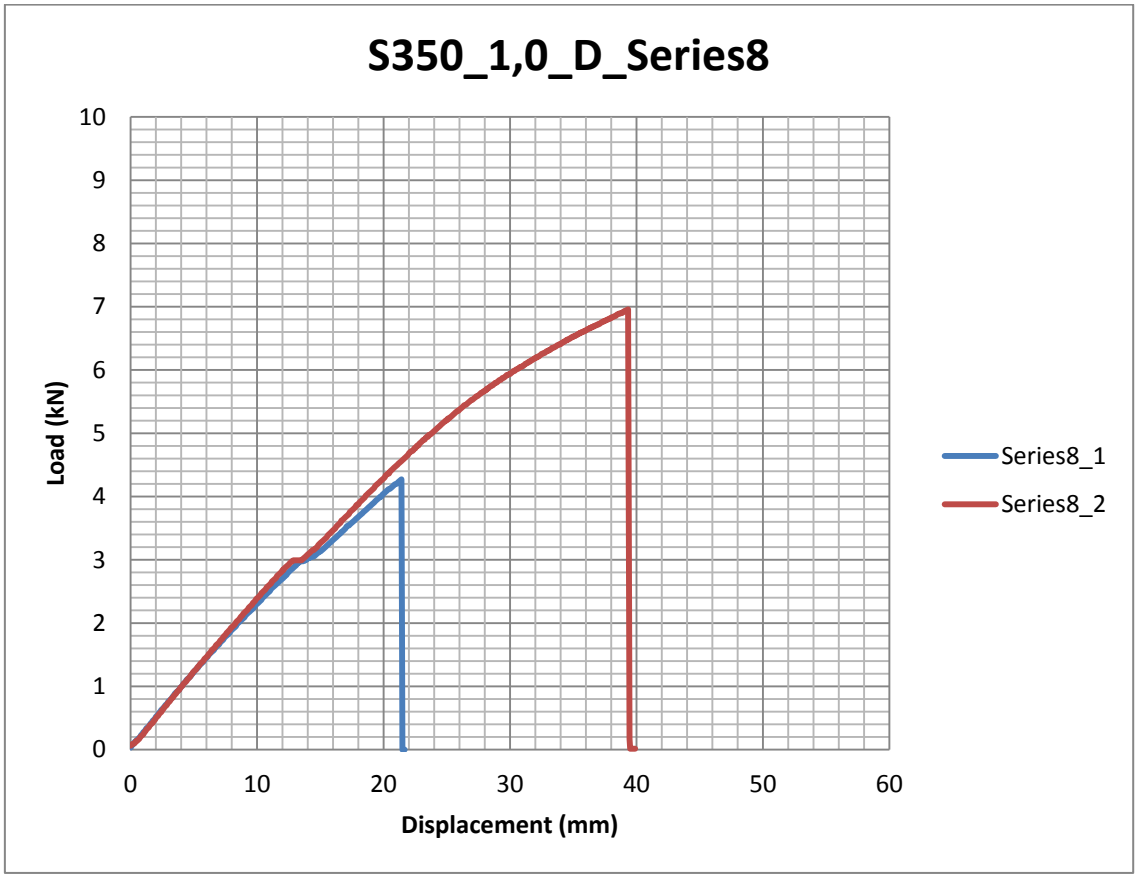

Figure 10 S350_1,0_D_Series8

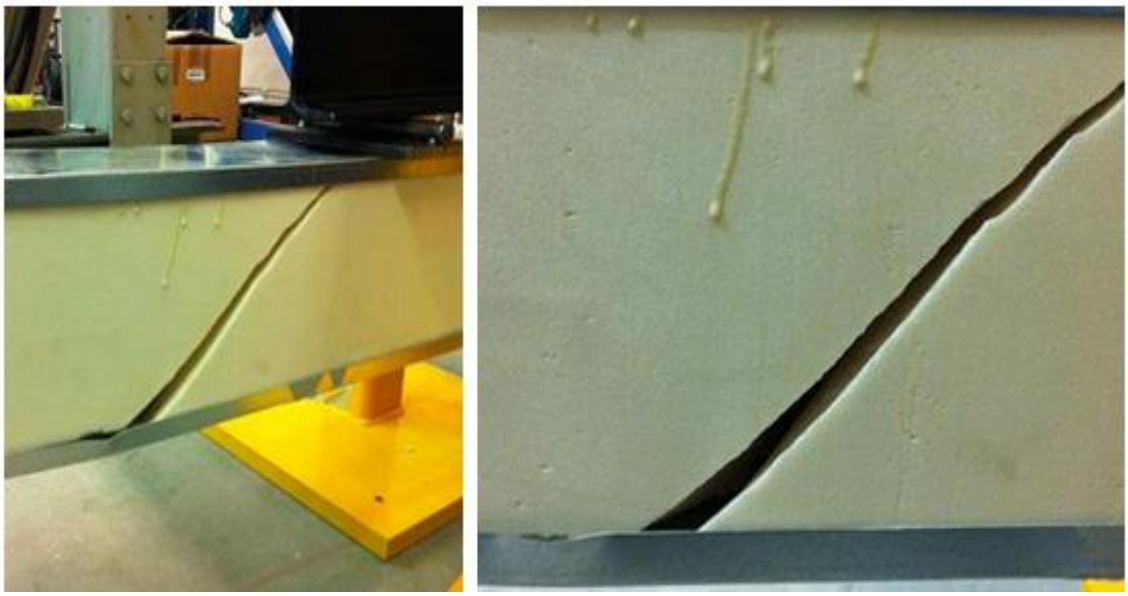

Figure 11 Shear failure of PU-board (Series 8_1)

Figure 12 Shear failure of PU-board (Series 8_2)

Appendix 3 (1/2)

INFORMATION OF THE USED GLUE DURING THE TEST SPECIMEN MANUFACTURE

Tekninen esite

Macroplast UK 8150

Henkel

Liuotinvapaa 2-komponenttiliima
Pohja: Polyuretaani

Versio: 03/2010

Tuotteen kuvaus

Macroplast UK 8150 on kaksikomponenttiliima, jonka pohjana on polyuretaani. Liima ei sisällä mitään liuotinaineita, eikä haihtuvia ainesosia. Perusosa (komponentti A) koostuu orgaanisista yhdisteistä, jotka sisältävät hydroksyyliryhmiä. Kovettajaosa (komponentti B) on isosyanaattipohjainen. Sekoittamalla molemmat osat A ja B seossuhteessa 5:1 painon mukaan, kemiallisen reaktion kautta aikaansaadaan kovaelastinen, sitkeä liima.

Käyttötarkoitus

Macroplast UK 8150 liiman pääkäyttökohde on Sandwich-elementtien valmistus. Yleisemmin käytetyt materiaalit ovat: EPS (styrox), vuori- ja lasivilla, polyuretaani, PVC, puu, erilaiset rakennuslevyt, alumiini ja teräs.

Tekniset tiedot

	Komponentti A Macroplast UK 8150	Komponentti B Macroplast UK 5400	Menetelmä
Väri:	vaalean beige	ruskea	
Koostumus:	neste	neste	
Tiheys (20°C):	1,60 ± 0,05 g/cm³	1,22 ± 0,06 g/cm³	
Viskositeetti *: (Brookfield RVT 6/20, 20° C)	13 000 ± 2 000 mPa s	250 ± 100 mPa s	M-10
Sekoitussuhde			
Massan mukaan:	5	: 1	
Tilavuuden mukaan:	3,8	: 1	

Seos (Komponentti A + B)

Koostumus:	neste	
Viskositeetti *: (Brookfield RVT 4/20, 25°C)	5 500 ± 1 000 mPa s	M-11
Potlife (100 g; 20 g, 20° C) *:	70 min ± 10 min	M-20
Avoin aika (23°C, 50% rh) *:	>100 min	M-30
Alkulujuus (23°C):	4 tunnin kuluttua	
Loppulujuus (23°C):	6-7 vrk:n kuluttua	
Kulutus: (Liimattavien materiaalien pinnan mukaan)	250 - 400 g/m²	
Vetomurtolujuus *:	> 12 MPa	M-40
Shore-D-kovuus (20°C):	80	ISO 868
Kuorimalujuus (Al/Al-levyt):	ei tiedossa	
Lämmönkesto:	-40°C - +100°C	
Lyhyt altistus (1 h):	+150°C	

Kaikki tekniset tiedot perustuvat Henkel Nordan Oy:n testimenetelmiin. *:llä merkityt tiedot on spesifioitu.

Työskentely

Alustava tiedotus

Ennen liiman levitystä on tärkeä lukea käyttöturvallisuustiedote. Siitä saa tietoa varovaisuustoimista sekä turvallisuussuosituksista. Myös sellaisten tuotteiden käyttöturvatiedotteisiin on syytä tutustua, jotka eivät lain mukaan vaadi varoitusmerkintöjä.

Ohjeet liimasauman valmisteluun ja pinnan esikäsittelyyn

Liimattavien pintojen tulee olla puhtaat, kuivat, pölyttömät, rasvattomat ja niissä ei saa olla muitakaan kontaminaatioita. Sopivan pohjusteen käyttö metallipinnoilla voi parantaa tartuntaa ja/tai parantaa liimasauman kestoa. Muovisten materiaalien pinnat tulee puhdistaa niin, että liimattavilta pinnoilta poistuvat kalkenlaiset liimaa irrottavat aineet Tartuntaa voidaan lisätä, materiaalista riippuen, pintaa karhentamalla tai hiekkapuhaltamalla.

Liiman sekoittaminen ja levittäminen

Liimakomponentit voidaan sekoittaa manuaalisesti, sekoittimella tai kaksikomponenttisekoittimella. Tuote voidaan levittää lastalla, telalla, valamalla tai ruiskuttamalla. Liimaa voidaan käyttää rajoitetun ajan sisällä (potlife). Tämän ajan jälkeen seos hyytyy, eikä sovellu enää käytettäväksi. Tämän vuoksi vain se määrä liimaa, joka voidaan levittää potlifen kuluessa, tulisi sekoittaa. Potlife riippuu sekoitetun liimaerän määrästä ja lämpötilasta. Liimamäärän kasvaessa ja lämpötilan kohotessa potlife alenee. Lämpötilan lasku pidentää potlifea.
Liimakomponentit eivät saa päästä kosketuksiin kosteuden kanssa säilytyksen eikä levityksen aikana. Kosteus (vesihöyry) aiheuttaa liiman vaahtoamista ja heikentää liimasidosta. Tämän vuoksi kaikki astiat tulisi sulkea tiiviisti ja suojata kosteudelta varastoinnin aikana.

Kovettuminen

Macroplast UK 8150 voidaan kovettaa 15°C - 60°C:een lämpötilassa. Lämpötilaa nostamalla lyhennetään kovettumisaikaa huomattavasti. Myös katalyyttien lisäys (kiihdyttäjien) nopeuttaa kovettumisreaktiota. (esim. potlife ja avoin aika).
Kontaktipaineen (painot, puristimet) ja kiinnityksen tulee olla riittävä kovettumisen aikana, jotta liitos pysyy paikoillaan. Hyvä merkki riittävästä liimamäärästä saumassa on, kun liima pursuaa ulos liimatusta saumasta.

Puhdistus

Tuore, kovettumaton liima (liimanlevityslaitteessa, liimattavilla pinnoilla jne.) voidaan poistaa esim. asetonilla, isopropanolilla tai metyleenikloridilla. Kovettunut liima voidaan poistaa ainoastaan mekaanisesti.

Varastointi

Tiiviisti suljettuna, kuivassa paikassa

Perusosa:	
Kylmän arkuus	ei ole
Suositeltava varastointilämpötila	15°C - 25°C
Varastoinnin kestävyys	12 kk alkuperäispakkauksessa
Kovettaja:	
Kylmän arkuus	kyllä
Suositeltava varastointilämpötila	15°C - 25°C (ei < 10°C eikä >50°C)
Varastoinnin kestävyys	12 kk alkuperäispakkauksessa

CALCULATION OF THE BENDING STIFFNESS FOR S350+Z275 C-PROFILE

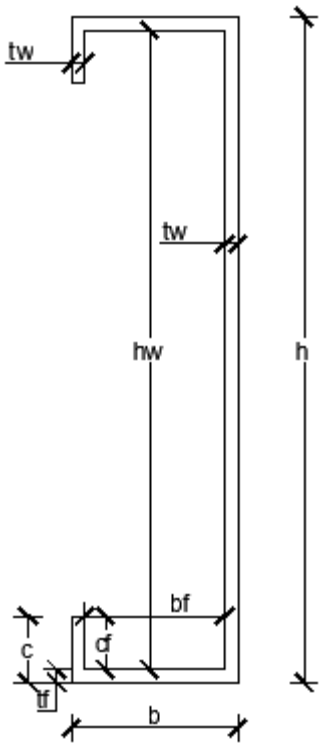

$h := 200mm$ Height of the profile

$h_w := 198mm$ Height of the web only

$t_w := 1.0mm$ Thickness of the web

$b := 50mm$ Breadth of the profile

$b_f := 48mm$ Breadth of flange only

$t_f := 1.0mm$ Thickness of the flange

$c := 20mm$ Length of the lip

$c_f := 19mm$ Length of lip omitting thickness of flange

$t := 1.0mm$ Thickness of the profile

$E := 210000\frac{N}{mm^2}$

$A_{tot} := t\cdot(2\cdot c + 2\cdot b_f + h) = 336\cdot mm^2$

Determination of Neutral axis:

$$x := \frac{(t\cdot c)\cdot\frac{c}{2} + (b_f\cdot t_f)\cdot\frac{t_f}{2} + (h\cdot t_w)\cdot\frac{h}{2} + (t_f\cdot b_f)\cdot\left(h - \frac{t_f}{2}\right) + (t\cdot c)\cdot\left(h - \frac{c}{2}\right)}{A_{tot}}$$

$x = 100\cdot mm$ Along x-axis

$$y := \frac{(h\cdot t_w)\cdot\frac{t_w}{2} + 2\cdot(t_f\cdot b_f)\cdot\left(\frac{b}{2}\right) + 2\cdot(t_f\cdot c)\cdot\left(b - \frac{t_f}{2}\right)}{A_{tot}}$$

$y = 13.333mm$ Along Y-axis

Now, calculating the Moment of Inertia for the given profile:

$$I := 2\cdot\left[\frac{t\cdot c_f^{\,3}}{12} + (t\cdot c_f)\cdot\left(\frac{h}{2} - t - \frac{c_f}{2}\right)^2\right] + 2\cdot\left[\frac{b\cdot t_f^{\,3}}{12} + (b\cdot t_f)\cdot\left(\frac{h - t_f}{2}\right)^2\right] + \frac{t_w\cdot(h - 2\cdot t_w)^3}{12}$$

$I = 1.942\times 10^6\cdot mm^4$

$E\cdot I = 407.911kN\cdot m^2$

For two profiles, $2\cdot E\cdot I = 815.821kN\cdot m^2$

This is the bending stiffness value of S350+Z275 C-profile brutto cross-section.

To calculate the maximum force a cold-formed C-purlin beam can take in a two point load arrangement where forces are equidistant from each other and from the supports, the total area of the cross-section that is bearing the stresses must be calculated first.
When a slender beam is loaded, it starts bending or buckling (depending on its cross-sectional properties) well before it reaches its yield limit. Similarly, in case of cold-formed sheet made purlins and beams, they behave the same way as slender beams as the purlins have very low thickness compared to the span of the beam. But, cold-formed purlins have a different characteristic on bending. When cold-formed purlins are loaded horizontally (point load or uniformly distributed load), part of the beam that is under pure tension (in our case the lower part of the beam comprising lower flange, lower lip and half of the web) will distribute the tensile stress very evenly so that the whole area of the tensile part of the beam (purlin) is effective. However in bending load on the other hand, the compressive part of the beam which is the upper half of the beam will have its ineffective parts that cannot contribute against the compressive stresses. As we know, steel perform very poorly against compressive forces in comparison to the very good performance against tensile forces. Also, in case of cold-formed profiles, profiles under compression have different characteristic which can be illustrated by taking an example of C-purlin.

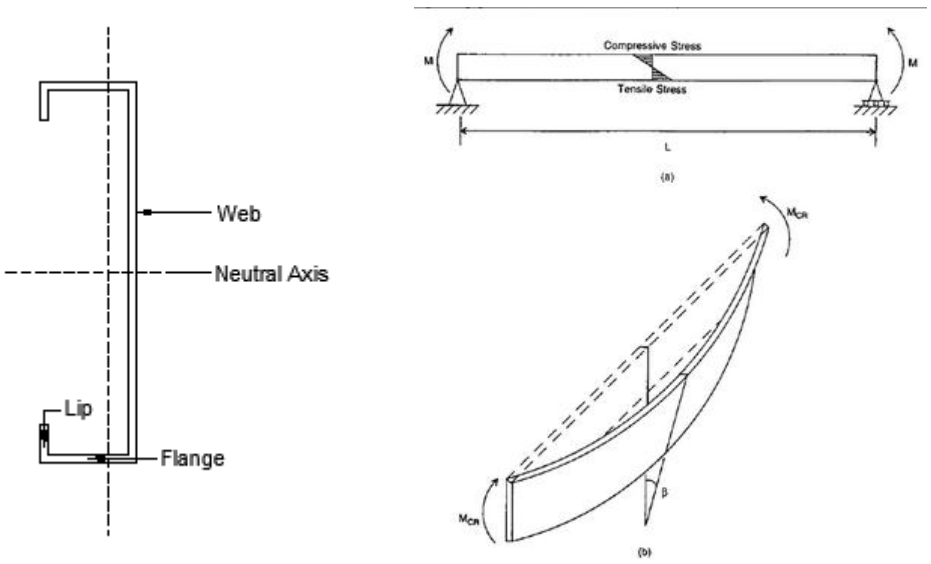

Here as we can see in the C-purlin given in the figure above, lower part of the web is under pure tensile stress when loaded whereas the upper half of the profile is in pure compression since the beam is loaded under bending. Sheet metal under tensile forces is fully efficient and all the tensile part of the profile yields at its yield point. However, under compressive stresses, sheet metal perform rather poorly as various buckling phenomenon occur within the compressive zone of the profile. Profile web and profile flanges are stiffened by their adjacent edges but not until the middle of the section (web or flange). So when the profile is loaded in bending, web part and flanges under compressive load starts buckling in various ways. Profile web on the compressive zone will experience buckling load failure takes place when the buckling load is over the yield limit. Compression flange in this case will experience buckling stress.

In our case, the upper part of the profile is in compressive stress comprising half of the profile web, flange and upper lip of the profile. So, we need to calculate the amount of area that is actually taking the compressive stress. For that we need to follow the Eurocode EN1993-1-1.

Local buckling of compression elements is accounted for in EN 1993-1-3 primarily by making reference to part 1.5 of the code. As explained in section 6.2.2 of this guide, an effective width approach is adopted, whereby "ineffective" portions of the cross sections are omitted and section properties may be determined based on the remaining effective portions. For cases where the maximum compressive stress in an element is less than the yield stress ($\sigma_{.com.Ed} < f_{yb}/\gamma_{M0}$), different expressions for the reduction factor ρ to those supplied in part 1.5 should be adopted, as given by equations D13.2 and D13.3:

When the cold-formed C-purlin is loaded under bending, the tensile end of the profile is fully utilized under the tensile stresses whereas the upper compressive part of the profile experiences different buckling phenomenon. As the beam gets flexure load, stresses distribute around the beam cross section which is less than the yield point. As the flexural loading increases, the compressive part of the beam initially starts buckling locally and then distortional buckling. When in local buckling, the edges or the lip of the profile prevents the local displacements of the nodal points (i.e. at the flange-to-lip junction). However, members like lips, flanges and web are free to bend. So, the flanges bends inwards while web and lips bend outwards like in the figure.

The test specimen manufactured was a simple C-purlin bent into the designed dimensions without any longitudinal stiffeners. So, according to the Eurocode EN1993-1-5 ...(4.4) Clause 4.1,

$A_{c.eff} := \rho \cdot A_c$

where,

$A_{c.eff}$	Effective area under compression
A_c	Area under compression
ρ	Reduction factor of the original width due to the Ineffective parts in the cross section

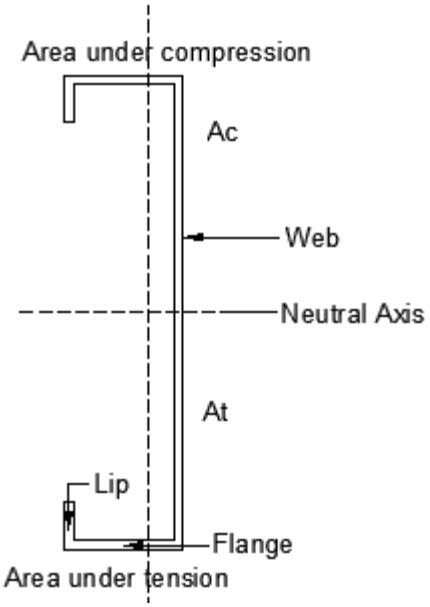

First, we need to check effects of local buckling in the profile to know to what extent the total area has reduced to the effective area that takes the compressive stress.
In our case, we have half the beam web, a flange and a lip in compression.
The beam web and flange are doubly supported by adjacent edges while the lip is supported only at one end hence being an outstand element.

4.4 Plate elements without longitudinal stiffeners

(1) The effective[P] areas of flat compression elements should be obtained using Table 4.1 for internal elements and Table 4.2 for outstand elements. The effective[P] area of the compression zone of a plate with the gross cross-sectional area A_c should be obtained from:

$$A_{c,eff} = \rho A_c \qquad (4.1)$$

where ρ is the reduction factor for plate buckling.

(2) The reduction factor ρ may be taken as follows:

- internal compression elements:

$$\rho = 1{,}0 \qquad \text{for } \bar{\lambda}_p \le 0{,}673$$

$$\rho = \frac{\bar{\lambda}_p - 0{,}055(3+\psi)}{\bar{\lambda}_p^2} \le 1{,}0 \qquad \text{for } \bar{\lambda}_p > 0{,}673 \text{ , where } (3+\psi) \ge 0 \qquad (4.2)$$

- outstand compression elements:

$$\rho = 1{,}0 \qquad \text{for } \bar{\lambda}_p \le 0{,}748$$

$$\rho = \frac{\bar{\lambda}_p - 0{,}188}{\bar{\lambda}_p^2} \le 1{,}0 \qquad \text{for } \bar{\lambda}_p > 0{,}748 \qquad (4.3)$$

where $\bar{\lambda}_p = \sqrt{\frac{f_y}{\sigma_{cr}}} = \frac{\bar{b}/t}{28{,}4\,\varepsilon\sqrt{k_\sigma}}$

$A_{c.eff} = \rho \cdot A_c$

The cross-section area for our profile under compression comprises of a 200mm high web, 50 mm long flange and 20mm long strip of lip. So, we will isolate the profile into each individual members compressed web, compressed flange and compressed lip.
For the compressed web being an internal compression member meaning a doubly supported compression element (element between two edge stiffeners), assuming slenderness ratio as A,

$$\rho_w = \frac{\lambda_p - 0.055(3+\psi)}{\lambda_p^{\,2}} \qquad \rho_w \le 1 \quad \text{for } A > 0.67 \quad \text{where } (3+\lambda) \ge 1$$

where,

$\lambda_p = \sqrt{\bar{\lambda}_p^2}$ Slenderness ratio of a plate for local buckling

The plate slenderness ratio $\bar{\lambda}_p^2$ is given by,

$$A = \sqrt{\frac{f_y}{\sigma_{cr}}} \qquad A = \frac{\frac{b_1}{t}}{28.4\varepsilon \cdot \sqrt{k_\sigma}}$$

To calculate the exact action and resistance of the elements under bending, we should subtract the thickness of the coating to the nominal thickness of the profile material. Since our material is S350+Z275, S350 meaning the nominal yield strength of the steel is 350N/mm^2 and Z275 meaning there is 275g/m^2 of zinc material distributed on each side of the surface as coating. Converting the numerical value in terms of coating thickness, we get 0.02mm. So, the new thickness of the profile is 1.0mm - 0.04mm=0.96mm

$t_{nom} := 1.0mm$	Nominal thickness of the profile
$t_{net} := 0.96mm$	Reduced thickness of the profile due t zinc coated surface

So, our new thickness of profile for EWC is,

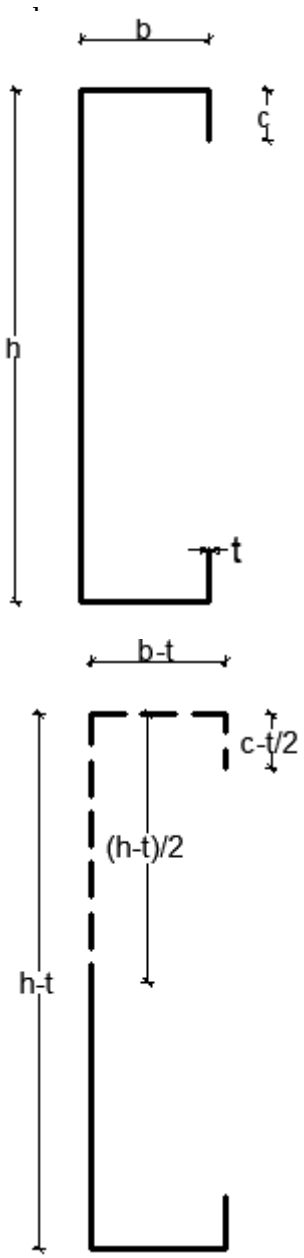

Determination of I-value of the C Profile:

Section properties for a 200 x 150 x 1.0 mm lipped C-profile:

$h = 200mm$	Height of the profile
$h_w = 198mm$	Height of the web only
$t_w = 1mm$	Thickness of the web
$b = 50mm$	Breadth of the profile
$b_f = 48mm$	Breadth of flange only
$t_f = 1mm$	Thickness of the flange
$c = 20mm$	Length of the lip
$c_f = 19mm$	Length of lip omitting thickness of flange
$t_{net} = 0.96mm$	Thickness of the profile
$r := 1.2mm$	Radius of curvature of the corners
$t_{coating} := 0.02mm$	Thickness of the coating per surface

When calculating the gross cross-sectional properties of the profile, we should avoid the thickness of the coating by subtracting it to the nominal thickness of the profile. However, the contribution of the coating thickness to the nominal thickness of the profile can be ignored.

$t_{net} = 0.96\,mm$

One of the easiest ways to calculate the gross area of the cross section is to consider the mid-line assumption.

$t = 1\cdot mm$

Idealized section properties of 200 x 50 x 20 of thickness 1.0 mm lipped C-profile after midline assumption:

$h - t = 199\,mm$ $\quad b - t = 49\,mm$ $\quad t - 2\cdot t_{coating} = 0.96\,mm$

$\frac{h - t}{2} = 99.5\,mm$ $\quad c - \frac{t}{2} = 19.5\,mm$ $\quad t_{net} = 0.96\,mm$

Gross area of the cross-section under compression:

$$A_{gross} := \left[\left[\frac{h - t}{2} + (b - t) + \left(c - \frac{t}{2}\right)\right]\cdot t_{net}\right] = 161.28\,mm^2$$

Total area of the cross-section is,

$$A_{tot} := 2\cdot A_{gross} = 322.56\,mm^2$$

Change in neutral axis towards horizontal direction due to reduced thickess of the profile:

$$y_g := \frac{\left[2\cdot(b - t)\cdot t_{net}\cdot\frac{(b - t)}{2} + 2\cdot\left(c - \frac{t}{2}\right)\cdot t_{net}\cdot(b - t)\right]}{A_{tot}}$$

$y_g = 12.833\,mm$

Calculation of effective widths:

Web:

Table 4.1: Internal compression elements

Stress distribution (compression positive)	Effective width b_{eff}
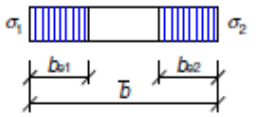	$\psi = 1$: $b_{eff} = \rho\ \bar{b}$ $b_{e1} = 0{,}5\ b_{eff}$ $\quad b_{e2} = 0{,}5\ b_{eff}$
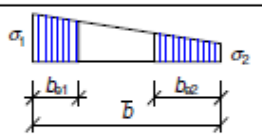	$1 > \psi \geq 0$: $b_{eff} = \rho\ \bar{b}$ $b_{e1} = \frac{2}{5 - \psi} b_{eff}$ $\quad b_{e2} = b_{eff} - b_{e1}$
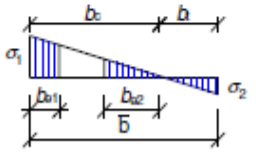	$\psi < 0$: $b_{eff} = \rho\ b_c = \rho\ \bar{b} / (1{-}\psi)$ $b_{e1} = 0{,}4\ b_{eff}$ $\quad b_{e2} = 0{,}6\ b_{eff}$

$\psi = \sigma_2/\sigma_1$	1	$1 > \psi > 0$	0	$0 > \psi > -1$	-1	$-1 > \psi > -3$
Buckling factor k_σ	4,0	$8{,}2 / (1{,}05 + \psi)$	7,81	$7{,}81 - 6{,}29\psi + 9{,}78\psi^2$	23,9	$5{,}98\ (1 - \psi)^2$

Since our profile is in bending, the upper half of the beam goes under compression whereas the lower half of the beam is in tensile force hence under full performance. Since, the section of the profile is divided into two different stresses, we also half the length of the web. Hence the new buckling length of the web under compression is half the total length of the profile.

$\psi = \frac{\sigma_2}{\sigma_1}$ $\psi = 0$ $\psi := 0$

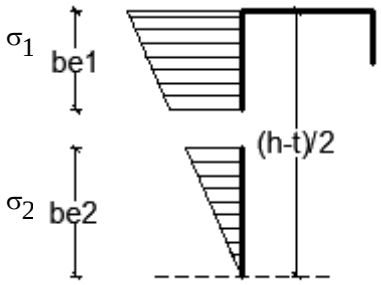

Value of σ_2 is zero as we run towards neutral axis.

So, from EN 1993-1-5 Table 4.1

$k_\sigma := 7.81$

$f_y := 350$ MPa

$\varepsilon := \sqrt{\frac{235}{f_y}}$ $\varepsilon = 0.819$

$\lambda_p := \frac{\frac{(h-t)}{2 \cdot t_{net}}}{28.4 \varepsilon \cdot \sqrt{k_\sigma}} = 1.594$ $\lambda_p > 0,673$ $3 + \psi > 1$

$\rho := \frac{\lambda_p - 0.055(3 + \psi)}{\lambda_p^{\,2}} = 0.563$ $\rho < 1$

$b_{eff} := \rho \cdot \frac{(h - t)}{2} = 55.969 mm$

56 mm effective out of 99.5 mm. WEE

Flange:

$k_{\sigma f} := 4.0$ Uniform compressive stress

$\varepsilon = 0.819$

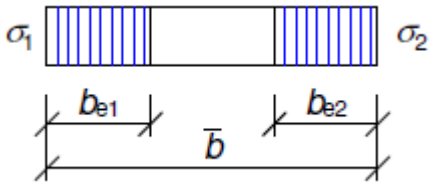

Uniform compressive stress

$\lambda_{pf} := \frac{\frac{(b-t)}{t_{net}}}{28.4 \varepsilon \cdot \sqrt{k_{\sigma f}}} = 1.097$ $\lambda_{pf} > 0.748$

$\rho_f := \frac{\lambda_{pf} - 0.188}{\lambda_{pf}^{\,2}} = 0.756$ $\rho_f < 1.0$

$b_{f.eff} := \rho_f \cdot (b - t) = 37.021 mm$

37.02mm effective out of 49mm. Flange

Lip:

For lip, we need to do an extra calculation of finding the stress at the end of the lip in order to calculate the buckling factor for lip.

If the material strength of the beam is 350 MPa and knowing the dimensions of our profile, we can easily calculate stresses in any place of the beam.

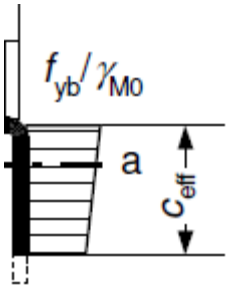

$f_y := 350MPa$

$e_{max} := 99.5mn$

$$e_b := \left[e_{max} - \left(c - \frac{t}{2}\right)\right] = 80 \cdot mn$$

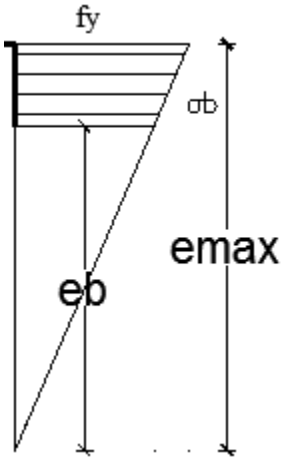

Stress at point B or at the end of lip, assume it is σ.b

$$\sigma_b := \left(\frac{e_b}{e_{max}}\right) \cdot f_y = 281.407MPa$$

Calculating the stress ratio,

$$\psi = \frac{\sigma_2}{\sigma_1} \qquad \psi := \frac{\sigma_b}{f_y} = 0.804 \qquad 0.802 < 1.0$$

Table 4.2: Outstand compression elements

Stress distribution (compression positive)	Effective[P] width b_{eff}
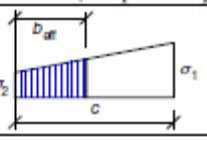	$1 > \psi > 0$: $b_{eff} = \rho\, c$
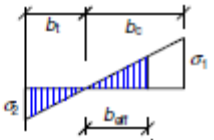	$\psi < 0$: $b_{eff} = \rho\, b_c = \rho\, c / (1-\psi)$

$\psi = \sigma_2/\sigma_1$	1	0	-1	$1 \geq \psi \geq -3$
Buckling factor k_σ	0,43	0,57	0,85	$0,57 - 0,21\psi + 0,07\psi^2$

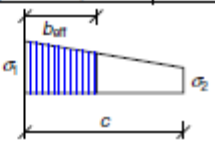	$1 > \psi > 0$: $b_{eff} = \rho\, c$
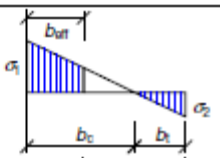	$\psi < 0$: $b_{eff} = \rho\, b_c = \rho\, c / (1-\psi)$

$\psi = \sigma_2/\sigma_1$	1	$1 > \psi > 0$	0	$0 > \psi > -1$	-1
Buckling factor k_σ	0,43	$0,578 / (\psi + 0,34)$	1,70	$1,7 - 5\psi + 17,1\psi^2$	23,8

From EN 1993-1-5 Table 4.2

$k_\sigma := \frac{0.578}{\psi + 0.34} = 0.505$ $\quad c - \frac{t}{2} = 19.5\,mm$

$\lambda_{lp} := \frac{\left(c - \frac{t}{2}\right)}{t_{net}} = 1.228$ $\quad \varepsilon = 0.819$

$\rho_{lp} := \frac{\lambda_p - 0.188}{\lambda_p^{\,2}} = 0.553$

$b_{lpeff} := \rho \cdot \left(c - \frac{t}{2}\right) = 10.969\,mm$

11mm effective of 20 mm lip.

According to EN 1993-1-5 Table 4.1, in case of the web member under tensile and compression the distribution of effective width is 40% to 60% where 40% zone being relatively more compressed side of the profile.

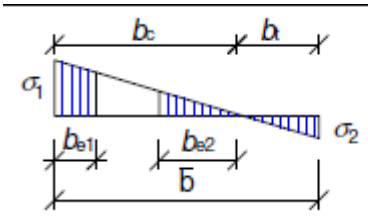

$\psi < 0$:

$b_{eff} = \rho\, b_c = \rho\, \bar{b} / (1-\psi)$

$b_{e1} = 0{,}4\, b_{eff}$ $\quad b_{e2} = 0{,}6\, b_{eff}$

So,

$b_{e1} := 0.4 b_{eff} = 22.388\,mm$ $\quad b_{e2} := 0.6 b_{eff} = 33.582\,mm$

Now, we should calculate the effective section properties of the profile:

Calculation of effective area:

$A_{eff} := b_{eff} \cdot t_{net} + b_{f.eff} \cdot t_{net} + b_{lpeff} \cdot t_{net} + \left(\frac{h - t}{2}\right) \cdot t_{net} + (b - t) \cdot t_{net} + \left(c - \frac{t}{2}\right) \cdot t_{net}$

$A_{eff} = 261.081\,mm^2$

The horizontal position of the neutral axis from the centerline of the web for the effective section is,

$b - t = 49\,mm$ $\quad c = 20\,mm$ $\quad b - t = 49\,mm$ $\quad c - \frac{t}{2} = 19.5\,mm$

$y_{eff} := \frac{\left[\left[\left(c - \frac{t}{2}\right) + b_{lpeff}\right] \cdot (b - t) + \left[(b - t) + b_{f.eff}\right] \cdot \left(\frac{b - t}{2}\right)\right] \cdot t_{net}}{A_{eff}}$

$y_{eff} = 13.239\,mm$

The vertical position of the neutral axis from the centerline of the lower flange for the effective section is,

$$\alpha := \left(c - \frac{t}{2}\right)^2 \cdot \frac{1}{2} + (h - t)^2 \cdot \frac{1}{8} = 5.14 \times 10^{-3}\,m^2$$

$$\beta := b_{e2} \cdot \left[\frac{(h - t)}{2} + \frac{b_{e2}}{2}\right] = 3.905 \times 10^{-3}\,m^2$$

$$\gamma := b_{e1} \cdot \left[(h - t) - \frac{b_{e1}}{2}\right] = 4.205 \times 10^{-3}\,m^2$$

$$\delta := b_{f.eff} \cdot (h - t) = 7.367 \times 10^{-3}\,m^2$$

$$\varepsilon := b_{lpeff} \cdot \left[(h - t) - \frac{b_{lpeff}}{2}\right] = 2.123 \times 10^{-3}\,m^2$$

$$x_{eff} := \frac{(\alpha + \beta + \gamma + \delta + \varepsilon) \cdot t_{net}}{A_{eff}} = 83.615\,mm$$

$x_{eff} = 83.615\,mm$

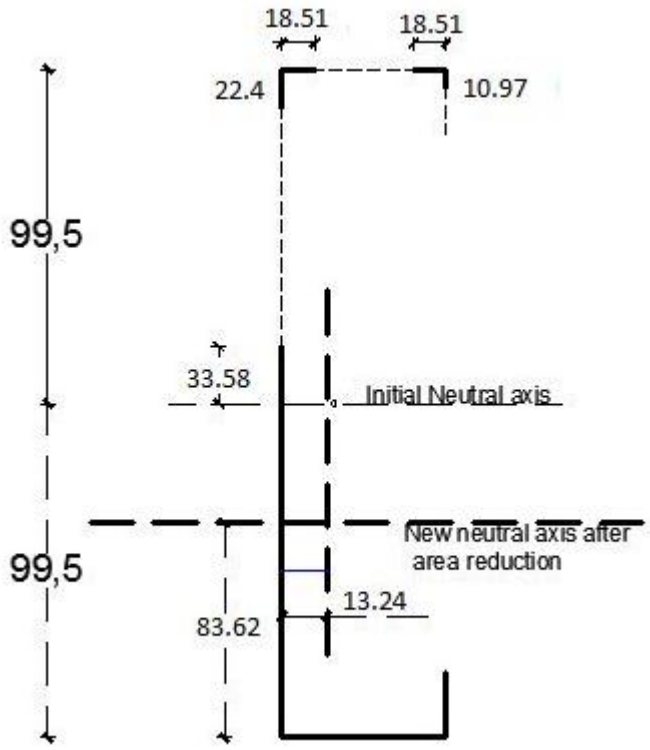

$b_{eff} = 55.969\,mm$

$b_{e1} = 22.388\,mm$ $b_{e2} = 33.582\,mm$ $b_{f.eff} = 37.021\,mm$

$b_{lpeff} = 10.969\,mm$

So the new moment of inertia of the C-profile only considering the effective cross-section of the profile is,

$$P := \frac{t_{net}\cdot\left(c-\frac{t}{2}\right)^3}{12} + \left[\left(c-\frac{t}{2}\right)\cdot t_{net}\right]\cdot\left[x_{eff}-\left(\frac{c-\frac{t}{2}}{2}\right)\right]^2 = 1.027\times 10^5\cdot mm^4$$

$$Q := \frac{(b-t)\cdot t_{net}^{\,3}}{12} + (b-t)\cdot t_{net}\cdot x_{eff}^{\,2} = 3.289\times 10^5\cdot mm^4$$

$$R := \frac{t_{net}\cdot\left[b_{e2}+\left(99.5mm-x_{eff}\right)\right]^3}{12} + \left(b_{e2}+99.5mm-x_{eff}\right)\cdot t_{net}\cdot\left(\frac{b_{e2}+99.5mm-x_{eff}}{2}\right)^2$$

$$R = 3.873\times 10^4\cdot mm^4$$

$$S := \frac{t_{net}\cdot b_{e1}^{\,3}}{12} + t_{net}\cdot b_{e1}\cdot\left(199.5mm-x_{eff}-\frac{b_{e1}}{2}\right)^2 = 2.365\times 10^5\cdot mm^4$$

$$T := \frac{b_{f.eff}\cdot t_{net}^{\,3}}{12} + \left(b_{f.eff}\cdot t_{net}\right)\cdot\left(199.5mm-x_{eff}-\frac{t_{net}}{2}\right)^2 = 4.733\times 10^5\cdot mm^4$$

$$U := \frac{t_{net}\cdot b_{lpeff}^{\,3}}{12} + \left(t_{net}\cdot b_{lpeff}\right)\cdot\left(199.5mm-x_{eff}-\frac{b_{lpeff}}{2}\right)^2 = 1.284\times 10^5\cdot mm^4$$

$$V := \frac{t_{net}\cdot x_{eff}^{\,3}}{12} + \left(t_{net}\cdot x_{eff}\right)\cdot\left(\frac{x_{eff}}{2}\right)^2 = 1.871\times 10^5\cdot mm^4$$

$$I_{eff} := P + Q + R + S + T + U + V = 1.496\times 10^6\cdot mm^4$$

$$E = 2.1\times 10^5\cdot\frac{N}{mm^2}$$

$$E\cdot I_{eff} = 314.089kN\cdot m^2$$

For two profiles, $2\cdot E\cdot I_{eff} = 628.178kN\cdot m^2$

This is the bending stiffness value of S350+Z275 C-profile effective cross-section.